Specification Criteria for Simple Performance Tests for Rutting, Volume I: Dynamic Modulus (E*) and Volume II: Flow Number and Flow Time

DETAILS

94 pages | | PAPERBACK
ISBN 978-0-309-42072-3 | DOI 10.17226/23120

AUTHORS

NATIONAL COOPERATIVE HIGHWAY RESEARCH PROGRAM

NCHRP REPORT 580

Specification Criteria for Simple Performance Tests for Rutting

Volume I: Dynamic Modulus (E)*
Volume II: Flow Number and Flow Time

M.W. Witczak
ARIZONA STATE UNIVERSITY
Tempe, AZ

Subject Areas
Pavement Design, Management, and Performance

Research sponsored by the American Association of State Highway and Transportation Officials
in cooperation with the Federal Highway Administration

TRANSPORTATION RESEARCH BOARD

WASHINGTON, D.C.
2007
www.TRB.org

NATIONAL COOPERATIVE HIGHWAY RESEARCH PROGRAM

Systematic, well-designed research provides the most effective approach to the solution of many problems facing highway administrators and engineers. Often, highway problems are of local interest and can best be studied by highway departments individually or in cooperation with their state universities and others. However, the accelerating growth of highway transportation develops increasingly complex problems of wide interest to highway authorities. These problems are best studied through a coordinated program of cooperative research.

In recognition of these needs, the highway administrators of the American Association of State Highway and Transportation Officials initiated in 1962 an objective national highway research program employing modern scientific techniques. This program is supported on a continuing basis by funds from participating member states of the Association and it receives the full cooperation and support of the Federal Highway Administration, United States Department of Transportation.

The Transportation Research Board of the National Academies was requested by the Association to administer the research program because of the Board's recognized objectivity and understanding of modern research practices. The Board is uniquely suited for this purpose as it maintains an extensive committee structure from which authorities on any highway transportation subject may be drawn; it possesses avenues of communications and cooperation with federal, state and local governmental agencies, universities, and industry; its relationship to the National Research Council is an insurance of objectivity; it maintains a full-time research correlation staff of specialists in highway transportation matters to bring the findings of research directly to those who are in a position to use them.

The program is developed on the basis of research needs identified by chief administrators of the highway and transportation departments and by committees of AASHTO. Each year, specific areas of research needs to be included in the program are proposed to the National Research Council and the Board by the American Association of State Highway and Transportation Officials. Research projects to fulfill these needs are defined by the Board, and qualified research agencies are selected from those that have submitted proposals. Administration and surveillance of research contracts are the responsibilities of the National Research Council and the Transportation Research Board.

The needs for highway research are many, and the National Cooperative Highway Research Program can make significant contributions to the solution of highway transportation problems of mutual concern to many responsible groups. The program, however, is intended to complement rather than to substitute for or duplicate other highway research programs.

NCHRP REPORT 580

Project 9-19
ISSN 0077-5614
ISBN 978-0-309-09913-4
Library of Congress Control Number 2007909329

COPYRIGHT PERMISSION

NOTICE

The project that is the subject of this report was a part of the National Cooperative Highway Research Program conducted by the Transportation Research Board with the approval of the Governing Board of the National Research Council. Such approval reflects the Governing Board's judgment that the program concerned is of national importance and appropriate with respect to both the purposes and resources of the National Research Council.

The members of the technical committee selected to monitor this project and to review this report were chosen for recognized scholarly competence and with due consideration for the balance of disciplines appropriate to the project. The opinions and conclusions expressed or implied are those of the research agency that performed the research, and, while they have been accepted as appropriate by the technical committee, they are not necessarily those of the Transportation Research Board, the National Research Council, the American Association of State Highway and Transportation Officials, or the Federal Highway Administration, U.S. Department of Transportation.

Each report is reviewed and accepted for publication by the technical committee according to procedures established and monitored by the Transportation Research Board Executive Committee and the Governing Board of the National Research Council.

The Transportation Research Board of the National Academies, the National Research Council, the Federal Highway Administration, the American Association of State Highway and Transportation Officials, and the individual states participating in the National Cooperative Highway Research Program do not endorse products or manufacturers. Trade or manufacturers' names appear herein solely because they are considered essential to the object of this report.

Published reports of the

NATIONAL COOPERATIVE HIGHWAY RESEARCH PROGRAM

are available from:

Transportation Research Board
Business Office
500 Fifth Street, NW
Washington, DC 20001

and can be ordered through the Internet at:

http://www.national-academies.org/trb/bookstore

Printed in the United States of America

THE NATIONAL ACADEMIES

Advisers to the Nation on Science, Engineering, and Medicine

The **National Academy of Sciences** is a private, nonprofit, self-perpetuating society of distinguished scholars engaged in scientific and engineering research, dedicated to the furtherance of science and technology and to their use for the general welfare. On the authority of the charter granted to it by the Congress in 1863, the Academy has a mandate that requires it to advise the federal government on scientific and technical matters. Dr. Ralph J. Cicerone is president of the National Academy of Sciences.

The **National Academy of Engineering** was established in 1964, under the charter of the National Academy of Sciences, as a parallel organization of outstanding engineers. It is autonomous in its administration and in the selection of its members, sharing with the National Academy of Sciences the responsibility for advising the federal government. The National Academy of Engineering also sponsors engineering programs aimed at meeting national needs, encourages education and research, and recognizes the superior achievements of engineers. Dr. Charles M. Vest is president of the National Academy of Engineering.

The **Institute of Medicine** was established in 1970 by the National Academy of Sciences to secure the services of eminent members of appropriate professions in the examination of policy matters pertaining to the health of the public. The Institute acts under the responsibility given to the National Academy of Sciences by its congressional charter to be an adviser to the federal government and, on its own initiative, to identify issues of medical care, research, and education. Dr. Harvey V. Fineberg is president of the Institute of Medicine.

The **National Research Council** was organized by the National Academy of Sciences in 1916 to associate the broad community of science and technology with the Academy's purposes of furthering knowledge and advising the federal government. Functioning in accordance with general policies determined by the Academy, the Council has become the principal operating agency of both the National Academy of Sciences and the National Academy of Engineering in providing services to the government, the public, and the scientific and engineering communities. The Council is administered jointly by both the Academies and the Institute of Medicine. Dr. Ralph J. Cicerone and Dr. Charles M. Vest are chair and vice chair, respectively, of the National Research Council.

The **Transportation Research Board** is one of six major divisions of the National Research Council. The mission of the Transportation Research Board is to provide leadership in transportation innovation and progress through research and information exchange, conducted within a setting that is objective, interdisciplinary, and multimodal. The Board's varied activities annually engage about 7,000 engineers, scientists, and other transportation researchers and practitioners from the public and private sectors and academia, all of whom contribute their expertise in the public interest. The program is supported by state transportation departments, federal agencies including the component administrations of the U.S. Department of Transportation, and other organizations and individuals interested in the development of transportation. **www.TRB.org**

www.national-academies.org

COOPERATIVE RESEARCH PROGRAMS

CRP STAFF FOR NCHRP REPORT 580

Christopher W. Jenks, *Director, Cooperative Research Programs*
Crawford F. Jencks, *Deputy Director, Cooperative Research Programs*
Edward T. Harrigan, *Senior Program Officer*
Eileen P. Delaney, *Director of Publications*
Hilary Freer, *Senior Editor*

NCHRP PROJECT 9-19 PANEL
Field of Materials and Construction—Area of Bituminous Materials

Hussain Bahia, *University of Wisconsin—Madison, Madison, WI*
Luis Julian Bendana, *New York State DOT, Albany, NY*
E. Ray Brown, *National Center for Asphalt Technology, Auburn, AL*
Dale S. Decker, *Bailey, CO*
Jon A. Epps, *Granite Construction Inc., Sparks, NV*
Eric E. Harm, *Illinois DOT, Springfield, IL*
Dallas N. Little, *Texas A&M University, College Station, TX*
Carl L. Monismith, *University of California—Berkeley, Berkeley, CA*
James A. Musselman, *Florida DOT, Gainesville, FL*
Linda M. Pierce, *Washington State DOT, Olympia, WA*
John Bukowski, *FHWA Liaison*
Thomas Harman, *FHWA Liaison*
Larry L. Michael, *Other Liaison*
Frederick Hejl, *TRB Liaison*

FOREWORD

By Edward T. Harrigan
Staff Officer
Transportation Research Board

This report summarizes in two volumes key information on three recommended simple performance tests for permanent deformation of hot mix asphalt (HMA). In the final phase of the work described here, the candidate tests for permanent deformation were validated with field performance data and specifications for their use were developed. The report will be of particular interest to materials engineers in state highway agencies, as well as to materials suppliers and paving contractor personnel responsible for designing and producing HMA.

A key objective of NCHRP Project 9-19, "Superpave Support and Performance Models Management," was to develop simple performance tests for permanent deformation and fatigue cracking for incorporation in the Superpave volumetric mix design method. The 2002 *NCHRP Report 465: Simple Performance Test for Superpave Mix Design* summarized analytical and experimental work conducted between 1995 and 2001 at the University of Maryland and Arizona State University to (1) survey the range of potential simple performance test methods and (2) select the most promising methods for a field validation program.

The resulting field validation and specification development programs were conducted between 2001 and 2005. Both plant mixes and laboratory-blended, short-term oven-aged mixes were tested in the field validation program. Mixtures from MnRoad, NCAT Test Track, Indiana, Nevada I-80, WesTrack, FHWA-ALF, and Arizona I-10 sites constituted the complete test matrix. The results of the validation program supported the selection of the dynamic modulus (E^*), flow number (Fn), and flow time (Ft) tests as simple performance tests for permanent deformation of HMA mixes.

The project findings summarized in this report were extensively reviewed with the research team by the NCHRP Project 9-19 panel. In 2004, the project panel formally recommended the dynamic modulus test as the primary simple performance test for permanent deformation. The panel further recommended the flow number test as an optional, complementary procedure for evaluating the resistance of an HMA mix design to tertiary flow. Subsequently, the research agency prepared a recommended specification, in the form of a Microsoft Excel spreadsheet, that determines a critical minimum E^* value for HMA, which is based on project-specific information on climate, traffic, pavement structure, and layer depth. The specification is based on a series of pavement design examples pre-solved using the Mechanistic-Empirical Pavement Design Guide software developed in NCHRP Projects 1-37A and 1-40. The agency also developed guidelines for using the flow number or flow time test to estimate the rutting potential of HMA mixes under specific project

conditions. These results, supported by the findings of the field validation program, are presented in Volumes I and II of this *NCHRP Report 580*.

Volumes I and II are abridgments of the full reports, which are available in their entirety as PDF Files 13-D and 13-E on NCHRP CRP-CD-46 and bundled with *NCHRP Report 547, Simple Performance Tests: Summary of Recommended Methods and Database*.

CONTENTS

VOLUME I

VOLUME II

VOLUME 1

Dynamic Modulus (E*)

CHAPTER 1

Introduction

1.1 Background

A serious shortcoming of the Superpave hot mix asphalt (HMA) mix design method is that it has lacked strength or material response tests that can be correlated to field performance. By contrast, strength tests have been available for the empirical Marshall and Hveem mix design methods for a long time.

The search for such a material response test was initiated by FHWA. In 1996, FHWA authorized the University of Maryland Superpave Models Team (under Phase II of FHWA Contract No. DTFH61-95-C-00100) to develop all of the test protocols, criteria, and guidelines needed for a so-called *simple performance test* (SPT). This test was intended to complement the Superpave volumetric mix design procedure. From 1999 to 2006, NCHRP Project 9-19 ("Superpave Support and Performance Models Management") continued this research effort, first at the University of Maryland and later at Arizona State University (ASU).

Three tests were selected as the final SPT candidates for evaluation. This selection process is summarized in *NCHRP Report 465: Simple Performance Test for Superpave Mix Design* (*1*), which defines an SPT as

> A test method(s) that accurately and reliably measures a mixture response characteristic or parameter that is highly correlated to the occurrence of pavement distress (i.e., cracking and rutting) over a diverse range of traffic and climatic conditions. (*1*)

Although it was not absolutely necessary for the SPT "to predict the entire distress or performance history of the HMA," (*1*) it was required to "allow a determination of a mix's ability to resist fracture and permanent deformation under defined conditions." (*1*)

NCHRP Report 465 details the selection of the final candidate tests for the Superpave SPT. An extensive laboratory testing program evaluated numerous candidate tests to determine their potential to discriminate between good and bad performing mixtures and to predict rutting. Three SPT candidates were selected for further evaluation because they showed the best potential to correlate laboratory results to field performance. The three candidate tests were

- Dynamic (complex) modulus—E^*,
- Repeated load testing—flow number (F_n) and
- Static creep—flow time (F_t).

NCHRP Report 465 also recommended the following two potential SPT candidates for fracture (fatigue cracking):

- Dynamic (complex) modulus—E^* and
- Indirect tensile strength.

Therefore, E^* was recognized as having a significant potential to become the SPT for two important pavement distresses—rutting and fracture. The use of the repeated load and static creep tests using flow number and flow time, respectively, to estimate rutting potential is presented in Volume II of this report.

The development of the *Mechanistic-Empirical Pavement Design Guide* (MEPDG) was performed concurrently with NCHRP Project 9-19 under NCHRP Project 1-37A, "Development of the 2002 Guide for the Design of New and Rehabilitated Pavement Structures," and NCHRP Project 1-40, "Facilitating the Implementation of the Guide for the Design of New and Rehabilitated Pavement Structures." Included in MEPDG research was evaluation and modeling of the major flexible pavement distresses, permanent deformation (rutting), fatigue cracking (alligator and longitudinal cracking), and thermal cracking. Models that predict the performance of the pavement structure were mechanistically developed and empirically calibrated using field test section data from the Long-Term Pavement Performance (LTPP) Database. In the MEPDG, mixture stiffness (E^*) is considered the main material characterization input for HMA mixtures. Of the

three SPT candidates identified in *NCHRP Report 465*, the only one that is currently implemented in the MEPDG is E*.

1.2 Objectives of This Research Project and Report

The primary objectives of the research reported herein were to (1) confirm that the E* test can be used as a Superpave SPT and (2) develop SPT criteria in order to fully implement E* as the selected SPT. It is important to note that the E* specification criteria evaluated for the rutting SPT are directly based upon the MEPDG. This analytical model, along with laboratory and field data from several national test sites (MnRoad, WesTrack, NCAT, and FHWA-ALF) used in NCHRP Project 9-19, provided the information needed to develop and validate the approach. The results showed that the measurement of E* is the basis for a robust, reliable SPT. Once this fact was established, the research turned to the development of methodology to implement the use of E* for several key situations commonly faced by an engineer:

- Pavement structure design,
- Asphalt mixture design,
- Interactive design of asphalt mixtures and pavement structures, and
- Construction quality control and assurance (QC/QA) for asphalt pavement systems.

Definition and validation of SPT criteria for these situations produced the E* SPT Specification Criteria Program, a predictive tool available as a Microsoft Excel spreadsheet and a C++ program that converts measured or calculated HMA E* values to rut depth predictions. This report provides an in-depth discussion of key aspects of the E* SPT Specification Criteria Program, viz.:

- The conceptual methodology used to create the program, which incorporated a database of pavement design scenarios pre-solved with the MEPDG to form interpolative estimates of potential rutting for any HMA mix design under project-specific traffic (loading), environmental, and multi-layer structural conditions,
- Validation of the approach to determine if the model provided a reasonable representation of the real-world system and to foster confidence in the accuracy of this predictive tool,
- User instructions for operating the program and understanding the interaction of its component worksheets.

1.3 SPT Criteria Definition for Rutting of Flexible Pavements Using E*

The SPT criteria are a set of guidelines the engineer uses to help select the most appropriate mix and structure combination during both the HMA mix and flexible pavement design process. Pavement construction quality control and assurance must also be accounted for once the appropriate HMA mixture is established.

A simple example of how these SPT criteria would be implemented is presented in Table 1-1. This table shows that for a given mix and structure combination (*XY*), at a given set of environmental (*C*) and traffic level (*N*) conditions, a minimum (allowable) SPT value would be required to limit a given pavement distress to a user-defined maximum desired value (*M*). This would be identical to selecting the maximum rut depth desired in the HMA pavement. When a laboratory or in situ measured mix SPT value is compared to this "allowable SPT," an assessment can be performed on the mix to determine whether it is acceptable or not, as shown in the table.

As stated previously, this study focused on the E* test as the potential rutting SPT. Therefore, Table 1-1 can be revised to show the E* criteria required to prevent rutting for specific, predetermined project conditions (see Table 1-2). What needs to be clarified in the final implementation scheme is

Table 1-1. General criteria example using any test as any distress SPT.

Specimen ID	Actual SPT Value Measured in the Laboratory or at the Project Site	Minimum Allowable SPT Value Calculated for Project Conditions	Decision: Yes or No?
A	150,000 units	200,000 units	Not Acceptable
B	225,000 units		Acceptable

NOTE: This is a typical table for a given environmental (*C*), traffic (*N*), and mix/structure combination (*XY*).

Table 1-2. Criteria example using E* as rutting SPT.

Specimen ID	Laboratory or In-Situ Measured E* (psi)	E* Criteria to Prevent Rutting > "x" Inches for Project Conditions (psi)	Decision: Yes or No?
A	150,000	200,000	Not Acceptable
B	225,000	200,000	Acceptable

NOTE: This is a typical table for a given environmental (*C*), traffic (*N*), and mix/structure combination (*XY*).The maximum allowable rutting value that the engineer used in the design process is represented by "x".

what specific set of conditions or scenarios the E* as rutting SPT criteria will utilize. The next section addresses this issue.

1.4 Potential Uses of the E* SPT Specification Criteria Program

Other scenarios in which the E* SPT Specification Criteria Program could be used are as follows:

1. During an interactive design process of HMA mix and flexible pavement design and
2. For quality control and assurance (QC/QA) of the pavement construction.

Under these proposed scenarios, four modes of the E* SPT Specification Criteria Program were envisioned within a comprehensive implementation system for evaluating the adequacy of an HMA mixture to resist permanent deformation to some allowable level. These modes are defined as follows:

- Mode 1—Full use of MEPDG developed under NCHRP Project 1-37A, along with the full use of the E*methodology developed under NCHRP Project 9-19;
- Mode 2—Use of an appropriate rut depth model based upon the MEPDG and full use of the E* methodology;
- Mode 3—Use of E* as a mix design tool; and
- Mode 4—Use of E* as a construction QC/QA tool.

These four modes are explained in greater detail in the following sections.

1.4.1 Mode 1 (Full MEPDG and E* Methodology)

This mode is the most reliable design procedure, under which all of the MEPDG predictable distresses would be calculated based on a specific set of material characterization parameters. The engineer would use the actual MEPDG software in a trial-and-error process to determine a combination of HMA mixture type and flexible pavement structure that yields adequate (i.e., tolerable) levels of distress selected by the designer.

E* tests would be performed in the full temperature-frequency factorial necessary to characterize the HMA mixture. This HMA material characterization would then be used as direct input for a simulation run in the MEPDG software. The distress predictions would be compared to those considered as failure values for each specific distress. If these predicted distress responses were found to be unacceptable, several trials would need to be performed until the desired mix/structure combination, satisfying all allowable (target) distress levels, is achieved.

The major problem with this mode is that it is a relatively time-consuming process because of the complexities of the MEPDG software. In addition, the real probability that numerous iterations (simulation runs) will be required results in the possibility that significant time may be required. With this limitation in mind, it is highly desirable to have a much quicker approach for using E* in an SPT specification criteria program that is based on the MEPDG.

1.4.2 Mode 2 (Shortcut of MEPDG and Full Superpave E* Methodology)

This mode uses approximate solutions obtained with the MEPDG software to predict rutting in HMA layers. It is based upon a database of rutting predictions constructed from the MEPDG, covering the greatest possible significant combinations of variables affecting the HMA rutting prediction. This allows the engineer to interpolate the HMA sublayer rutting within any pavement structure for any traffic and climatic condition chosen from the database.

With this abbreviated methodology, E* versus rutting relationships may be constructed for all possible combinations of traffic, climatic, and structural conditions. Then, by knowing the specified mix properties (i.e., E* values), the appropriate rutting value may be calculated within a given confidence level.

Figure 1-1 provides an example of such an E* versus rutting relationship for a given set of design input values. Here,

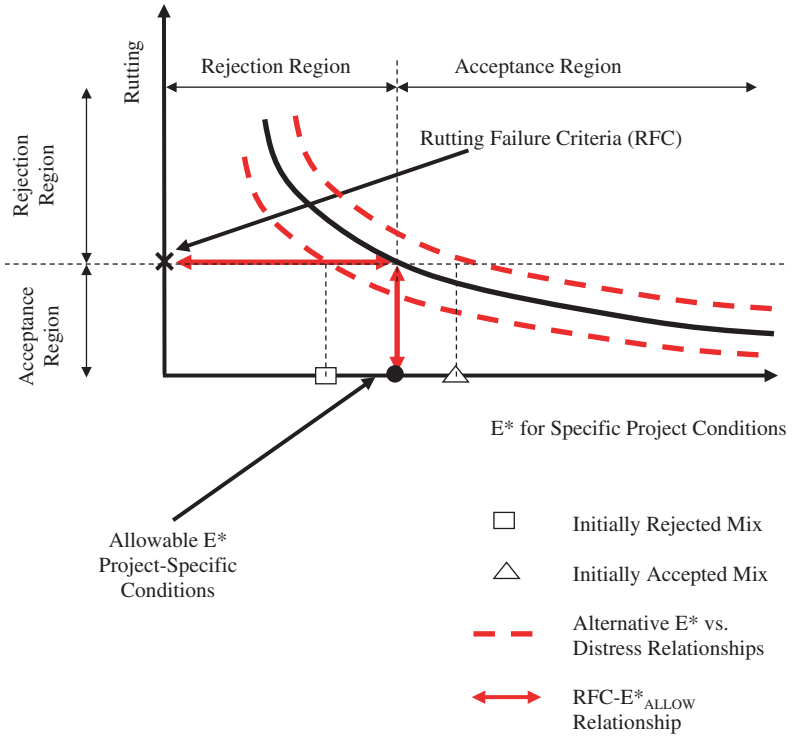

Figure 1-1. Mode 2 use (shortcut for MEPDG and full E* master curve).

the engineer inputs the HMA rutting (by HMA sublayer) that is allowed for the design conditions. This limit value is called the rutting failure criterion (RFC) or, simply, the criterion. By using the E* versus rutting relationship, the RFC can be converted to a minimum allowable E* value (E^*_{ALLOW}). The two-way arrows shown in the figure correspond to the unique failure criteria relationship between E* and rutting for the specific traffic, environmental, and pavement structural conditions of the project.

The engineer can then evaluate different mixes and compare them with this unique RFC-E^*_{ALLOW} relationship. For example, if there is a mix that has a lower E* than the E^*_{ALLOW} (see square denoting initially rejected mix in Figure 1-1), then the mix design should be considered inappropriate for the project conditions and should be rejected (rejection region). On the other hand, if the E* is higher than the E^*_{ALLOW} (triangle denoting acceptance region in Figure 1-1), then the mix is appropriate for the project conditions and should be accepted.

In the case where the mix falls into the rejection region, the engineer has the option of searching for another mix or changing the structural design in such a way that the E* versus rutting relationship changes (dashed curved lines in Figure 1-1), thus varying the RFC-E^*_{ALLOW} relationship. Similarly, the engineer can use a mix that falls within the acceptance region, or consider an alternate structural design (e.g., thickness reduction) in such a way that the design will not be overly conservative (cost reduction/design optimization). As a general rule, the sensitivity of rutting to changes in the specific HMA mixture properties will be many times greater than to changes in the flexible pavement structure.

For this mode only, the acceptance/rejection regions can be analyzed on both axes. That is, the engineer can define the failure based on the E* values or on the pavement distress.

1.4.3 Mode 3 (E* as a Mix Design Tool)

One of the primary goals of developing an SPT was to provide the engineer with a tool for determining whether the mix designed with the Superpave volumetric approach was appropriate for withstanding the unique project conditions according to the design limits specified by the engineer. In order to better explain this mode, a schematic example similar to the one shown in Figure 1-1 is presented in Figure 1-2.

Having a defined and constant E* versus rutting relationship (and RFC-E^*_{ALLOW} relationship) for the project traffic, environmental, and structural conditions, the engineer only has the opportunity to assess the mix E*. If it is found to be unsatisfactory, the design can be changed until the mix surpasses the set criteria. This mode is different from Mode 2, because the engineer does not have the ability to change the structural design and thus move the E* versus rutting (RFC-E^*_{ALLOW}) relationship.

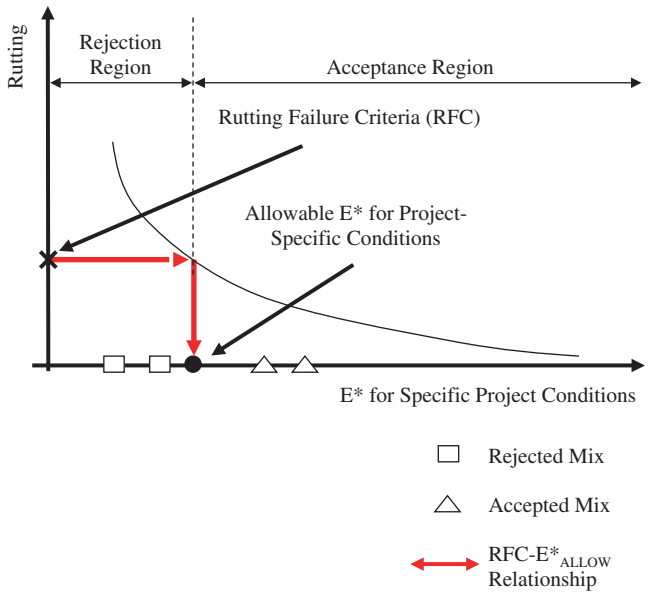

Figure 1-2. Mode 3 use (E* as a mix design tool).

Therefore, the engineer can test mixes that will fall in the rejection region (squares in Figure 1-2) or acceptance region (triangles in Figure 1-2) and, based on these tests, define the appropriate mix for the project. What is critical in this approach, as well as the others, is to have a methodology that is able to determine the HMA mix effective temperature and frequency associated with the design input conditions.

1.4.4 Mode 4 (Use of E* as a Construction QC/QA Tool)

The RFC-E^*_{ALLOW} relationship in Figure 1-2 is robust enough to be used in a reverse manner for QC/QA purposes. For Mode 3, the user starts from the RFC and then determines an allowable E* for the design. For Mode 4, however, the user starts from an E* value tested in the field from samples taken during the construction of the project. The E* values obtained in the tests are then converted, using the E* versus rutting relationship, to potential rut depth magnitude predictions and the comparison is made with the RFC. Figure 1-3 shows a schematic example of this mode.

In this figure, two E* values (squares in Figure 1-3) are lower (less stiff) than E^*_{ALLOW}. It is observed that the respective rutting would be higher than the RFC. Since the as-constructed/compacted mix has not met the required specifications, the mix is considered to be unsatisfactory. However, mixtures having an E* value higher than E^*_{ALLOW} (triangle in Figure 1-3) will yield a lower distress (rut depth) than the RFC. A statistical analysis aimed at developing a frequency distribution of the predicted rut depth within the HMA layers provides the basis for a rational, logical penalty-bonus methodology between the contractor and the owner agency.

This completes the definition and scope of the modes of the E* as rutting SPT criteria developed in this research study. The following chapters provide the full details of the methodology and findings of this comprehensive study. A summary of these chapters and their scope are presented next.

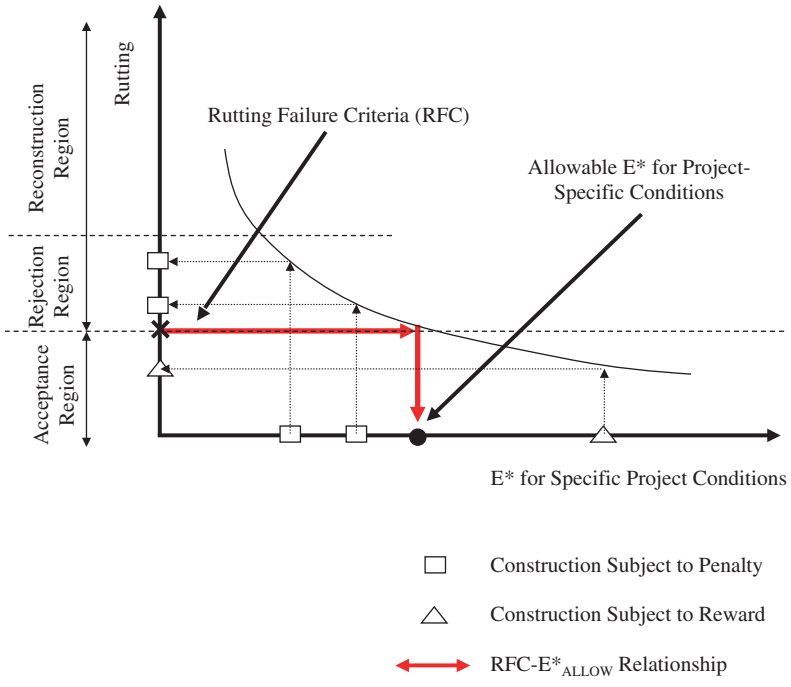

Figure 1-3. Use of SPT for quality control and assurance.

1.5 Organization of This Report

In addition to this introductory information presented in Chapter 1, Chapter 2 of this report focuses on validation of the E* SPT conceptual methodology using laboratory and field data collected for NCHRP Project 9-19, as well as LTPP data used in NCHRP Project 1-37A. Chapter 3 provides a user-friendly guide for the E* SPT Specification Criteria Program. Chapter 4 concludes this report with a summary of findings.

This report is an abridgment of Reference 2, which is available in its entirety as PDF File 13-D on NCHRP CRP-CD-46 and bundled with *NCHRP Report 547: Simple Performance Tests: Summary of Recommended Methods and Database*.

CHAPTER 2

E* SPT Specification Criteria Program Validation

Knowing the final methodology developed to implement E* as the SPT, the goal of this chapter is to test the validity of this method. This validation study was performed with the aid of the statistical tools explained in Section 2.1.1, and through interpretation of graphical plots of measured versus predicted data.

The data to be compared in this validation study are mainly the rutting predictions. Since the E* SPT Specification Criteria Program Mode 2 is an accurate, sound shortcut for the MEPDG, its rutting predictions are as close as possible to those from the MEPDG. Therefore, "measured data" stands for the MEPDG predictions, while the "predicted data" stands for rutting predicted by the E* SPT Specification Criteria Program, obtained from the master curves of E* data input in any of the four options available. Real and simulated pavement system scenarios have been used to perform this validation. The chapter will go into the details of the measured versus predicted comparisons, including some of the enhancements required to improve the correlations.

2.1 Comparison of MEPDG and E* SPT Specification Criteria Program Rutting Predictions

2.1.1 E* SPT Specification Criteria Program Database

The first step in the validation process was to determine if the E* SPT Specification Criteria Program could autopredict itself; that is, to predict the rutting values that are used in the extensive rutting database. The first comparison between the MEPDG rutting database values and the predictions from the E* SPT Specification Criteria Program is shown in Figure 2-1. At the time that this comparison was performed, the temperature variable was only characterized with the mean annual air temperature (MAAT), and the calibration factor used in both programs came from the national calibration factors developed by El-Basyouny (*3*). As can be noticed, there is no bias in the prediction ($y = 1.0079\ x$), but the precision is quite low for a program that is expected to be the shortcut of the MEPDG ($S_e = 0.172$ inches). To increase the precision of the program, extensive studies regarding the T_{eff} and temperature factor that would replace the MAAT factor were developed (see Reference 3, Section 3.1, and Appendix C), and the regional calibration factor approach was also implemented. The results of these additions can be seen in Figure 2-2.

As shown, once the new T_f variable was used to replace the old MAAT and the regional calibration approach was implemented, a significant improvement in the MEPDG versus E* criteria rutting comparison was achieved. There is still no significant bias ($y = 0.9877\ x$), and the precision has considerably increased, with the standard error reduced from 0.172 inches to 0.0703 inches, and the R^2_{adj} increased from 0.9455 to 0.9892. At 6.7%, the resulting coefficient of variation (CV) was also found to be quite low when compared to the original CV, which was equal to 18.7%.

2.1.2 NCHRP 1-37A LTPP Sections

The next step in the validation process was to use the E* SPT Specification Criteria Program for other groups of pavement sections. First, 61 of the 72 LTPP sections used in the national calibration of the MEPDG performed by El-Basyouny (*3*) were used. Table 2-1 provides a list of the LTPP sites used in this study. For details on each section, refer to El-Basyouny (*3*).

Figure 2-3 compares the MEPDG to the E* SPT Specification Criteria Program rutting predictions using the program as it was developed for the previous comparison (i.e., with the temperature factor as the temperature characterization parameter and the regional calibration factor approach).

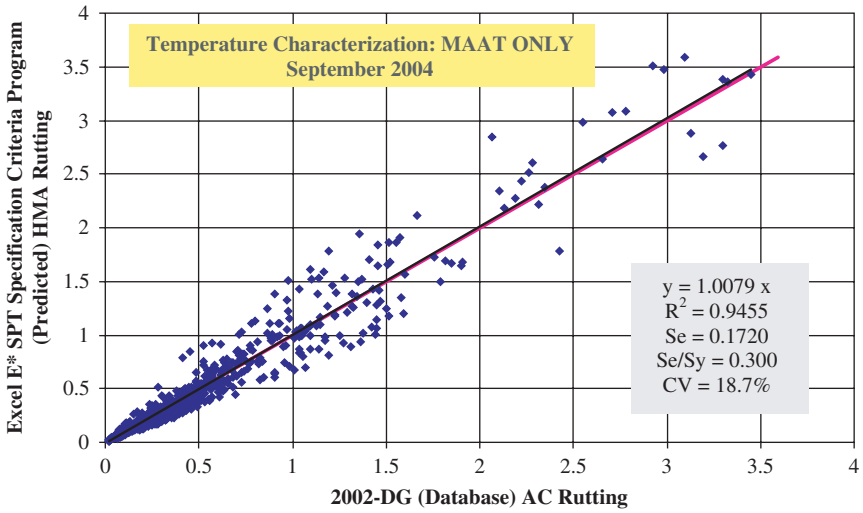

Figure 2-1. Initial comparison between MEPDG and E* SPT Specification Criteria Program rutting predictions for the program rutting database.

NOTE: Temperature characterization = MAAT only; calibration factors are $\beta_{r1} = 0.623$, $\beta_{r2} = 0.9$, $\beta_{r3} = 1.2$.

Of the original 72 LTPP sections, 10 were eliminated because of negative trends, and 1 was eliminated because it was shown to be an outlier. As can be observed, the 61 LTPP sections used showed an insignificant bias toward an under-prediction from the Excel *E** SPT Specification Criteria Program (y = 0.9414 x), with a lower precision than the one observed in Figure 2-2 (good $R^2_{adj} = 0.7349$). Some reasons associated with this decrease in precision were as follows:

1. Effect of the continuity and peak-prediction problems,
2. Reduced effect of the temperature characterization parameter, and
3. Intrinsic variability of the E* SPT Specification Criteria Program itself (Figure 2-2, $S_e = 0.0703$).

The standard error associated with Figure 2-3 ($S_e = 0.0529$, lower in absolute value but higher relatively; see highest rutting value for Figures 2-2 and 2-3) was thought to be distributed at varying depths in the HMA layer due to (1) the way that the environmental effects model in the MEPDG handles sublayers; (2) continuity and peak problems in early versions of the MEPDG software; (3) the variability associated with the determination of the value of T_{eff}; and (4) the variability of the program itself (see Figure 2-2).

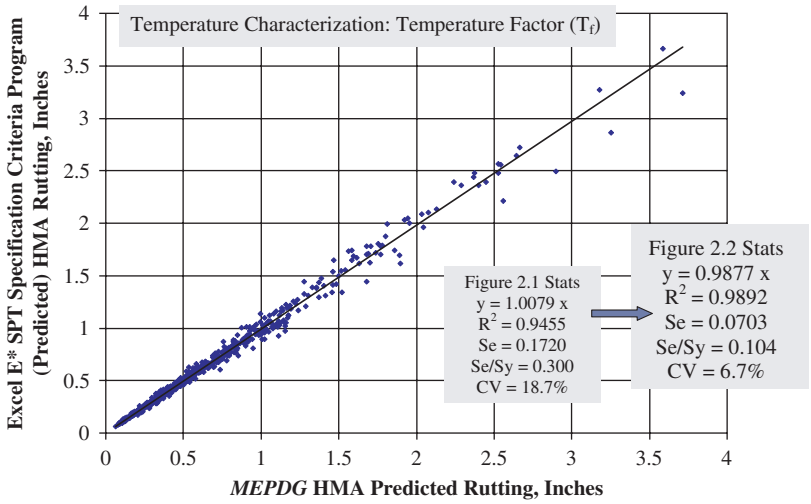

Figure 2-2. Final comparison between MEPDG and E* SPT Specification Criteria Program rutting predictions for the program rutting database.

Table 2-1. LTPP sections used/eliminated throughout study.

011019	161001	351005
014126 †	161009 *	351022
021001	161021	371024 †
021002	169034	371802 †
040114 †	201009 *	371817 *
040115 †	251003	371992
040116 †	251004	404087
040117 †	261001	404163
040118 †	261004 *	421599 †
041007 †	271087 * †	451011
041016	291008	480001
081029	307088 *	481060
081047 *	308129	481077
081053	321020 †	481109
091803	341011	481178
123997	341031	481183
124105	341033	501002
124106	341034	501004
124107	350101	511002
124108	350102 †	511023
131031	350103 †	512021
134111	350104 †	531801 *
134112 + ‡	350105 †	561007 *
134119 * †	350106 †	841684 †

NOTE:
* Sections eliminated because of negative trends = 10.
† Sections eliminated from T_{eff} / Temperature Factor Study = 20.
‡ Outlier section.

It should be realized that Figure 2-2 is the comparison of the program database itself, run for structures at whole-number thickness values (i.e., 2, 3, 4, 8, 12, etc.). The 61 LTPP sections, on the other hand, had thickness values that were quite variable, and distributed as follows:

1. Six sections with whole-number thickness values;
2. Thirty sections with values between (x).5 and (x + 1).0 values (e.g., 3.5 inches, 4.6 inches, 6.7 inches, 10.9 inches, etc.);
3. Twenty-five sections with values between (x).0 and (x).5 (e.g., 2.1 inches, 3.2 inches, etc.); and
4. Six sections with values between 2 and 3 inches.

Thus, 30 out of 61 sections may be most affected by the continuity problem of Version 0.7 of the MEPDG, and 7 may be affected by the peak-prediction problem, which leads to the mentioned reduction in predictive precision.

The remaining error is associated with variability present within the temperature factor and effective temperature equations, and the variability of the E* SPT Specification Criteria Program itself. Although the new temperature characterization methodology greatly improves the correlations (compare Figures 2-1 and 2-2), there is still variability within the relationships that leads to small errors that add to those from the continuity and peak problems, as well as to the embedded variability of the program. Nevertheless, as a tradeoff for the simplification provided by the E* SPT Specification Criteria Program, such errors (S_e = 0.0529 inches) are considered small and acceptable.

Although the results from the LTPP sections were very encouraging, the analysis of more data was needed. Thus, 20 additional random sections were created exclusively for this project, including some NCHRP Project 9-19 sections described in Chapter 3 of *NCHRP Report 547, Simple Performance Tests: Summary of Recommended Methods and Database.*

2.1.3 Random Sections

Additional sections were desired with varying temperature, traffic, material, and structural conditions and characteristics. Twenty sections were randomly created, increasing the number of environmental sites from 73 (61 LTPP plus 12 environmental sites for the E* SPT Specification Criteria Program) to 93 sites. A list of the climatic sites, as well as the

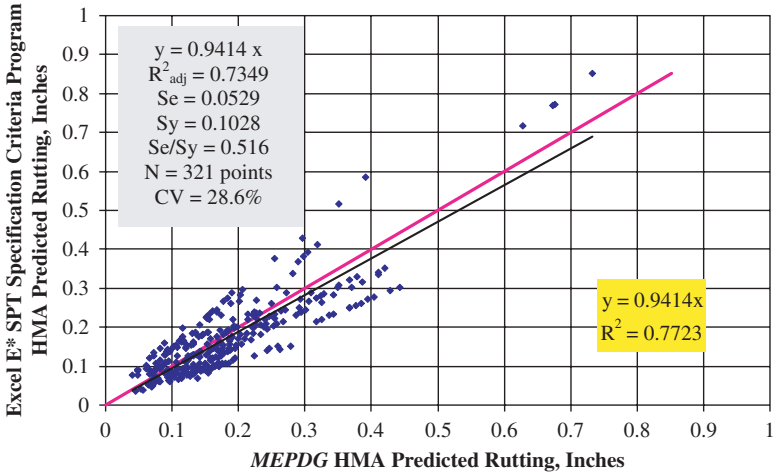

Figure 2-3. Comparison between MEPDG and E* SPT Specification Criteria Program rutting predictions for 61 LTPP sections.

temperature parameters used for them, is presented in Table 2-2. Similarly, Table 2-3 presents the summary of the traffic, structural, and mix characteristics of the 20 randomly generated sections.

Figure 2-4 shows the comparison of measured (MEPDG-predicted data) versus predicted (E* SPT Specification Criteria Program) rutting values. As shown, from the 20 random sections, only one section was considerably underpredicted (Random Section No. 17; MEPDG predicted 1.516 inches while E* predicted 0.986 inches).

A detailed study on this section concluded that the error was solely derived from the temperature characterization variable. Although the regression model that was developed was appropriately correlated for the significant number of sections used, its uncertainty was still considerable. However, for the purposes and scope of this project, it was concluded that the temperature factor and effective temperature approaches were valid and sufficient.

It is important to highlight that comparisons using the data from the 20 random sections, as well as from the E* SPT Specification Criteria Program Database, produce quite high and unrealistic rutting predictions (higher than 0.5 inches) in some cases. In both comparison studies, some of the sections were either purposefully susceptible to rutting (rutting database) or were randomly created in such a way (20 random sections).

Such simulation scenarios, although unrealistic and extreme, proved to yield appropriate comparisons between the MEPDG and the E* SPT Specification Criteria Program. However, standard deviations increase as the magnitude of rutting becomes large. For example, the S_e for the realistic LTPP sections was 0.0529, while the S_e for the unrealistic high-rutting random sections was 0.1476 (mainly driven by the sections with rutting greater than 1 inch).

Since the standard error proved to be a function of the average predicted rutting, the CV was determined to be a better parameter to represent the variability of data used. For these random sections, it was found that the CV was 15.4%. Meanwhile, the CV for the LTPP sections was found to be equal to 28.6%, while the CV for the program database itself was found to be equal to 6.7% (see Figure 2-2).

Thus, this gap between the program CV of 6.7% and the CV of the LTPP (28.6%) and random sections (15.4%) mainly results from (1) the continuity and peak problems in Version 0.7 of the MEPDG, (2) the different subdivision schemes for the environmental effects model in the MEPDG, and (3) the errors associated with the temperature factor and effective temperature concepts (as was shown in Figure 2-4 with Random Section No. 17).

With the acquisition of more simulations and real measured data, the models may be further improved and the current CV will be further reduced.

2.1.4 NCHRP Project 9-19 Sections

The final comparison between predicted E* SPT Specification Criteria Program and predicted MEPDG rutting values was performed using the final NCHRP Project 9-19 sections (MnRoad, NCAT, WesTrack, and FHWA-ALF) described in Chapter 3 of Reference 2.

Table 2-2. Environmental characteristics of the 20 random sections.

No.	Location	Mean Annual Air Temp (°F)	Mean Monthly Air Temp SD (°F)	Mean Annual Wind Speed (mph)	Mean Annual Sunshine (%)	Annual Cumulative Rainfall Depth (Inches)
1	Columbus	65.5	15.5	5.2	67.7	36.6
2	Charleston	65.4	14.6	6.8	66.9	53.9
3	Albuquerque	57.3	17.8	7.1	60.4	9.1
4	Madison	47.6	20.6	6.5	52.5	31.6
5	New York	55.0	16.7	6.0	58.1	45.1
6	Anchorage	37.9	17.8	3.7	26.3	12.9
7	Miami	76.6	7.8	7.1	44.4	62.0
8	Denver	50.1	19.6	8.6	42.9	16.1
9	Grand Canyon	46.8	19.2	5.4	74.1	13.3
10	Juneau	42.5	11.6	6.6	17.8	65.8
11	Seattle	51.4	10.6	6.2	27.5	38.5
12	International Falls	39.7	23.6	6.7	52.6	24.7
13	El Paso	65.1	17.4	7.4	70.1	7.2
14	Las Vegas	68.9	18.5	7.6	68.8	4.5
15	Raleigh	59.7	16.7	5.1	44.3	46.3
16	Lincoln	51.8	21.9	8.4	63.7	28.0
17	Ontario	51.6	18.7	5.2	71.4	9.7
18	New Orleans	69.7	13.3	7.1	54.2	56.4
19	Honolulu	76.5	4.7	9.6	70.5	7.6
20	Cedar Rapids	48.8	21.5	8.5	52.6	30.0

Table 2-3. Traffic and mix/volumetric characteristics of the 20 random sections.

No.	Location	18-kip ESALs (x 1,000)	Avg Speed (mph)	Total Thickness (Inches)	AV (%)	Vbeff (%)	Ret ¾ (%)	Ret 3/8 (%)	Ret N4 (%)	Pass N200 (%)
1	Columbus	5,747	51	1.6	9	11	7.2	27.4	43.5	4.5
2	Charleston	31,536	51	7.6	8	11	9.5	25.4	55.2	5.2
3	Albuquerque	65,969	17	1	6	9	5.5	15.3	57.3	4.4
4	Madison	17,481	51	6.6	6	8	0.5	16.7	56.5	3.9
5	New York	21,094	15	6.4	6	9	2.7	30.1	53.5	7.6
6	Anchorage	33,450	13	11.3	8	15	7.3	33.1	48.5	5.8
7	Miami	14,279	52	6.8	7	11	9	16	41	6
8	Denver	53,491	28	3.1	7	12	1.1	30.2	49.6	7.3
9	Grand Canyon	29,645	6	8.5	8	14	6.5	30	44.5	8.5
10	Juneau	18,057	67	8	9	11	5	26.1	52.1	3.7
11	Seattle	68,913	23	10.9	5	8	0	31.6	51.9	3.9
12	International Falls	10,052	63	8.6	7	10	3.5	13.8	41.6	3.4
13	El Paso	74,931	51	2.3	7	10	1.1	16.5	56.2	5.5
14	Las Vegas	7,358	68	2	7	12	9.6	29.1	59.6	3.3
15	Raleigh	22,729	6	11.3	8	12	3.3	13.4	43.6	7.7
16	Lincoln	61,287	28	7.2	12	15	7.8	22.1	51.6	5.4
17	Ontario	35,044	14	4.3	9	12	4	22.8	49.9	4.9
18	New Orleans	43,664	27	9.7	5	11	0	27.4	47.4	3.7
19	Honolulu	23,394	21	9.1	7	14	5.4	16.7	51.1	5.2
20	Cedar Rapids	40,982	34	11.4	7	13	9.7	26.1	40.6	9

Similar to the LTPP and random sections study, this part also implements the regional calibration factor approach using Equation 3.20 in Reference 2.

The comparisons for MnRoad proved to be fair (Figure 2-5, $R^2_{adj} = 0.5408$) with a moderate underprediction ($y = 0.7724\ x$) and an associated CV equal to 26.3%.

For the WesTrack sections, however, the correlations were good (Figure 2-6, $R^2_{adj} = 0.7605$) with a slight tendency to underpredict the MEPDG predictions ($y = 0.9171\ x$) and a null CV (in fact, the standard deviation, a constant value of 0.089 inches, did not change with the average value). The correlations were improved by the application of a correction factor to account for the lack of wander present at WesTrack. By running the MEPDG for various WesTrack sections, the predicted rutting when the standard deviation of wander (σ_{wander}) was equal to 10 inches (conventional value) was found to be 1.25 times lower than the predicted rutting when the standard deviation of wander was equal to 3.5 inches

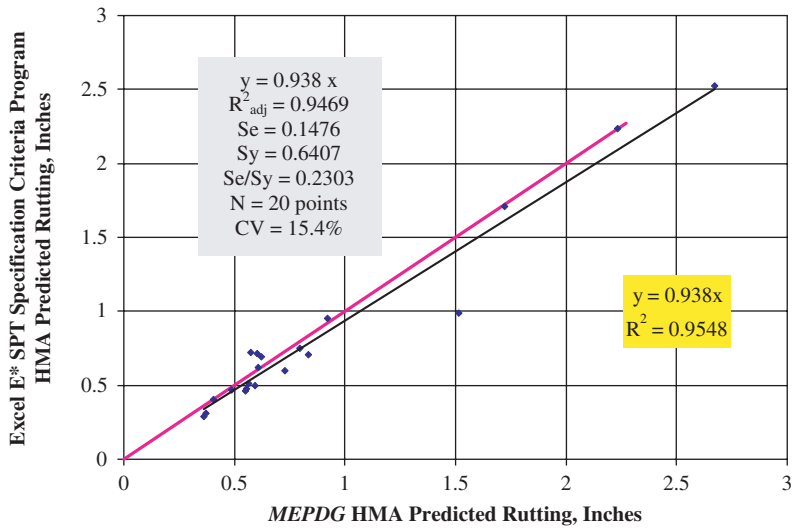

Figure 2-4. Comparison between MEPDG and E* SPT Specification Criteria Program rutting predictions for 20 random sections.

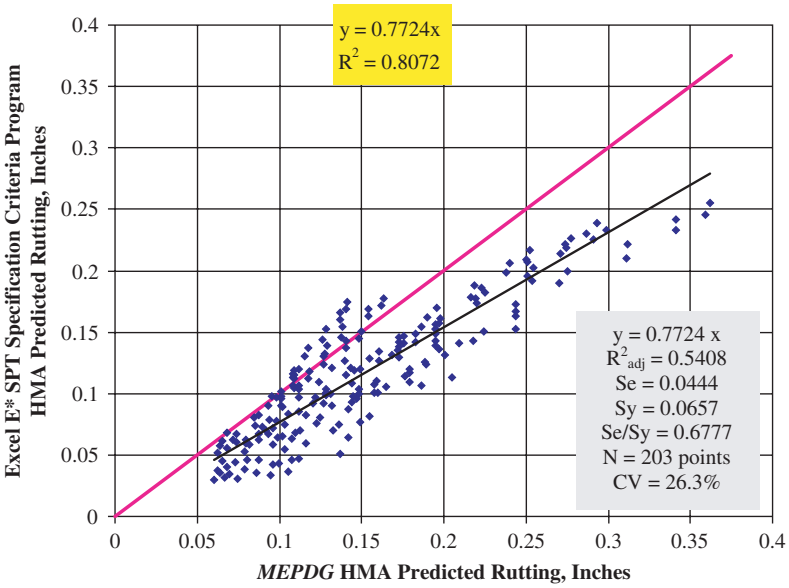

Figure 2-5. Comparison between MEPDG and E* SPT Specification Criteria Program rutting predictions for MnRoad sections.

(arbitrarily selected value for WesTrack and applied in MEPDG simulation runs). Thus, all the Excel predictions were multiplied by the 1.25 wander factor.

For the FHWA-ALF sections, a slight overprediction was present ($y = 1.1919\ x$) with a good correlation ($R^2_{adj} = 0.8505$; see Figure 2-7). For these sections, the temperature was kept constant throughout the structure, as was done in the MEPDG runs to try to reflect what was reported in Reference 4. Similar to WesTrack, a 2.12 wander factor was applied to account for the different MEPDG predictions when the standard deviation of wander was equal to 10 inches and zero inches (values reported at FHWA-ALF). The associated CV found was equal to 22.9%.

Finally, for the NCAT sections (Figure 2-8), the correlation was only fair ($R^2_{adj} = 0.5031$), with a slight overprediction ($y = 1.0887\ x$) and a null CV (in fact, the variation decreases as the rutting increases, and therefore a constant value of the CV is not available).

The main reason for the fair correlations ($R^2_{adj} < 0.60$) for the NCAT and MnRoad sections is likely the summer-winter

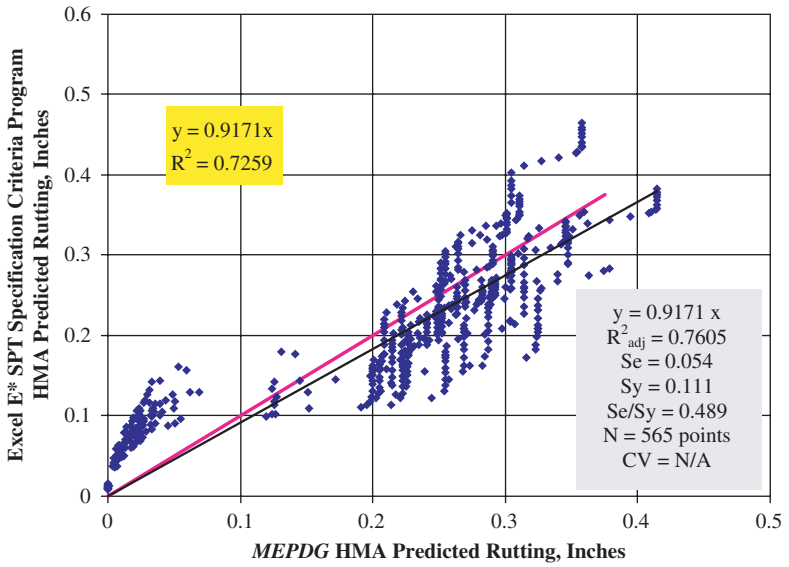

Figure 2-6. Comparison between MEPDG and E* SPT Specification Criteria Program rutting predictions for WesTrack sections.

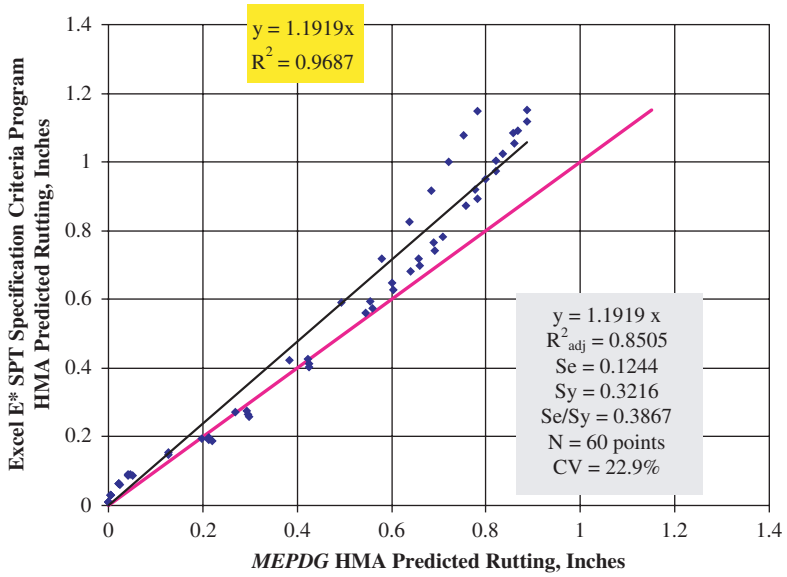

Figure 2-7. Comparison between MEPDG and E* SPT Specification Criteria Program rutting predictions for FHWA-ALF sections.

effect (particularly severe at NCAT, see Figure 2-8), and the intrinsic error in the T_{eff} relationship, respectively.

2.1.5 Summary of Comparisons

Figure 2-9 provides a summary of all of the comparisons in which the results of the original database, the LTPP sections, the random sections, and the NCHRP Project 9-19 sections are combined. The R^2_{adj} associated with this comparison was 0.979 (excellent), with an S_e of 0.069 and CV of 10.1%. Without the database and random sections (see Figure 2-10), which provided unrealistic and non-measured field rutting values that may erroneously affect the relationship, the R^2_{adj} was equal to 0.835 (good correlation), the S_e was equal to 0.067, and CV was equal to 22.0%. These values are considered acceptable and very satisfactory for the simplifications performed by this E* SPT Specification Criteria Program, with no significant under- or over-prediction between Excel and the MEPDG (y = 0.9926 x), which is what is expected from such a shortcut program.

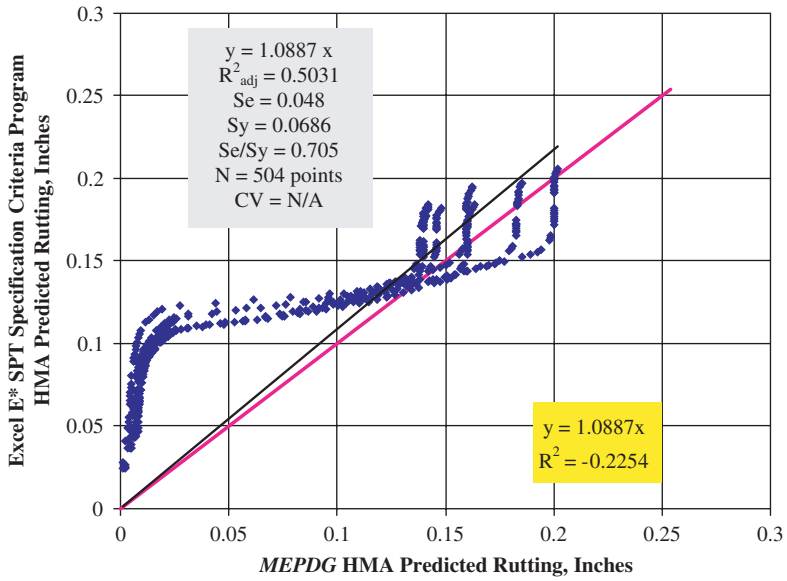

Figure 2-8. Comparison between MEPDG and E* SPT Specification Criteria Program rutting predictions for NCAT sections.

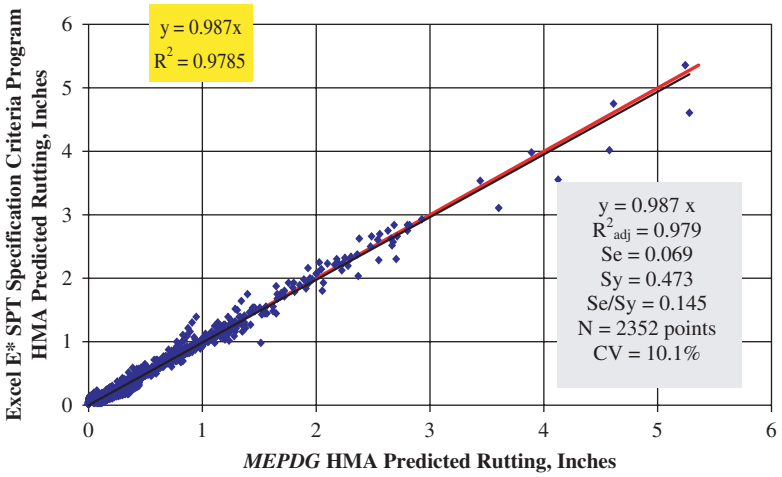

Figure 2-9. Comparison between MEPDG and E* SPT Specification Criteria Program rutting predictions for all validation study sections (LTPP, random, and NCHRP Project 9-19).

2.1.6 Initial Assessment of the Use of E* as an SPT

Since the E* SPT Specification Criteria Program predictions have proven satisfactory with respect to the MEPDG predictions, this section assesses the use of E* as an SPT. As explained in Chapter 5 of Reference 2, the final output of the program is not a pavement thickness or mix design, but a prediction of rut depth associated with an E* at T_{eff} and loading frequency conditions, which are then compared with what the engineer considers a failure rut depth and its associated critical E*.

Figure 2-11 is a schematic of how the comparison between the system capacity (whatever the proposed mix and structural design yields as performance) and the system demand (the failure criteria defined by the user) is performed.

This comparison was performed for all of the LTPP sites available, as well as the NCHRP Project 9-19 sections (those that have real measured data in the field). The system demand for this comparison was set to be equal to the field-measured rut depth, and the system capacity to the rut value predicted by the E* SPT Specification Criteria Program. The graphical comparison in Figure 2-12 indicates that the correlation is slightly worse than the field-measured versus MEPDG-predicted rutting correlation (see Figure 2-13), as expected due to the numerous shortcut relationships and assumptions in the derivation of the E* SPT Specification Criteria Program.

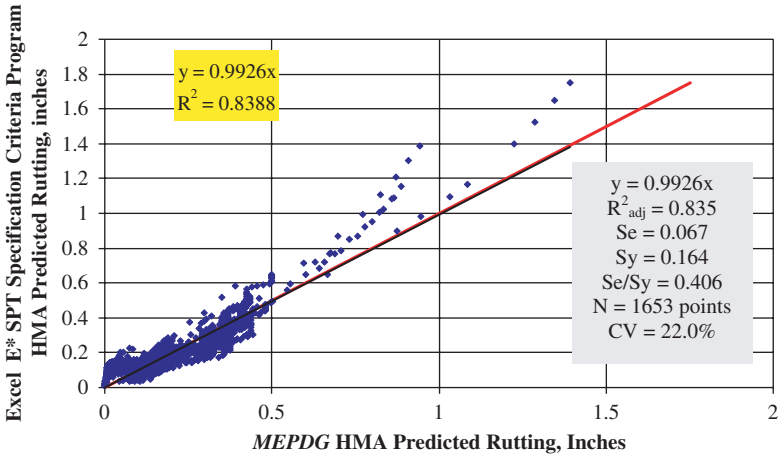

Figure 2-10. Comparison between MEPDG and E* SPT Specification Criteria Program rutting predictions for validation study sections with field-measured data.

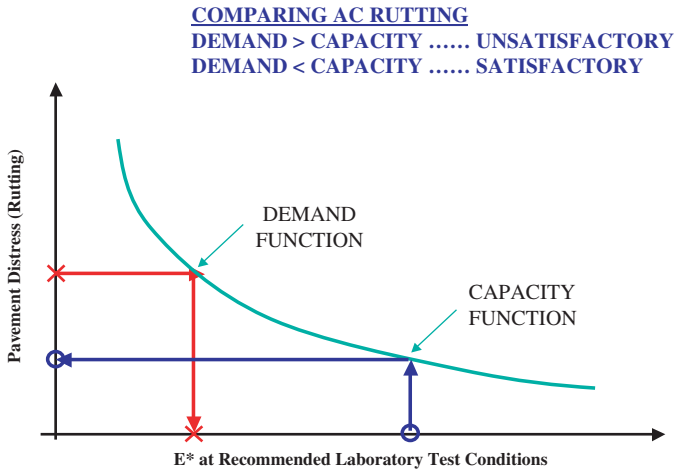

Figure 2-11. System demand versus system capacity comparison.

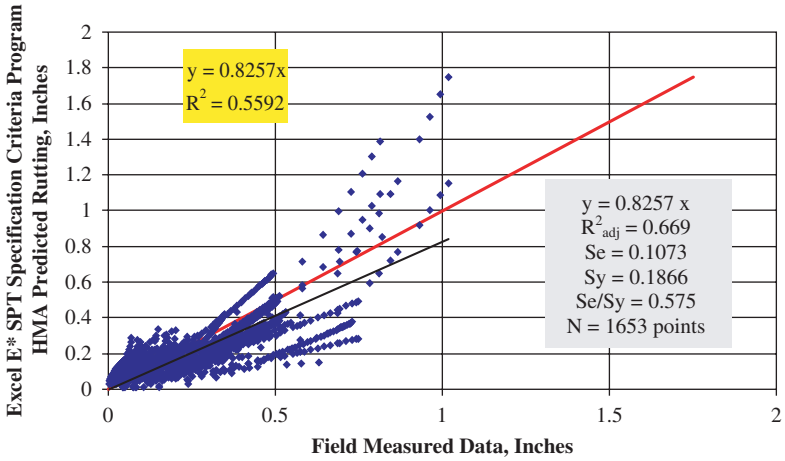

Figure 2-12. System demand (field-measured rutting data) versus system capacity (E SPT Specification Criteria Program rutting predictions) comparison for LTPP, MnRoad, WesTrack, FHWA-ALF, and NCAT sections with regional calibration approach applied.*

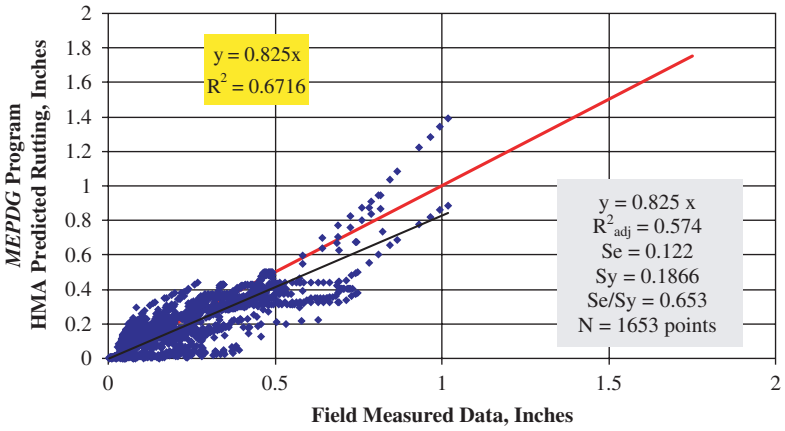

Figure 2-13. Field-measured rutting data versus MEPDG comparison for LTPP, MnRoad, WesTrack, FHWA-ALF, and NCAT sections with regional calibration approach applied.

Section 3.9 of Reference 2 shows that the MEPDG predicted the field-measured data (once regionally calibrated) with an R^2_{adj} equal to 0.672. By comparison, Figure 2-12 indicates that the R^2_{adj} equals 0.669. This small difference is mainly due to a change in traffic characterization for the LTPP sections. For the comparison in Reference 2, the axle load spectra approach was used, while here the results with the ESAL approach are necessary because the spreadsheet solution must be analyzed using ESALs and not axle load spectra results.

The decrease between R^2_{adj} equals 0.669 and S_e equals 0.1073 inches for the MEPDG and R^2_{adj} equals 0.574 and S_e equals 0.122 inches can be considered minor for the simplifications performed. When the data were analyzed per site/mix type, the following comparison based on S_e was obtained:

OVERALL	$Se_{MEPDG} = 0.107$	$Se_{EXCEL} = 0.122$	$Sy = 0.186$
LTPP	$Se_{MEPDG} = 0.081$	$Se_{EXCEL} = 0.078$	$Sy = 0.116$
MnRoad (L)	$Se_{MEPDG} = 0.107$	$Se_{EXCEL} = 0.114$	$Sy = 0.113$
MnRoad (P)	$Se_{MEPDG} = 0.087$	$Se_{EXCEL} = 0.093$	$Sy = 0.094$
WesTrack (L)	$Se_{MEPDG} = 0.190$	$Se_{EXCEL} = 0.233$	$Sy = 0.163$
WesTrack (P)	$Se_{MEPDG} = 0.129$	$Se_{EXCEL} = 0.138$	$Sy = 0.138$
FHWA-ALF (L)	$Se_{MEPDG} = 0.183$	$Se_{EXCEL} = 0.182$	$Sy = 0.283$
FHWA-ALF (C)	$Se_{MEPDG} = 0.193$	$Se_{EXCEL} = 0.328$	$Sy = 0.283$
NCAT (P)	$Se_{MEPDG} = 0.062$	$Se_{EXCEL} = 0.078$	$Sy = 0.057$

NOTE: L = laboratory mix, P = plant mix, and C = cores.

It is clear that the S_e values increased slightly for all combinations in various degrees, with the greatest effect in the FHWA-ALF sections evaluated with field sample cores and the WesTrack sections evaluated with lab blended mixes. For the majority of cases, this S_e increase can be attributed mainly to the intrinsic error between the Excel program and the MEPDG, and also to the summer-winter effect that is handled differently in the two programs.

For example, the comparison of the measured data versus the MEPDG and the Excel predictions for the NCAT sections is presented in Figure 2-14. Values for both prediction sources are quite close; however, the path to reach those values is different, with a stair-step trend for the MEPDG and a straight-line increase for the spreadsheet program.

Nevertheless, the overall conclusion is that the spreadsheet program provides results that are quite close to those provided by the MEPDG (as expected and desired), giving credence to the predictive capabilities of the E* SPT Specification Criteria Program.

The next step was to perform comparisons using the predicted effective E* versus the critical E*. Theses results did not provide as good a trend as the system demand versus system capacity had shown, but the critical E* was found to be within 100 ksi and 1000 ksi of the effective E* for all of the studied cases. The final critical E* value depends on many factors, the most important of which are

- Region of study (the hotter the site, the higher E* required); and
- HMA total thickness and related critical depth (the deeper the critical depth, the higher the critical E*).

Figure 2-15 compares the resultant predicted versus the critical (threshold) E*. As shown, there are two significant (and unsatisfactory) outliers in the plot. These outliers developed from the conditions of the project falling outside the range of the project's universal E* versus rut depth relationship (UR), a situation that would only occur when

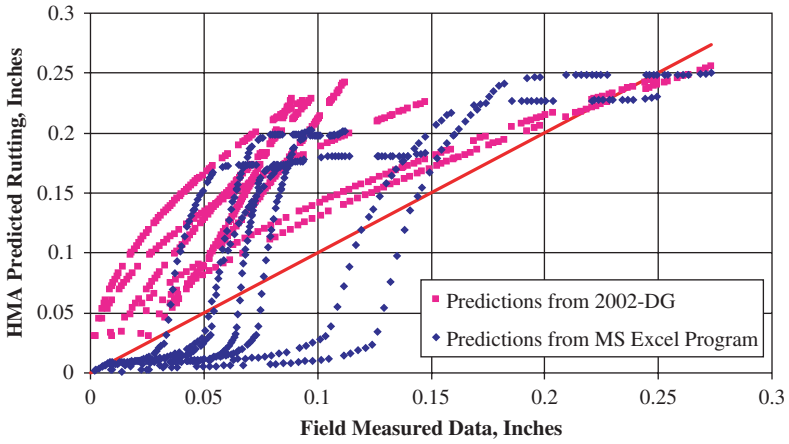

Figure 2-14. Comparison of field-measured rutting data versus predicted data by source for NCAT sections with regional calibration approach applied.

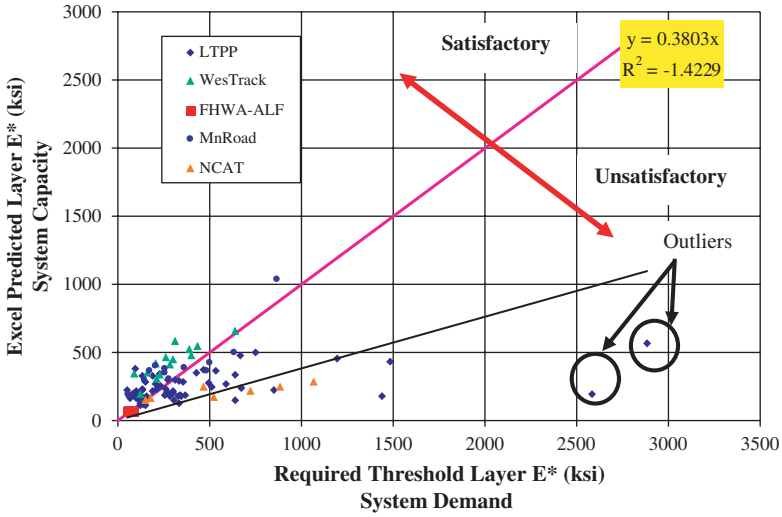

Figure 2-15. E* associated with system demand (Critical E*) versus E* associated with system capacity (criteria program Predicted E*) comparison for LTPP and NCHRP Project 9-19 sections—full database.

1. The mix placed in the field was extremely stiff (stiffer than a conventional dense graded PG 82-10 mix) or extremely soft (softer than the corresponding PG 52-40 mix), or
2. The RFC was too strict (extremely low rutting value compared to what the structure/mix design can withstand) or too relaxed (a rutting value much higher than the structure/mix design would possibly reach).

For this study, a strict RFC was used (i.e., the actual measured rutting appeared to be below what the spreadsheet program expected). In this case, the UR would have to be extrapolated, giving rise to the two severe outliers. In fact, evaluating the required threshold values (X-axis), it was found that extrapolations because of strict RFC occurred when the E* values were required to be higher than 800 ksi. Thus, special care should be taken care when looking at such values.

Figure 2-16 shows how the predicted versus critical (threshold) E* graphical comparison would appear without the extrapolated sections. The correlation is closer to y is equal to x (y = 0.7851 x), although the variability is high, which is understandable because of the various conditions of the sections used in the study.

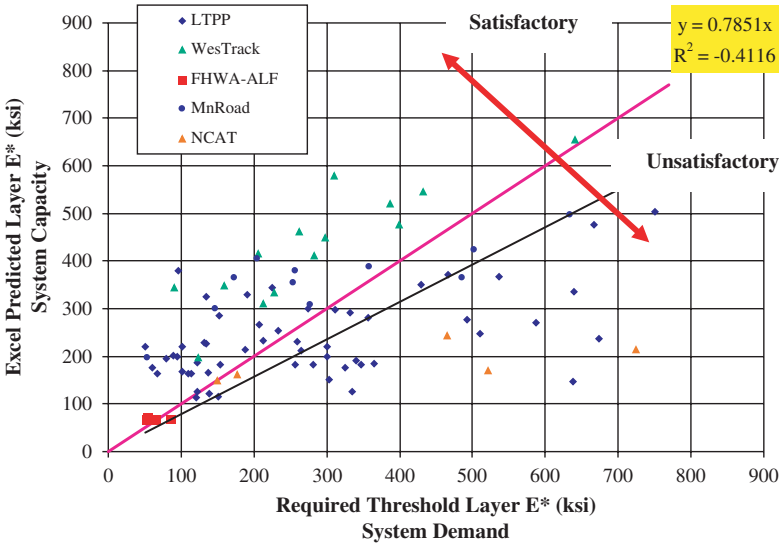

Figure 2-16. E* associated with system demand (Critical E*) versus E* associated with system capacity (criteria program Predicted E*) comparison for LTPP and NCHRP Project 9-19 sections—database without extrapolated sections.

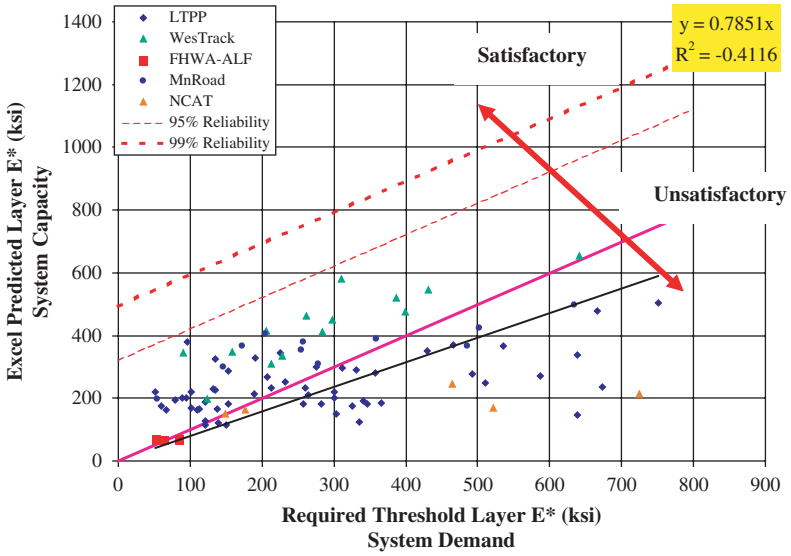

Figure 2-17. Reliability levels on comparison between Critical E* (associated with system demand) and Predicted E* (associated with system capacity).

Overall, the following conclusions can be drawn from this E* comparison study:

1. The UR covers a wide range of mix/structural conditions and provides results (between 50 and 800 ksi for E* values) that meet the test of engineering reasonableness, and
2. When the UR does not cover the mix/structural combination proposed, it may become quite unreliable, yielding E* greater than 800 ksi.

Fortunately, Figure 2-17 suggests that most mix/structural combined designs will fall within the developed universal rut depth-E* relationship if extrapolations are not to be performed.

2.2 General Conclusion from the Validation Studies

The good trends shown by the comparison between system demand and capacity, the realistic E* values obtained as critical E*, as well as the good correlations between MEPDG predictions and the spreadsheet program predictions reinforce the conclusion that E* can be used as a Superpave SPT using the implementation program developed here, along with the MEPDG regional calibration factor approach developed and implemented in this study and described in Reference 2.

Mode 2 rutting predictions are based on the universal E* versus rut depth relationships developed in this research study. This universal relationship is based on (1) E* values calculated from the effective temperature and loading frequency explained in Chapter 3 of Reference 2, and (2) rutting values obtained from the MEPDG. The correlations between the E* SPT Specification Criteria Program and the MEPDG range from fair to excellent ($R^2_{adj} > 0.49$ at least), allowing the conclusion that using E* is appropriate to predict rutting performance.

Problems with correlation with field-measured data are not related to the E* calculation, but on the original rutting data used for the universal relationship (i.e., the MEPDG methodology). Although the regional calibration factor approach has improved the correlations greatly (from very poor with the national calibration to $R^2_{adj} = 0.728$ when LTPP and NCHRP Project 9-19 sections were evaluated), future versions of the MEPDG software will need to make improvements in several areas. For example, a better summer-winter effect characterization needs to be implemented, as well as a better rutting prediction mechanism for rut predictions between different HMA thickness ranges. If these problems are solved, the correlations between the MEPDG and the E* SPT Specification Criteria Program may be greatly improved, making E* an even stronger SPT.

Thus, it is concluded that the E* SPT Specification Criteria Program, developed as an Excel spreadsheet, can be used to implement E* as a simple performance test for rutting.

CHAPTER 3

E* SPT Specification Criteria Program User Guide

This chapter presents a concise user guide for the E* SPT Specification Criteria Program. The program is available in two formats: (1) a spreadsheet-based program running in Excel and (2) a Microsoft Windows-based, stand-alone program written in C++ programming language. The user guide presented here applies to either version. The chapter also provides illustrative examples covering several common situations.

3.1 Receiving User Information—Input

3.1.1 Selection of Program Mode and Option

The user is first required to provide project information within several spreadsheets. Figure 3-1 shows the initial Welcome Worksheet. In this worksheet, the user selects the mode (described in Chapter 1) and E* data input option combination. The *Option* selection designates the source of the E* data for each HMA layer as follows:

- Option 1, use laboratory-measured values for all HMA mixes and layers;
- Option 2, use sigmoidal master curve coefficients for all HMA mixes and layers;
- Option 3, use Witczak predictive equation (WPE) with job mix formula data for all HMA mixes and layers; and
- Option 4, use any combination of Options 1, 2, or 3 for the HMA layers.

The program can handle 12 combinations of mode and option, as presented in the mode-option table in the Welcome Worksheet. These combinations are

- A: Mode 2 and Option 1,
- B: Mode 2 and Option 2,
- C: Mode 2 and Option 3,
- D: Mode 2 and Option 4,
- E: Mode 3 and Option 1,
- F: Mode 3 and Option 2,
- G: Mode 3 and Option 3,
- H: Mode 3 and Option 4,
- I: Mode 4 and Option 1,
- J: Mode 4 and Option 2,
- K: Mode 4 and Option 3, and
- L: Mode 4 and Option 4.

Choosing the desired option selects the next set of worksheets. For example, if Combination D (Mode 2 and Option 4) is selected in the table and placed in the yellow cell shown in Figure 3-1, then the title in the User Input Worksheet changes to Mode 2 (Figure 3-2a). Similarly, the three worksheets shown in Figures 3-2b and 3-3 are now titled Option 4 and permit the use of a combination of laboratory-measured E* values (Option 1) or E* values calculated with sigmoidal master curve coefficients or job mix formula data (Options 2 and 3, respectively) for the various HMA layers.

If the combination selected had been E instead of D (Mode 3 and Option 1), Figures 3-2 and 3-3 would change as shown in Figures 3-4 and 3-5. In Figure 3-4a, the title is changed to "Mode 3 = E* as a SPT (Simple Performance Test)." In Figure 3-4b, the title changes to "Option 1 Dynamic Modulus Laboratory Measurement Input Worksheet."

Changes in the E* input option also update the Layer Label ID cells and their color code. In the example shown in Figures 3-2 and 3-3 for Mode-Option Combination D, two HMA layers are used (labeled *top* and *bottom*); the WPE is used to calculate E* for the top layer, and laboratory-measured E* values are used for the bottom layer. Thus, in Figure 3-2b, the Layer Label ID for the top layer is off and color-coded red (i.e., data cannot be input), while for the bottom layer it is on and color-coded yellow (i.e., data must be input). In Figure 3-3, the Layer Label IDs for both layers

E* IMPLEMENTATION PROGRAM Version 1.0 (August 15, 2005)

Developed By

Andres Sotil, Graduate Research Assistant

Under the Guidance of

Dr. Matthew W. Witczak, Professor

ARIZONA STATE UNIVERSITY

Sponsored By

NCHRP

ADOT

WELCOME!!!

The following MS Excel Spreadsheet has been designed to help you in your Mix and/or Structural Design. You have the capability of using the program for Asphalt Mix Design, only for Quality Control and Assurance during your project construction, and also for simultaneous Asphalt Mix and Structural Each different use represents what is called a **MODE.** The following list shows the 4 MODES identified by the Research Team:

MODE 1 = M-E 2002-DG fully implemented (Not Possible in the MS Excel Program).
MODE 2 = Simultaneous Asphalt Mix and Pavement Structural Design (MODE 1 Shortcut).
MODE 3 = Asphalt Mix Design Only
MODE 4 = Quality Control and Assurance Process Only

For this MS Excel Spreadsheet, it is required that you input the material characteristics of your asphalt mixes. Your have 4 different options to do it.

OPTION 1 = Use Laboratory Measured E* Values for all the Mixes
OPTION 2 = Use Sigmoidal Master Curve Coefficients for all the Mixes
OPTION 3 = Use Job Mix Formula for all the Mixes (Witczak E* Predictive Equation)
OPTION 4 = Allow Combination of Option 1, 2, and 3 according to Engineer's input

Please, select what condition you require:
Indicate the letter from A to P that produces your desired combination: D

OPTION \ MODE	1	2	3	4
1		A	E	I
2		B	F	J
3		C	G	K
4		D	H	L

Figure 3-1. E SPT Specification Criteria Program Welcome Worksheet.*

(a)

MODE 2 = E * AS MIX / STRUCTURAL DESIGN TOOL

Please Locate Your Input in these Cells	All current values are just examples
Do not Input Data in these Cells	No values should be placed in these cells

PROJECT GENERAL INPUT DATA

Project ID =	Example 1
Project Location =	Anytown, US
Date of Analysis =	9/25/2005
Operator's Name =	Andres Sotil

DESIGN SPECIFIED TOTAL AC RUTTING

Rutting Criteria (in) =	0.35

PROJECT TRAFFIC AND CLIMATIC CONDITIONS

Design Average Speed (mph) =	60
Design Total Traffic (ESALs) =	7,500,000

Mean Annual Air Temperature (oF) =	48.1
Mean Monthly Air Temp St. Dev. (oF) =	15.0
Mean Annual Wind Speed (mph) =	5.0
Mean Annual Sunshine (%) =	69.0
Annual Cumulative Rainfall Depth (in) =	44.0

(b)

OPTION 4 DYNAMIC MODULUS LABORATORY MEASUREMENT INPUT WORKSHEET

INSTRUCTIONS: PLEASE INPUT DYNAMIC MODULUS VALUES IN YELLOW TABLE. THEN RUN SOLVER AS IT IS GIVEN AND YOUR RESULTS WILL BE THE ONES IN TABLE A. MORE INSTRUCTIONS BELOW

Bottom		
Temp. (oF)	Freq. (Hz)	E* (10^6 psi)
14.0	25	2.841
14.0	10	2.667
14.0	5	2.531

OPTIMIZED NUMBER =	0.0000
RUN SOLVER TO PROVIDE YOUR RESULTS	
Σ e2 =	0.0127
Σ e =	-0.0003

Figure 3-2. User Input and Option Input Worksheets for Mode-Option Combination D.

OPTION 4 INPUT THE SIGMOIDAL MASTER CURVE PARAMETERS FOR CORRESPONDING MIXES

Sigmoidal Function Parameters	δ			
	α			
	γ			
	β			
Shift Factors Polynomial Coefficients	Constant			
	X-value			
	X^2-value			

OPTION 4 INPUT THE JOB MIX FORMULA FOR CORRESPONDING MIXES

								Binder Characterization ***		
Layer Label ID	Target Air Voids (%)	Effective Binder (%)	Ret. 3/4"	Ret. 3/8"	Ret. No.4	Pass. No.200	Enter 1 or 2	Type of Binder (PG)	A	VTS
Top	5	7	0	25.6	51.8	4.2	2		11.787	-3.981

*** Choose the Type of Binder Characterization: (1) Type of Binder (2) A and VTS

Figure 3-3. Master Curve and Job Mix Formula Input Worksheets for Mode-Option Combination D.

are off and color-coded red as the E* values are calculated rather than input by the user.

The example in Figures 3-4 and 3-5 shows the worksheets presented when the user chooses a mode-option combination that includes Option 1 (A, E, or I). The Layer Label IDs turn on for both the top and bottom layers, indicating that the user must input laboratory-measured E* values for both layers. In Figure 3-5, the title for each table changes to "Go To Option 1," indicating to the user that the corresponding tables do not require data as the E* values will not be calculated from other material properties.

Another change that occurs between Combinations D and E is seen by comparing Figures 3-2b and Figure 3-4b. In Figure 3-2b, a numeric value appears in the green cell labeled *Optimized Number* =, while in Figure 3-4b, the cell contains the error warning #!VALUE!. This error value appears because the program is expecting E* laboratory data for both layers. However, as can be seen, only data for the bottom layer are available, and a division-by-zero-error is declared.

Another possible scenario involves selecting either Option 2 or 3. Such changes, regardless of the corresponding mode, would result in a change in the Option Worksheet, as shown

(a)

MODE 3 = E* AS A SPT (SIMPLE PERFORMANCE TEST)

Please Locate Your Input in these Cells	All current values are just examples
Do not Input Data in these Cells	No values should be placed in these cells

PROJECT GENERAL INPUT DATA

Project ID =	Example 1
Project Location =	Anytown, US
Date of Analysis =	6/5/2007
Operator's Name =	Andres Sotil

DESIGN SPECIFIED TOTAL AC RUTTING

Rutting Criteria (in) =	0.350

PROJECT TRAFFIC AND CLIMATIC CONDITIONS

Design Average Speed (mph) =	60
Design Total Traffic (ESALs) =	7,500,000

Mean Annual Air Temperature (oF) =	48.1
Mean Monthly Air Temp St. Dev. (oF) =	15.0
Mean Annual Wind Speed (mph) =	5.0
Mean Annual Sunshine (%) =	69.0
Annual Cumulative Rainfall Depth (in) =	44.0

(b)

OPTION 1 DYNAMIC MODULUS LABORATORY MEASUREMENT INPUT WORKSHEET

INSTRUCTIONS: PLEASE INPUT DYNAMIC MODULUS VALUES IN YELLOW TABLE. THEN RUN SOLVER AS IT IS GIVEN AND YOUR RESULTS WILL BE THE ONES IN TABLE A. MORE INSTRUCTIONS BELOW

Top			Bottom					
Temp. (oF)	Freq. (Hz)	E* (10^6 psi)	Temp. (oF)	Freq. (Hz)	E* (10^6 psi)			
			14	25	2.841			
			14	10	2.667			
			14	5	2.531			

OPTIMIZED NUMBER =	#VALUE!
RUN SOLVER TO PROVIDE YOUR RESULTS	
Σ e2 =	#VALUE!
Σ e =	#VALUE!

Figure 3-4. User Input and Option Worksheets for Mode-Option Combination E.

GO TO OPTION 1

Sigmoidal Function Parameters	δ			
	α			
	γ			
	β			
Shift Factors Polynomial Coefficients	Constant			
	X-value			
	X^2-value			

GO TO OPTION 1

								Binder Characterization ***		
Layer Label ID	Target Air Voids (%)	Effective Binder (%)	Ret. 3/4"	Ret. 3/8"	Ret. No.4	Pass. No.200	Enter 1 or 2	Type of Binder (PG)	A	VTS
	5	7	0	25.6	51.8	4.2	2		11.787	-3.981

*** Choose the Type of Binder Characterization: (1) Type of Binder (2) A and VTS

Figure 3-5. Master Curve and Job Mix Formula Input Worksheets for Mode-Option Combination E.

in Figures 3-6a and 3-6b for Option 2 and 3, respectively. The active option worksheets for Options 2 and 3 are shown in Figures 3-7 and 3-8, respectively.

The program is designed to lead the user to the appropriate tables for the selected mode-option combination. For example, in Figure 3-6a the user is instructed to go to Option 2. In both Figures 3-6a and 3-6b, the Layer Label IDs are turned off and color-coded red, indicating that data cannot be input by the user.

In the same way, Figure 3-7 shows that the program will provide the appropriate title for Option 2 and refer the user in the Option 3 table to the appropriate one (Go To Option 2). In Figure 3-8 the table titles are reversed, as well as the color coding of the cells, indicating that the user should go to Option 3. Thus, the Layer Label IDs and colors change according to the user selection, turning on and off as the input option is varied.

It is important to understand how the data are handled by the program when options are changed. For example, in Figure 3-7, the program requests data in the upper Option 2 table (the Layer Label ID is on for both layers). If no data are provided in the output worksheets, error messages will appear. In the same figure, data are available in the Option 3 table (left for purposes of this example). The program will not use these data, and leaving them there will not affect the final calculations. Only missing data, where the program is expecting input (layer labels are on and color-coded yellow), will produce error values like the one shown in Figure 3-4b.

(a) Option 2 Selected

GO TO OPTION 2

DO NOT USE THIS WORKSHEET
DO NOT USE THIS WORKSHEET

			14.0 14.0	25 10	2.841 2.667			

(b) Option 3 Selected

GO TO OPTION 3

DO NOT USE THIS WORKSHEET
DO NOT USE THIS WORKSHEET

			14.0 14.0	25 10	2.841 2.667			

Figure 3-6. Option worksheets for an option selection different than 1.

OPTION 2 INPUT THE SIGMOIDAL MASTER CURVE PARAMETERS FOR CORRESPONDING MIXES

		Top	Bottom	
Sigmoidal Function Parameters	δ			
	α			
	γ			
	β			
Shift Factors Polynomial Coefficients	Constant			
	X-value			
	X^2-value			

GO TO OPTION 2

								Binder Characterization ***		
Layer Label ID	Target Air Voids (%)	Effective Binder (%)	Ret. 3/4"	Ret. 3/8"	Ret. No.4	Pass. No.200	Enter 1 or 2	Type of Binder (PG)	A	VTS
	5	7	0	25.6	51.8	4.2	2		11.787	-3.981

*** Choose the Type of Binder Characterization: (1) Type of Binder (2) A and VTS

Figure 3-7. Option 2-3 Worksheets for selection of Option 2.

Finally, the selection of the mode-option combination will also turn on and off the appropriate output worksheet.

3.1.2 General Project Input Data

Information about the project location and ID, the date of the analysis, and name of the user are optional cells that can be filled out for proper control of a project. No restrictions are placed on the cells, and the values provided by the user are repeated in the output worksheets.

3.1.3 Rutting Failure Criterion (RFC)

An input cell is provided for entry of an RFC for the entire HMA structure (see Figure 3-9). The program accepts numeric values greater than zero, with guidance that a normal HMA layer RFC will generally range from 0.2 to 0.5 inches.

3.1.4 Traffic and Environmental (Climatic) Characteristics

The program accepts positive numeric values for the traffic and climatic input variables. None of the 900 climatic sites contained in the MEPDG climatic database have a MAAT below 0° F (the lowest temperature for a site was approximately 10° F). Similar to the RFC, the program provides suggestions for the average traffic speed, indicating that it may be between 0.5 to 60.0 mph.

3.1.5 Structural Characteristics

The program is limited to the analysis of no more than three different HMA layers: surface or wearing course, intermediate or binder course, and bottom or base course.

GO TO OPTION 3

Sigmoidal Function Parameters	δ			
	α			
	γ			
	β			
Shift Factors Polynomial Coefficients	Constant			
	X-value			
	X^2-value			

OPTION 3 INPUT THE JOB MIX FORMULA FOR CORRESPONDING MIXES

								Binder Characterization ***		
Layer Label ID	Target Air Voids (%)	Effective Binder (%)	Ret. 3/4"	Ret. 3/8"	Ret. No.4	Pass. No.200	Enter 1 or 2	Type of Binder (PG)	A	VTS
Top	5	7	0	25.6	51.8	4.2	2		1 1.787	-3.981
Bottom										

*** Choose the Type of Binder Characterization: (1) Type of Binder (2) A and VTS

Figure 3-8. Option 2-3 Worksheets for selection of Option 3.

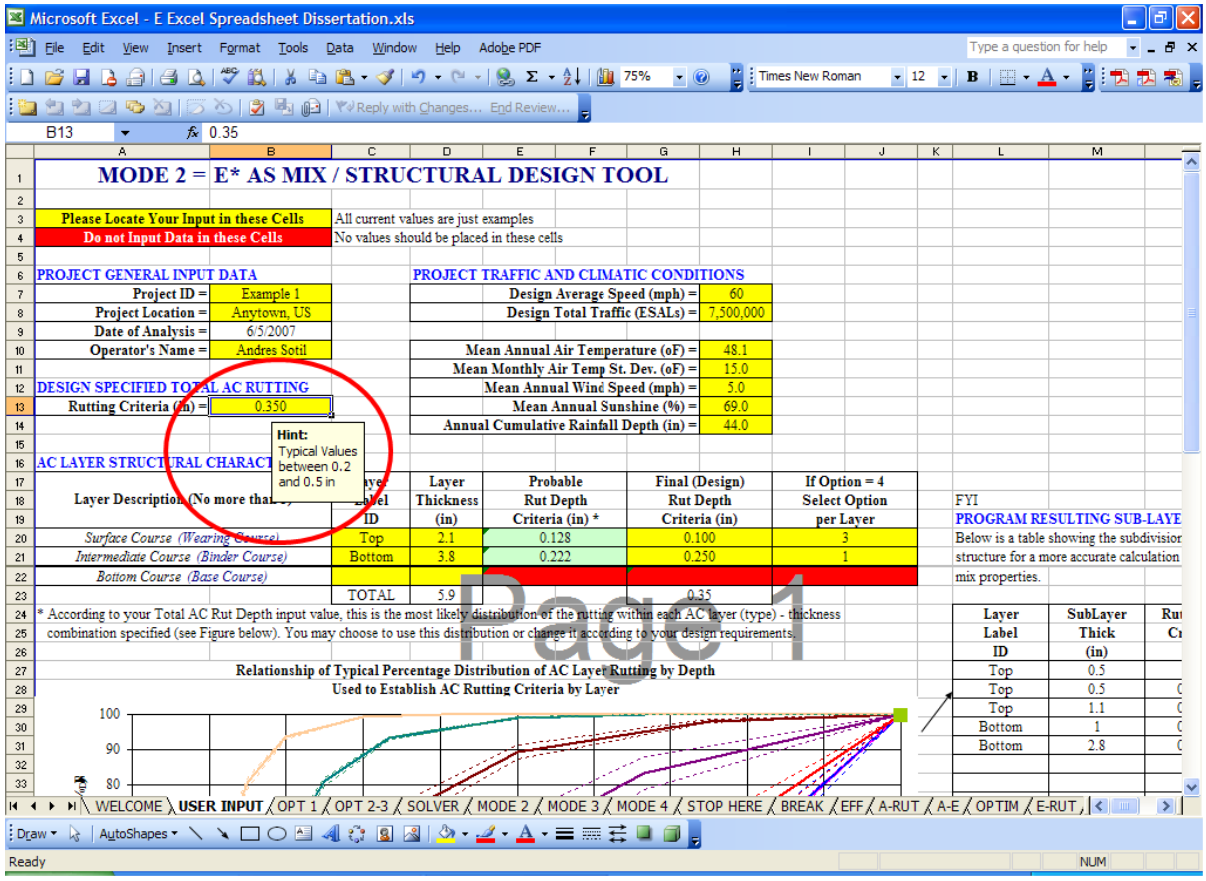

Figure 3-9. Rutting failure criteria.

The asphalt concrete (AC) layer structural characteristics section provides the space required for the input of the necessary structural data. Each layer receives an AC Layer Label ID, which is an alphanumeric value of no more than 10 characters (see Figure 3-10a).

The thickness of each layer is entered next. A screen message points out that the program cannot analyze an HMA layer thickness value less than 1 inch (see Figure 3-10b).

The next two input columns correspond to the layer RFC values. In the column for *Probable Rut Depth Criteria (Inches)*, the program suggests a subdivision of the total HMA structure RFC. In the column for *Final (Design) Rut Depth Criteria*, the user can either accept the proposed subdivision or modify these values with non-negative values (see Figure 3-10c).

The last column is available only when Option 4 is selected; it permits the selection of different options for different layers. A message related to this condition is provided as an aid to the user (see Figure 3-10d). The only acceptable input values are 1, 2, and 3.

3.1.6 Understanding Available Charts and Tables in the User Input Worksheet

The following three examples illustrate the use of the plot and table provided in the User Input Worksheet:

Example 1:
Layer A = 3.5 inches
Layer B = 4.2 inches
Structure RFC = 0.5 inches

Example 2:
Layer Full = 5.6 inches
Structure RFC = 0.3 inches

Example 3:
Layer Top = 1.8 inches
Layer Medium = 3.4 inches
Layer Bottom = 6 inches
Structure RFC = 0.45 inches

The rut depth versus HMA thickness distribution relationship for Examples 1, 2, and 3 is presented in Figures 3-11, 3-12, and 3-13, respectively. Similarly, Tables 3-1a, 3-1b, and 3-1c are the output of the E* SPT Specification Criteria Program based upon user input of the required information for Examples 1, 2, and 3, respectively.

3.1.6.1 Results for Example 1

Figure 3-11 illustrates the distribution of rut depth versus HMA thickness for seven of the standard HMA structures contained in the program's database. The heavy dashed line

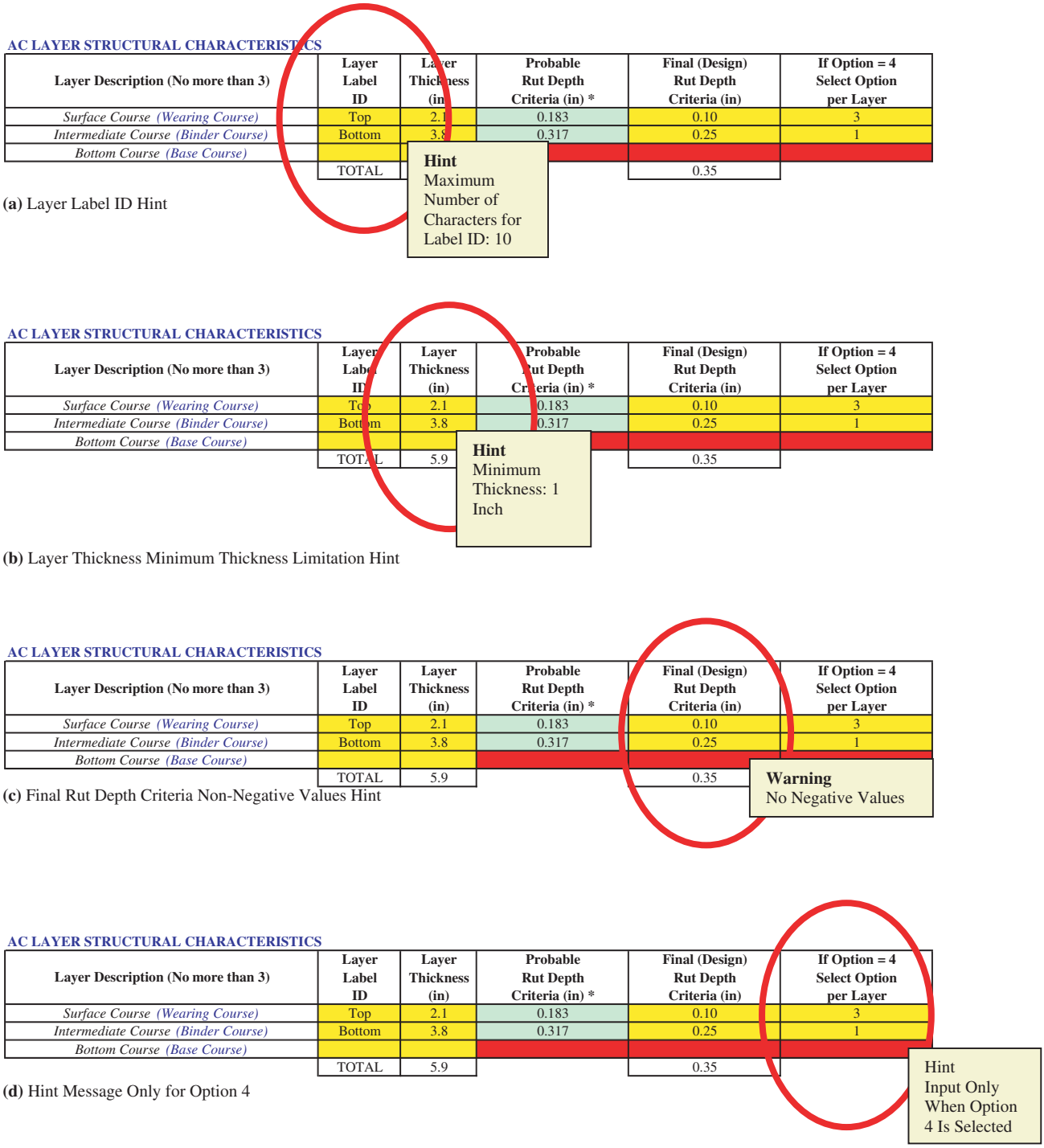

Figure 3-10. HMA layer structural characteristics.

in Figure 3-11 shows the distribution of HMA layer rutting in the 7.7-inch-thick example structure (labeled *Your Structure*) estimated by interpolation between the relationships for the 6- and 9-inch standard structures.

Since the total HMA thickness is 7.7 inches, 7.7 inches is represented by 100% on the X-axis. The corresponding RFC input by the user is 100% on the Y-axis.

The structure is then subdivided into two layers. The first HMA layer has a thickness of 3.5 inches, which represents 45% of the total HMA layer thickness (X-axis). By interpolation, this thickness percentage is estimated to yield approximately 80% total HMA rut depth. Therefore, the first 3.5-inch layer will have 80% of the total rutting within the HMA, while the remaining 4.2-inch layer will only contribute 20% of the total rutting.

For more accurate results, the layers provided by the user are subdivided as shown in Table 3-1a. Thus, for this example, the first layer (3.5 inches) was subdivided into four sublayers

$$0.5 + 0.5 + 1.0 + 1.5 = 3.5 \text{ inches}$$

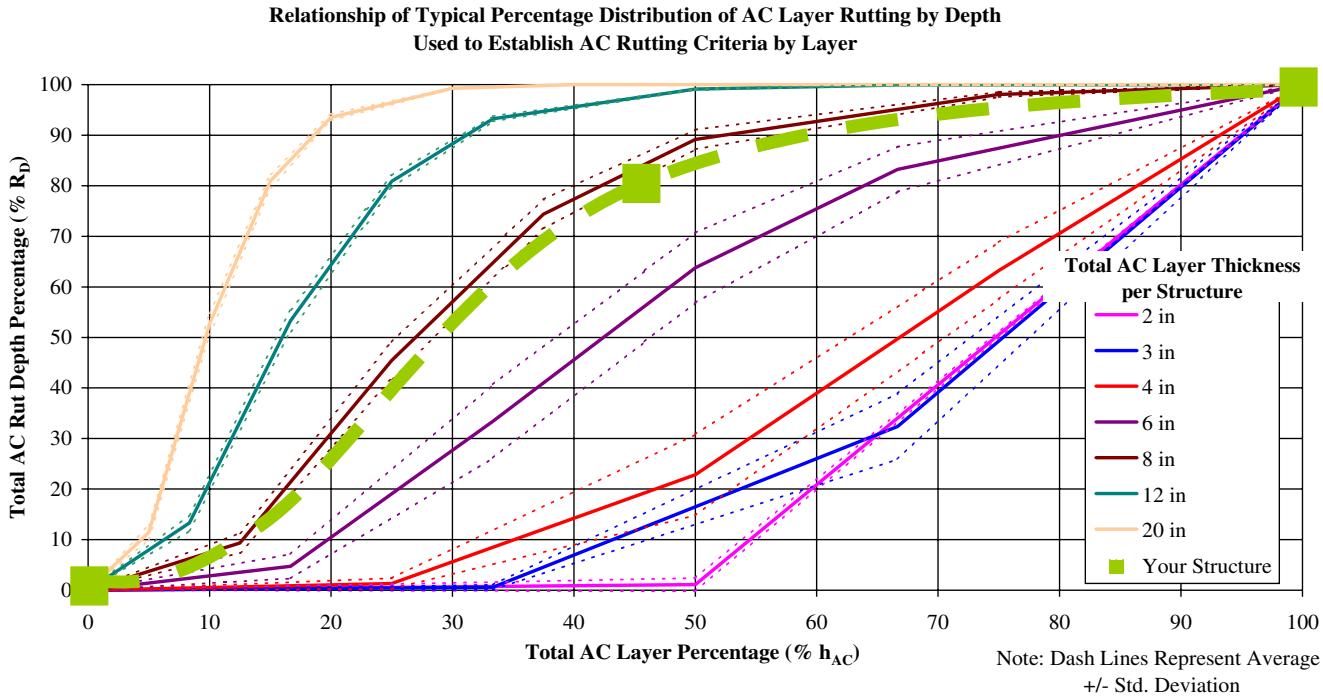

Figure 3-11. Rut depth versus HMA thickness distribution relationship—Example 1.

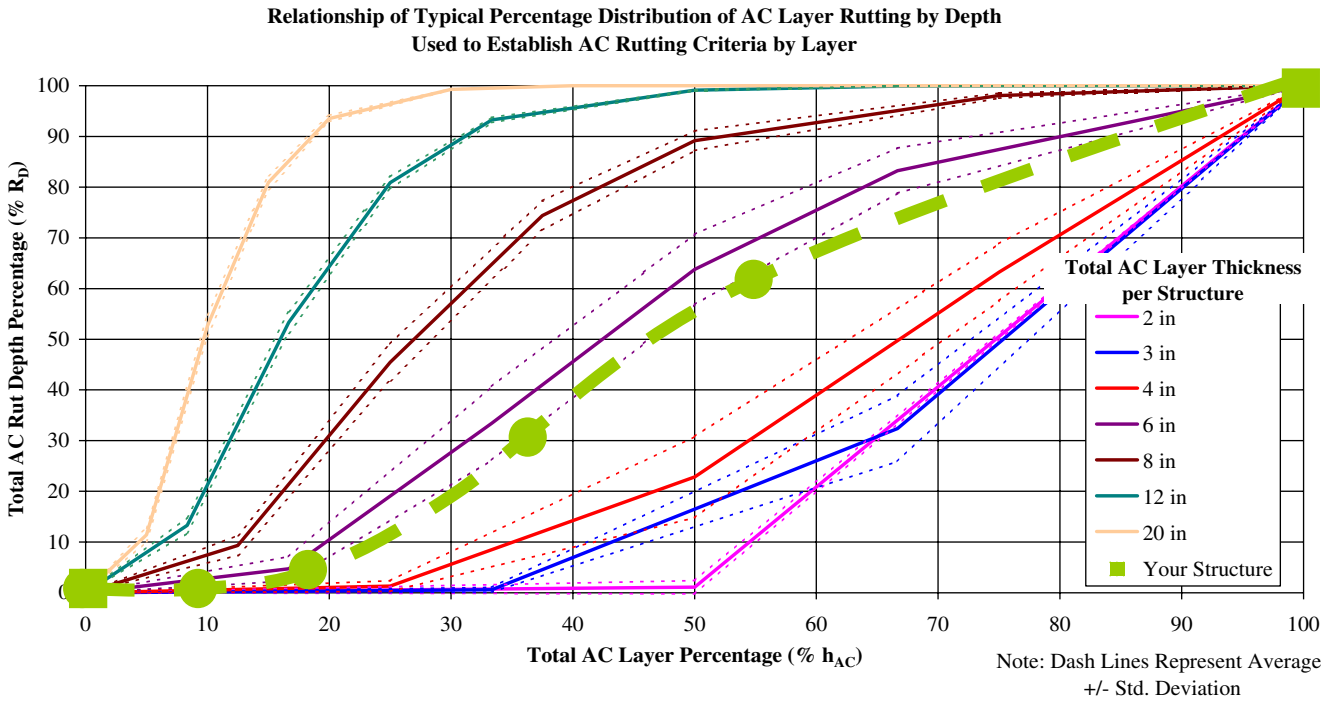

Figure 3-12. Rut depth versus HMA thickness distribution relationship—Example 2.

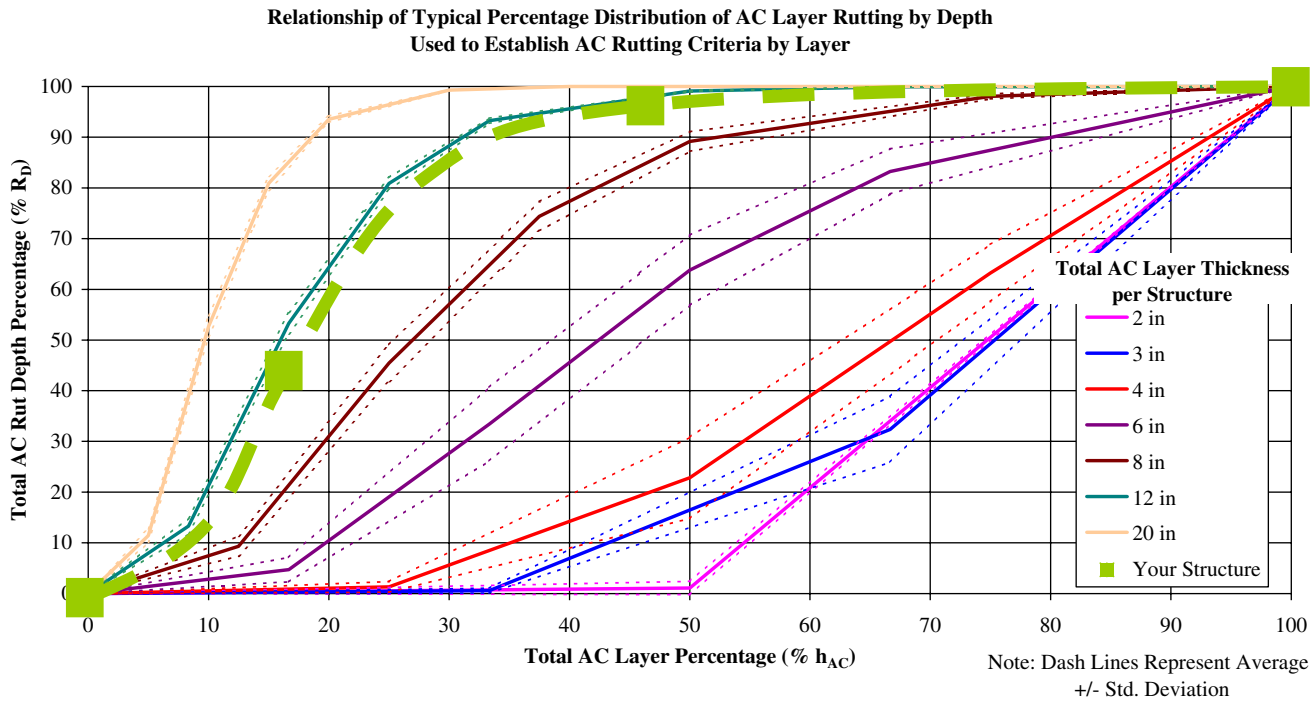

Figure 3-13. Rut depth versus HMA thickness distribution relationship—Example 3.

Table 3-1. Resulting sublayering for examples provided.

FYI
PROGRAM RESULTING SUB-LAYERING
Below is a table showing the subdivision of your structure for a more accurate calculation of your mix properties.

(a) Example 1

Layer Label ID	SubLayer Thick (in)	Rut Depth Criteria (in)
A	0.5	0.00
A	0.5	0.04
A	1	0.18
A	1.5	0.18
B	1	0.05
B	3.2	0.05

(b) Example 2

Layer Label ID	SubLayer Thick (in)	Rut Depth Criteria (in)
FULL	0.5	0.00
FULL	0.5	0.01
FULL	1	0.08
FULL	1	0.10
FULL	2.6	0.11

(c) Example 3

Layer Label ID	SubLayer Thick (in)	Rut Depth Criteria (in)
TOP	0.5	0.00
TOP	1.3	0.20
MEDIUM	1	0.14
MEDIUM	1	0.07
MEDIUM	1.4	0.03
BOTTOM	2	0.01
BOTTOM	4	0.00

The corresponding sublayer RFC from the structure RFC of 0.5 inches was

0 + 0.04 + 0.18 + 0.18 = 0.40 inches

This yields 80% (0.4/0.5) of total RFC in the first layer. The second layer was divided into two sublayers

1.0 + 3.2 = 4.2 inches

The sublayer RFC was

0.05 + 0.05 = 0.10

This yields 20% of the total rutting (0.1/0.5).

3.1.6.2 Results for Example 2

The rut depth versus HMA thickness distribution for the desired structure is shown in Figure 3-12. With a total HMA thickness of 5.6 inches, a distribution between 4 to 6 inches is used.

The dashed, curved line shown in Figure 3-12 represents the approximate distribution of HMA layer rutting in the example structure. Since the total thickness is 5.6 inches, 5.6 is represented by 100% on the X-axis. The user inputs a corresponding RFC of 100% on the Y-axis.

For this structure, there is only one layer available and only the 0% and 100% square dot will appear. However, the points in between will be used for the sublayer RFC calculations, as shown in Table 3-1b. To help explain this table, circular dots have been placed on Figure 3-12, along the dashed, curved line assumed for the 5.6-inch structure.

The subdivision of the total 5.6 inches is shown in Table 3-1b. The structure was divided into five sublayers as follows:

0.5 + 0.5 + 1.0 + 1.0 + 2.6 = 5.6 inches

The corresponding division of the sublayer RFC (using the total HMA structure RFC of 0.3 inches) is

0.0 + 0.01 + 0.08 + 0.10 + 0.11 = 0.30 inches

For the first sublayer of 0.5 inches, the rutting will be zero. This is a direct consequence of the derivation of the solutions from the MEPDG. The next 0.5 inches is estimated to contribute 3.33% (0.01 of 0.30 inches); followed by the third sublayer with 26.67% of the total RFC (0.08/0.30). The RFC of the last two sublayers is subdivided as 33.33% and 36.67% with 0.10/ 0.30 and 0.11/0.30 inches of rutting, respectively. The cumulative percentages per layer are represented in Figure 3-12 by the squares and dots.

3.1.6.3 Results for Example 3

In this final example, the desired structure was subdivided into three sublayers: 1.8, 3.4, and 6.0 inches in thickness. The total 11.2 inches represent 100% HMA thickness (X-axis), and an RFC of 0.45 represents 100% HMA rut depth (Y-axis).

As shown in Figure 3-13, the first layer represents 1.8/11.2, or 16% of the total thickness. Plotting that value on the resulting heavy dashed line between the 8- and 12-inch structures shows that approximately 45% of the rutting for that structure is within the first layer. The next layer (from 1.8 to 5.2 inches, or 16% to 46% of the total HMA thickness) represents the next 50% of the RFC, leaving the final 55% of the asphalt structure to contribute just 5% of the total RFC. This example clearly shows how the rutting is concentrated within the top 4 inches of the structure, leaving the rutting in the HMA layer below 5 to 6 inches of depth to produce a minimal effect on the total pavement distress. Table 3-1c shows the numerical results associated with Figure 3-13.

3.1.7 Asphalt Mix Characteristics

This section addresses the last variable input by the user, E* values from either laboratory test results, historical databases, or the WPE.

3.1.7.1 Option 1: E from Laboratory-Measured Data*

E* obtained from laboratory test measurements is input in the Option 1 Worksheet. The following data are required:

- Temperature (°F),
- Frequency (Hz), and
- Dynamic modulus, E* (10^6 psi).

The program is capable of handling 42 sets of E* test results for each HMA layer used (three layers maximum). As explained in Section 3.1.1, the user inputs the E* values in spaces where the Layer Label IDs are on and color-coded yellow. This was previously illustrated in Figure 3-2b, for a case where only the second layer was required and its label was on, and the first layer was not required and its label was off.

The E* SPT Specification Criteria Program is capable of handling up to seven test temperatures and six test frequencies, which are input in increasing and decreasing order; respectively. Different test conditions may be used for different HMA layers.

Figure 3-14 is an example of how the program requests and receives E* data, as well as the automatic method of analyzing the data within the program. Figure 3-15 shows both automatic and manual methods of analyzing the E* data to obtain the E* master curve.

In Figure 3-14, only 15 E* points are input (3 temperatures and 5 frequencies) for the first HMA layer, leaving the rest of the cells blank. For the second layer, however, 30 points are

OPTION 1 DYNAMIC MODULUS LABORATORY MEASUREMENT INPUT WORKSHEET

INSTRUCTIONS: PLEASE INPUT DYNAMIC MODULUS VALUES IN YELLOW TABLE. THEN RUN SOLVER AS IT IS GIVEN AND YOUR RESULTS WILL BE THE ONES IN TABLE A. MORE INSTRUCTIONS BELOW

TOP			MEDIUM		
Temp. (oF)	Freq. (Hz)	E* (10^6 psi)	Temp. (oF)	Freq. (Hz)	E* (10^6 psi)
30.0	25	2.3866	14.0	25	2.8289
30.0	10	2.3139	14.0	10	2.7377
30.0	1	2.2365	14.0	5	2.6967
30.0	0.5	1.9841	14.0	1	2.4474
30.0	0.1	1.8748	14.0	0.5	2.3361
70.0	25	1.3354	14.0	0.1	2.0908
70.0	10	1.2163	39.9	25	1.9442
70.0	1	0.8229	39.9	10	1.8901
70.0	0.5	0.7330	39.9	5	1.7762
70.0	0.1	0.5463	39.9	1	1.5207
120.0	25	0.2741	39.9	0.5	1.4134
120.0	10	0.2138	39.9	0.1	1.1851
120.0	1	0.1211	70.0	25	1.4057
120.0	0.5	0.1028	70.0	10	1.2803
120.0	0.1	0.0706	70.0	5	1.1519
			70.0	1	0.9143
			70.0	0.5	0.8144
			70.0	0.1	0.6070
			100.0	25	0.4050
			100.0	10	0.3171
			100.0	5	0.2659
			100.0	1	0.1786
			100.0	0.5	0.1503
			100.0	0.1	0.0998
			129.9	25	0.1431
			129.9	10	0.1104
			129.9	5	0.0929
			129.9	1	0.0637
			129.9	0.5	0.0553
			129.9	0.1	0.0415

DYNAMIC MODULUS INPUT INSTRUCTIONS

INPUT IN INCREASING ORDER YOUR TEMPERATURE AND IN DECREASING ORDER YOUR FREQUENCY YOU HAVE UP TO SEVEN TEMPERATURES AND SIX FREQUENCIES. IF EXTRA SPACE IS LEFT, LEAVE IT BLANK.

OPTIMIZED NUMBER = 2.1379

RUN SOLVER TO PROVIDE YOUR RESULTS

Σ e2 = 0.8767

Σ e = -1.0221

Sigmoidal Function Parameters

	TOP	MEDIUM	
δ	4.07020	4.07020	4.07020
α	2.56364	2.56364	2.56364
γ	-0.93073	-0.93073	-0.93073
β	0.49917	0.49917	0.49917

Shift Factors Polynomial Coefficients

	TOP	MEDIUM	
Constant	6.55808	6.55808	6.55808
X-value	-0.10719	-0.10719	-0.10719
X^2-value	0.00019	0.00019	0.00019

SOLVING PROBLEM SPECIFIED

(ONLY IF LAB E* IS TO BE USED)

AUTOMATIC METHOD
PUSH TO RUN MACRO

Figure 3-14. Example of how to input E* data in Option 1 Worksheet.

input (5 temperatures and 6 frequencies). The E* input is totally independent between HMA layers.

The right side of Figure 3-14 shows the automatic method for calculating the E* master curve. The E* data are optimized with a sigmoidal master curve model by an iteration process that can be easily performed in Excel with the aid of the Solver function. All of the computational steps have been placed together in a Visual Basic program (a macro) and made available to the user by simply clicking the *Solving Problem Specified* button (Figure 3-14).

The main difficulty in developing this macro was to input the Solver function into the macro, which involves updating some files on the user's computer. The program contains a Solver.xla file for installation on the user's computer and an accompanying text file that presents all steps required to properly install this Solver.xla file.

When the macro is initialized, it automatically performs a two-step non-linear optimization solution on the E* master curve for each required layer (for a total of up to six optimizations). In Figures 3-14 and 3-15, the optimized number is equal to 2.1379, which indicates that the macro has not yet completed the optimization and reduced the optimized number to as close to zero as possible.

The optimized number is calculated with one of two equations, depending on the type of optimization the macro is using. When the program is performing a biased optimization, the optimized number (*ON*) is computed with Equation 3.1 as follows:

$$ON = \sum_{i=1}^{n} \sum_{j_i=1}^{k_i} e_{j_i}{}^2 \qquad (3\text{-}1)$$

where

i = ith HMA layer required by the user,
n = total number of required HMA layers (up to three),
j_i = jth E* test result for the ith HMA layer,
k_i = total number of E* test results for the ith HMA layer (up to 42), and
e_{ji} = jth error (laboratory-measured E* minus predicted E*) for ith layer.

T WORKSHEET

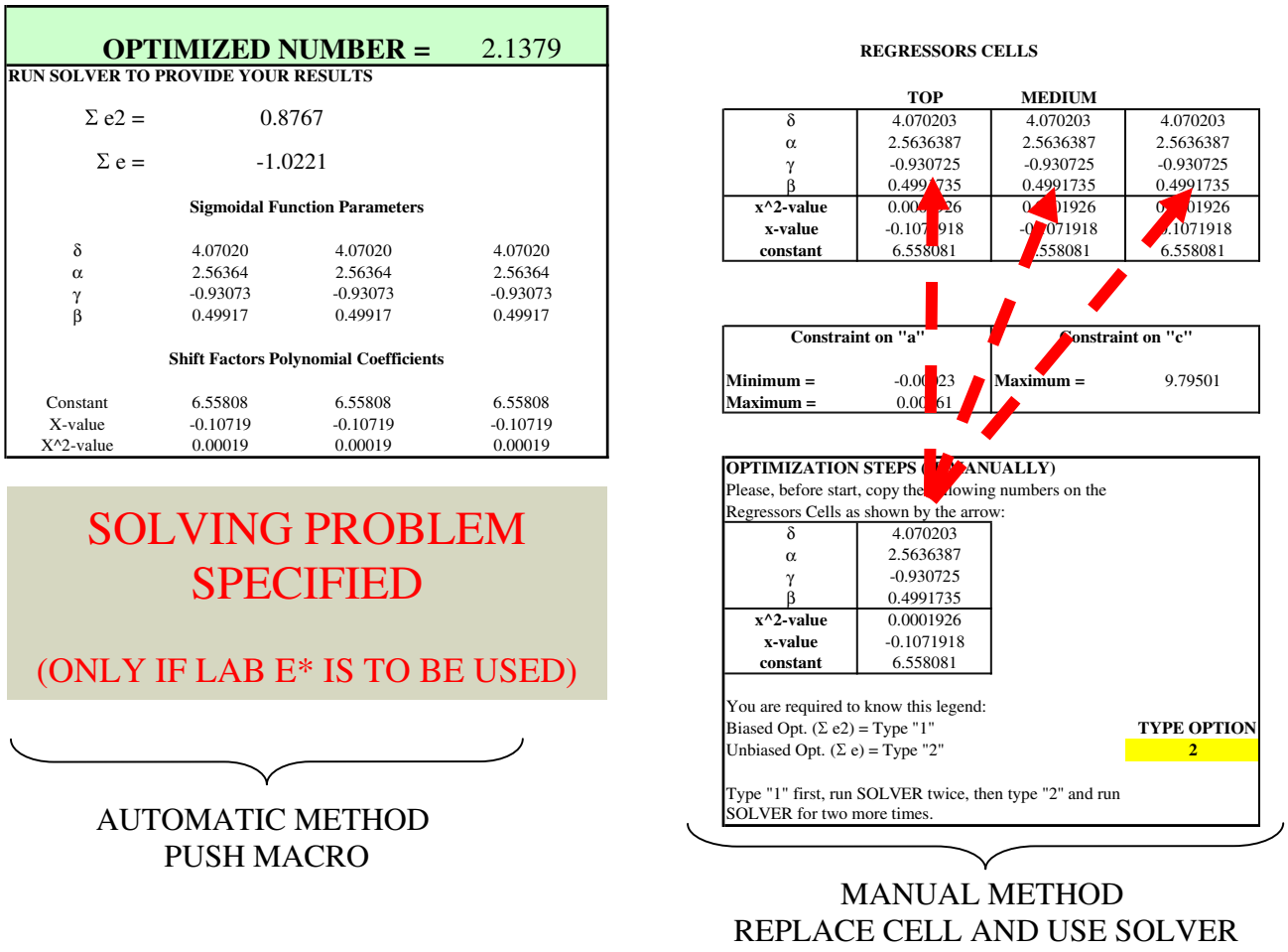

Figure 3-15. Comparison of automatic and manual methodologies for E* master curve calculation.

Thus, *ON* is the summation of errors associated with all of the E* test results for all the included layers.

On the other hand, when unbiased optimization is desired (this should be used after the biased option), *ON* is expressed by the following relationship:

$$ON = \sum_{i=1}^{n} \left(\sum_{j_i=1}^{k_j} e_{ji} \right)^2 \qquad (3\text{-}2)$$

This represents the sum of the squares of the sum of errors, per layer. The biased optimization will lead to a sum of errors near zero, the unbiased optimization will lead to zero.

If the macro is not available, the program can be run manually using the following steps (Figure 3-15):

1. Scroll right in the Option 1 Worksheet until the manual method section appears.
2. In the yellow cell labeled *Type Option*, select Type 1, which directs the program to run a biased optimization following Equation 3.1.
3. Copy and paste the default optimization values located in the table next to the Type Option cell to the regressor cells for the required layers, as indicated by the label ID.
4. Go to the Excel Tools menu, and select the Solver option.
5. In the Solver window, select *Solve* (already configured by default).
6. Repeat the process until there is no further reduction in the optimized number. Generally, one iteration is enough, since the second iteration usually offers only marginal improvement. Because of this, the macro only performs one biased iteration.
7. In the Type Option cell, select Type 2, which directs the program to perform an unbiased optimization following Equation 3.2.

8. In the Tools menu, select the Solver option and click on *Solve* for the unbiased iteration.
9. Repeat the process until there is no further reduction in the optimized number. Again, one iteration is generally enough.

The next part of this section covers the input of E* for Options 2 and 3.

3.1.7.2 Option 2: E* from Laboratory-Measured Data

If historical databases are used, the four sigmoidal coefficients, α, β, γ, and δ, may be determined by use of Equation 3.3 as follows:

$$\log(E^*) = \delta + \frac{\alpha}{1 + e^{\beta+\gamma(\log t_r)}} \quad (3\text{-}3)$$

where

E^* = dynamic modulus, 10^5 psi,
t_r = time of loading at the reference temperature (reduced time),
δ = minimum value of E*,
$\delta + \alpha$ = maximum value of E*,
β, γ = parameters describing the shape of the sigmoidal function, and the three regression coefficients from Equation 3.4 are input.

$$a(T) = a\,T^2 + b\,T + c \quad (3\text{-}4)$$

where T is temperature of interest in °F, and a, b, and c are regression coefficients.

The fitting parameters δ and α depend on aggregate gradation, binder content, and air void content. The fitting parameters β and γ depend on the characteristics of the asphalt binder and the magnitude of δ and α. The sigmoidal function describes the time dependency of the modulus at the reference temperature. The shift factors describe the temperature dependency of the modulus. Equation 3.4 provides the general form of the shift factors.

The value of a(T) is normally between −5 to 5, but the program allows a range of −10 to 10 to cover various combinations of the regression coefficients. It is recommended that the intercept term c in Equation 3.4 should not be higher than 10.2930 and that the x^2-term a in Equation 3.4 should be between −0.000175 and 0.000625.

Similar to Option 1, the program in Option 2 can independently handle up to three HMA layers.

3.1.7.3 Option 3: E* from the WPE

In Option 3, E* is calculated from mix and volumetric properties using the WPE. Recommendations for each of the input variables are as follows:

1. Target Air Voids (%)—Positive numeric values are expected, with initial in situ air voids generally between 6% and 12%, with a typical mean value of 8%.
2. Effective Volumetric Binder (%)—Positive numeric values are expected, with the effective binder content by volume generally between 7% and 13%, or about 2 to 2.2 times the effective binder content by weight.
3. Percent retained on ¾-inch, 3/8-inch, and No. 4 sieves, and passing the No. 200 sieve—Positive numeric values are expected.
4. Binder Characterization—There are two alternate, user-defined ways to input this important variable:
   - Binder Characterization 1: provide the performance grade of the asphalt binder (preferred), or
   - Binder Characterization 2: provide values of the regression parameters A and VTS calculated from asphalt binder characteristics such as softening point, penetration, and rotational viscosity. Specifically, A and VTS are defined by the following equation:

$$\log\log\eta = A + VTS\log T_R \quad (3\text{-}5)$$

where

η = viscosity, cP,
T_R = temperature, Rankine,
A = regression intercept, and
VTS = regression slope of viscosity temperature susceptibility.

The next section will cover the calculations required by the user.

3.2 Performing Required Calculations with E* SPT Specification Criteria Program (Solver in Macros)

Once all required variables are input, and if necessary, the macro for the calculation of the laboratory-measured E* master curve is run, the iteration process related to the calculation of E*, effective temperature, frequency, and critical depth is performed.

Three iteration procedures are required, as follows:

1. Iteration for user-specified mix, environmental, and traffic conditions.
2. Iteration for the high stiffness mix at 13 environmental sites (the project site and 12 locations predefined in the program), user-selected thickness, traffic speed, and design number of repetitions.
3. Iteration for the low stiffness mix at the same 13 environmental sites, user-selected thickness, traffic speed, and design number of repetitions.

For each iteration procedure, the program is capable of accommodating rutting predictions for up to 12 sublayers. Since only one site is desired for the first iteration process, 12 variables are iterated. For the last two iteration procedures, 13 sites are evaluated. This yields 156 variables to be optimized. The total iteration process may optimize up to a grand total of 324 variables. Since the Solver function is capable of handling no more than 200 variables per iteration, the three-step procedure previously described is used.

For simplicity, the three Solver procedures have been put together in a macro. The specific Solver Worksheet is shown in Figure 3-16.

After all required variables are input, the cells Solver 1, Solver 2, Solver 3, and Total Solver will be different from zero (as shown in Figure 3-16). Clicking on *Solving Problem Specified* will generally minimize Total Solver to 0.0000 within one iteration. If not, clicking on *Continue Solving* as many times as needed will continue the iteration process until Total Solver = 0.0000 is obtained and the Regional Calibration cell changes color from red to yellow.

The value in the yellow cell (1.100 in the example in Figure 3-16) is the recommended regional calibration factor, α_{r1}, that is a direct multiplier of the national calibration factor, β_{r1} (= 0.623), in the rutting model shown in the figure. A range of α_{r1} values is provided (upper and lower limits) to give a better idea of what the regional calibration might be, but the ultimate value used by the program must be input by the user.

The last row of the table shows the final calibration factor, χ_{r1} ($= \alpha_{r1} \times \beta_{r1}$), applied in the rutting model.

3.3 Manually Performing Required Calculations with E* SPT Specification Criteria Program

When necessary, the macro discussed in the previous section can be manually replicated to calculate the required regional calibration factor. The steps are as follows:

First iteration

1. Go to Solver Worksheet.
2. Scroll down and select the cell range A37:A48.
3. Delete everything to start the iteration at default conditions. By deleting all of the previous values, the SES (sum of errors squared) and SE (sum of errors) cells will change to higher values.
4. Go to the Tools menu, and select the Solver option.
5. In the Solver Parameters window (see Figure 3-17), input the following parameters:

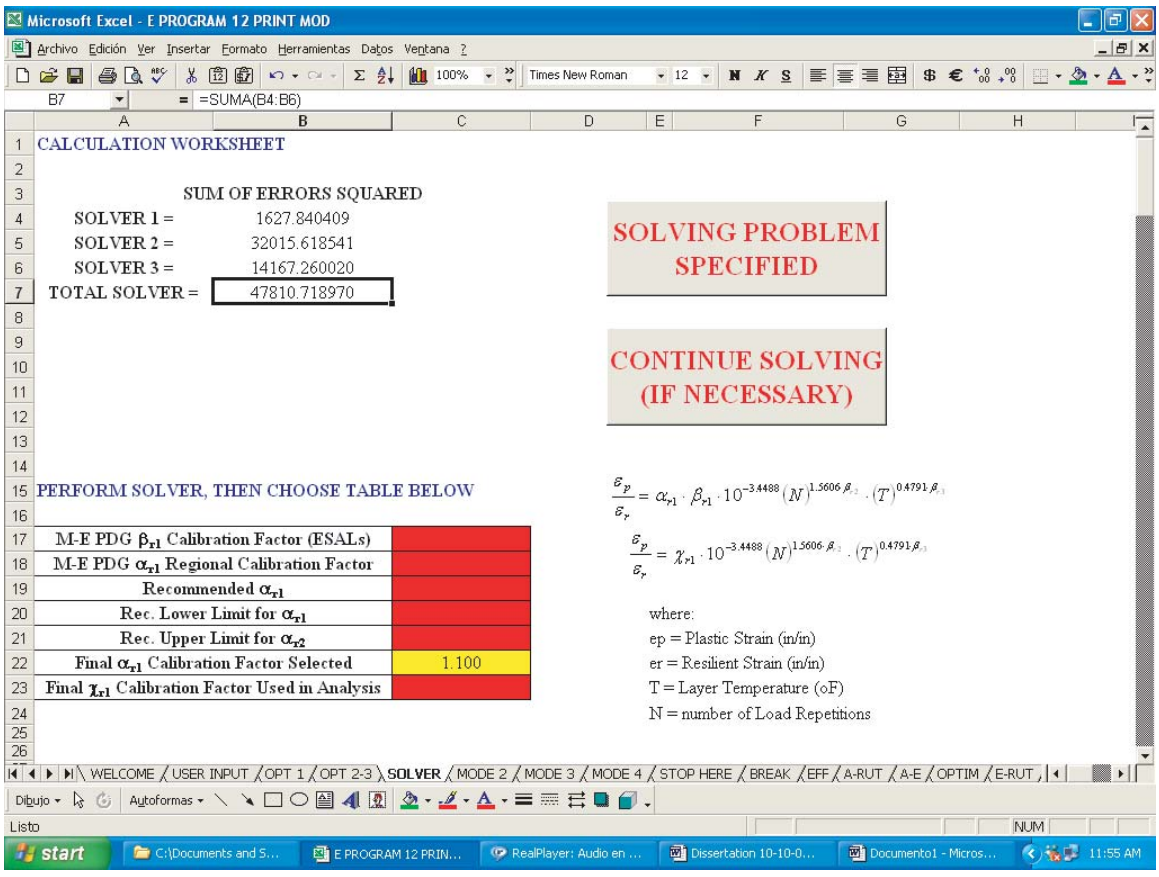

Figure 3-16. Typical Solver Worksheet.

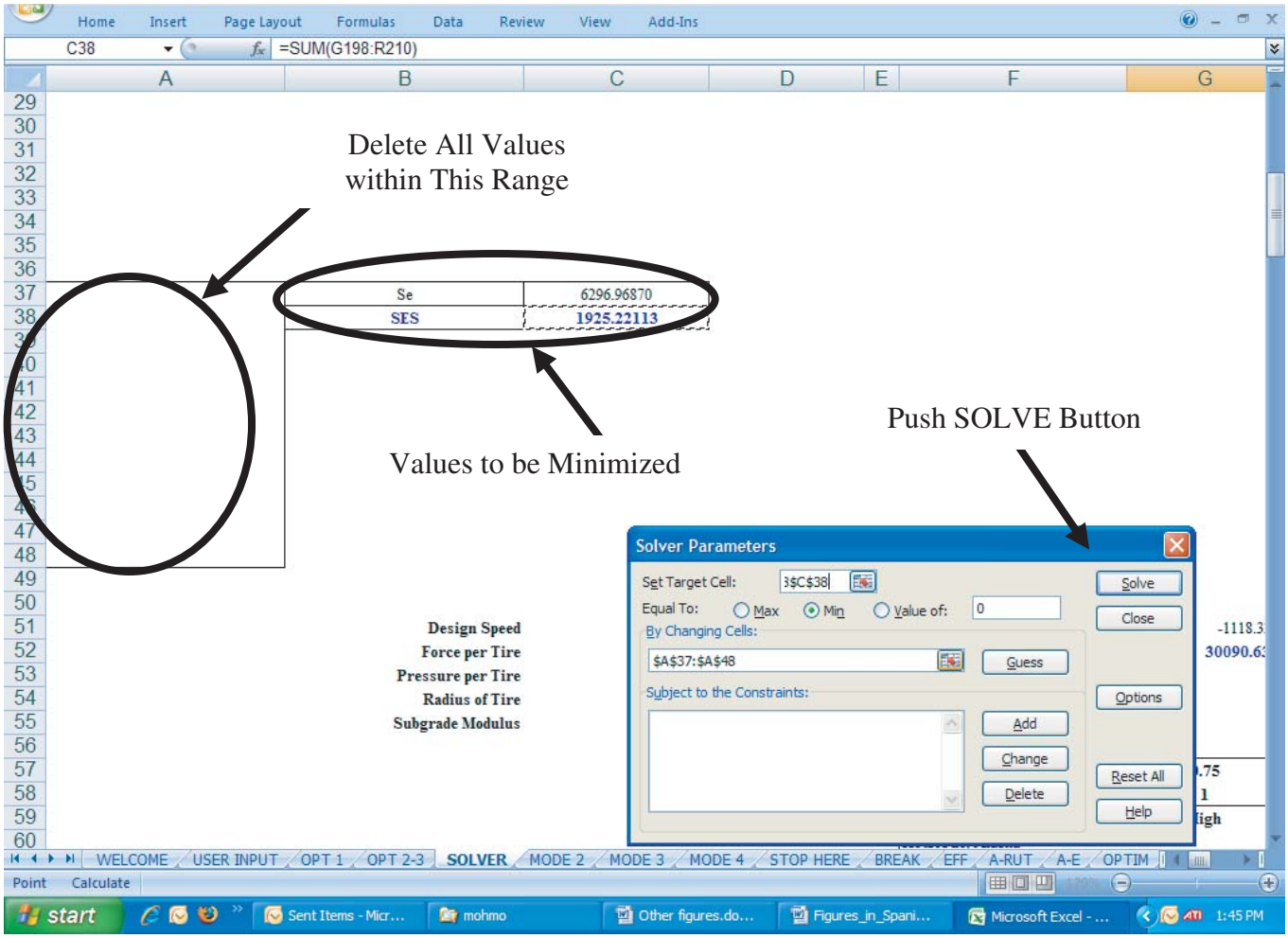

Figure 3-17. Manual solution of first iteration procedure.

Set Target cell to $C$38,
Select *Minimum* radio button, and
Place $A$37:$A$48 in the Changing Cells box.

6. Click on *Solve*. Generally, one iteration will minimize SES and SE values to 0.0000.

Second Iteration

1. Scroll down the page and select the cell range G60:R72.
2. Delete all values. SES and SE (cells G52 and G51, respectively) are changed to non-zero values.
3. Go to the Tools menu and select Solver.
4. On the Solver Parameters window (Figure 3-18), input the following parameters:
   Set Target cell to $G$52,
   Select *Minimum* radio button, and
   Place $G$60:$R$72 in the Change Cells box.
5. Click on *Solve*. Generally, with only one Solver iteration the SES and SE values will be minimized to 0.0000. This step, however, will take more time than the first iteration procedure because of the number of variables considered.

Third Iteration

1. Scroll down the page and select the cell range G170:R182
2. Delete all values. SES and SE (cells G162 and G161, respectively) are changed to non-zero values that may be larger than before the deletion.
3. Go to the Tools menu and select Solver.
4. On the Solver Parameters window (Figure 3-19), input the following parameters:
   Set Target cell to $G$162,
   Select *Minimum* radio button, and
   Place $G$170:$R$182 in the Change Cells box.
5. Click on *Solve*. Generally, one Solver iteration will minimize SES and SE to 0.0000.

When these three iteration procedures are completed, the output can be accessed in one of the Mode 2; Mode 3; or Mode 4 Worksheets as appropriate.

The warning message in Figure 3-20 is displayed if the initial iteration process does not successfully achieve an optimized solution.

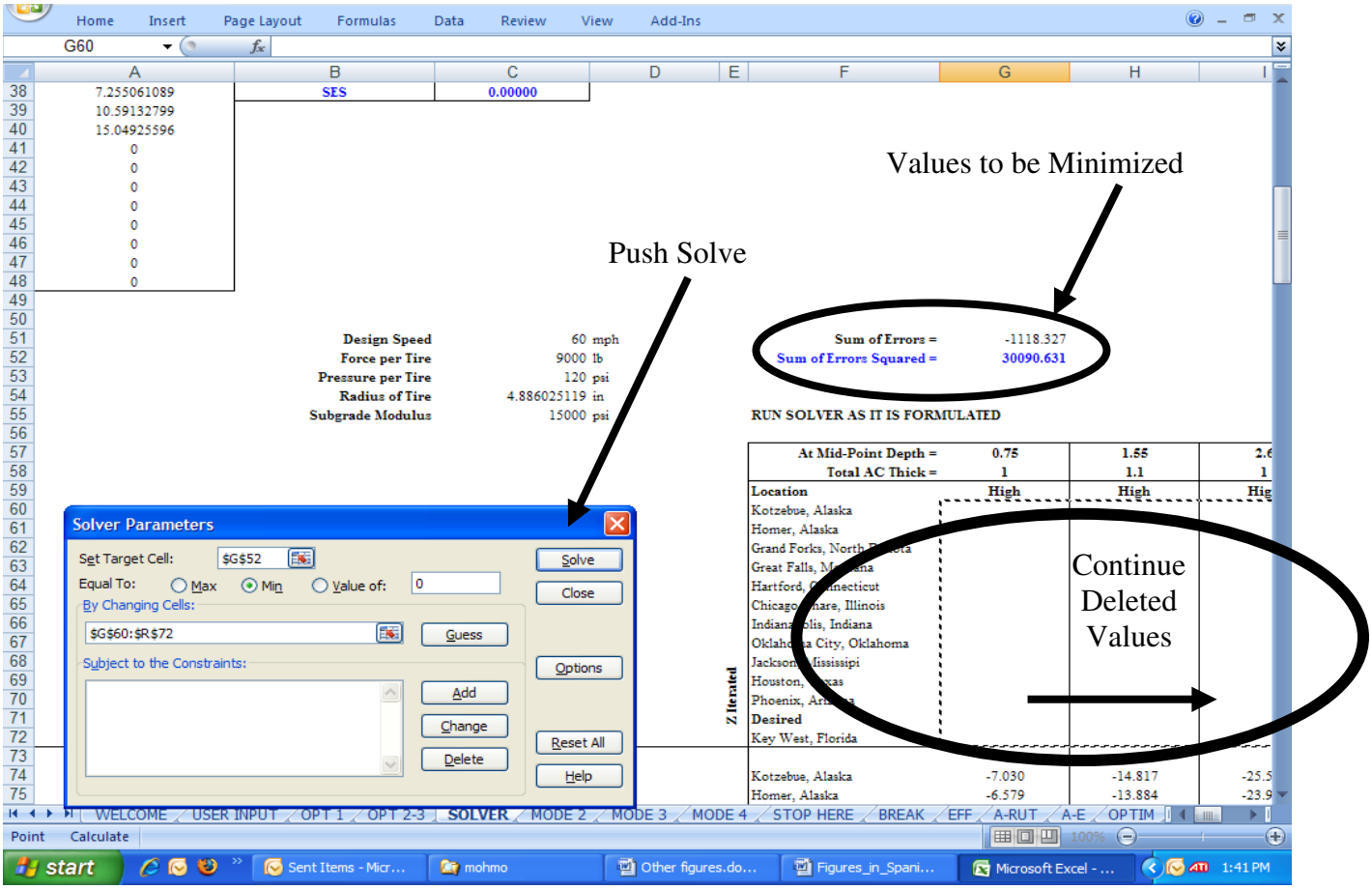

Figure 3-18. Manual solution of second iteration procedure (high stiffness mix).

3.4 Reading Desired Output

The program output is presented on one of three worksheets, which are described in the following sections.

3.4.1 Mode 2

Figure 3-21 shows a typical Mode 2 Output Worksheet.

Tables at the top left and top right provide selected input data on project general input data and project traffic and climatic conditions, respectively.

The table at the bottom of Figure 3-21 presents a summary of program output for the layers specified by the user. In this mode, layer comparisons are possible between:

- Allowable rut depth (RFC) and allowable layer E*, and
- Predicted rut depth and predicted layer E*.

The program provides an objective, deterministic comparison for the layer and E* values. If the allowable rut depth is higher than the predicted rut depth, the program defines the layer design (thickness and mix characteristics) as acceptable. Similarly, if the allowable layer E* is higher than the predicted layer E*, then the program considers the layer design as unacceptable.

A final output of this worksheet is to provide information on the desired effective and SPT recommended temperature and frequency. The effective temperature and frequency are those conditions calculated from the iterations performed by the user following the directions provided in Section 3.2. If E* tests would be used to assess different mixtures for the project conditions and structural design, then E* tests would have to be performed at these effective temperature and frequency conditions. However, if the effective frequency is higher than 25 Hz, it may not be possible to perform the E* test because of equipment limitations. This is why a space is provided for the user to input a new user-defined frequency value (lower than, or equal to, 25 Hz) that will yield an equivalent testing temperature. These equivalent temperature and frequency values are designated as the SPT recommended temperature and frequency values. These values are calculated using the Time-Temperature Superposition Principle for the specific mixture master curve defined.

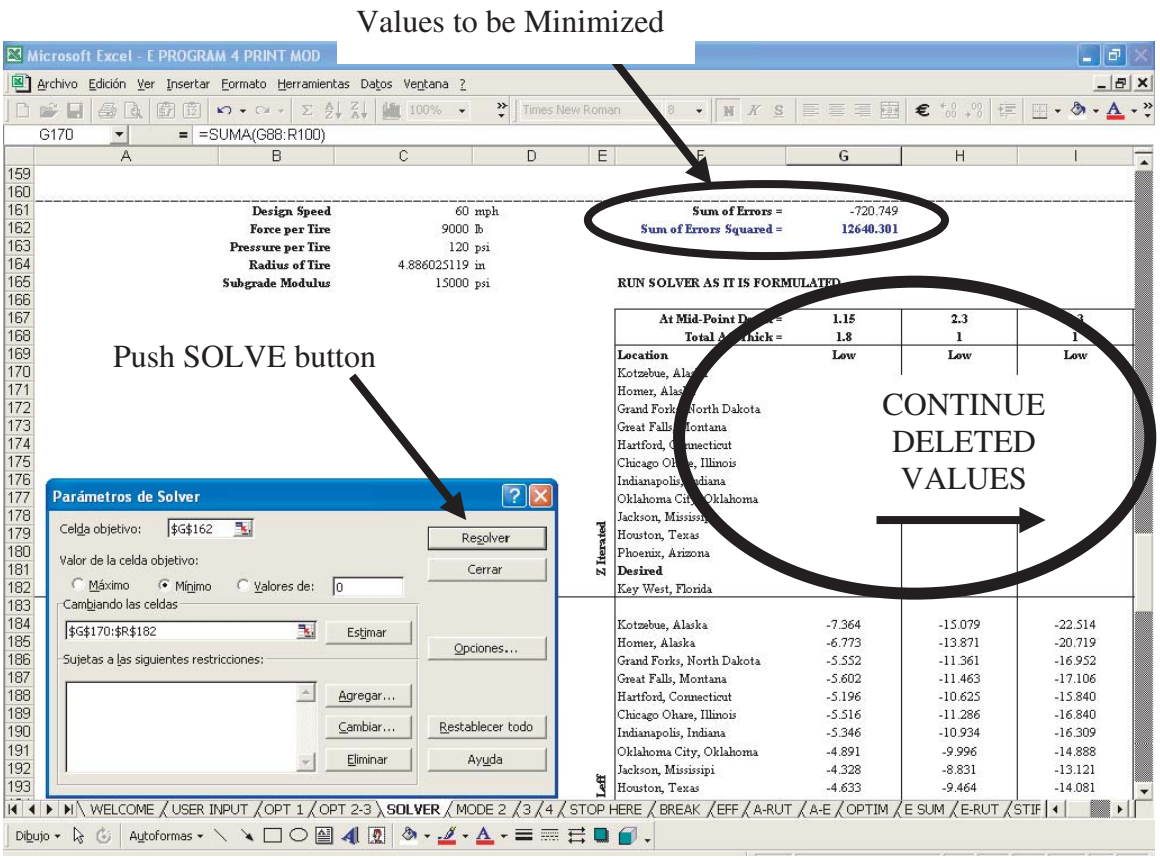

Figure 3-19. Manual solution of third iteration procedure (low stiffness mix).

E* AS MIX / STRUCTURAL DESIGN TOOL

PROJECT GENERAL INPUT DATA

Project ID	Example 1
Project Location	Anytown, US
Date of Analysis	9/25/2005
Operator's Name	Andres Sotil

PROJECT TRAFFIC AND CLIMATIC CONDITIONS

Desired Speed (mph)	60
Desired Traffic (ESALs)	7,500,000
Mean Annual Air Temperature (oF)	48.1
Mean Monthly Air Temp St. Dev. (oF)	15
Mean Annual Wind Speed (mph)	5
Mean Annual Sunshine (%)	69
Annual Cumulative Rainfall Depth (in)	44

SUMMARY OF PROGRAM OUTPUT

WARNING!!!
GO BACK TO 'SOLVER' TO OPTIMIZE THE PROBLEM

Layer Label ID	A	B	
Layer Thickness (in)	3.5	4.2	
Effective Frequency (Hz) **	35.0	44.0	
Effective Temperature (oF)	98.1	86.0	
SPT Recom. Frequency (Hz)	25.00	25.00	
SPT Recom. Temperature (oF)	95.8	82.4	
Allowable Rut Depth (in)	**0.10**	**0.25**	
Allowable Layer E* (ksi)	**1176.1**	**85.5**	
Predicted Rut Depth (in)	**0.28**	**0.06**	
Predicted Layer E* (ksi)	**389.9**	**512.7**	
Acceptable (Rut) ???	**NO**	**YES**	
Acceptable (E*) ???	**NO**	**YES**	

WARNING!!!
GO BACK TO 'SOLVER' TO OPTIMIZE THE PROBLEM

Figure 3-20. Typical warning messages for a non-optimized problem.

E* AS MIX / STRUCTURAL DESIGN TOOL

PROJECT GENERAL INPUT DATA

Project ID	Example 1
Project Location	Anytown, US
Date of Analysis	9/25/2005
Operator's Name	Andres Sotil

PROJECT TRAFFIC AND CLIMATIC CONDITIONS

Desired Speed (mph)	60
Desired Traffic (ESALs)	7,500,000
Mean Annual Air Temperature (oF)	48.1
Mean Monthly Air Temp St. Dev. (oF)	15
Mean Annual Wind Speed (mph)	5
Mean Annual Sunshine (%)	69
Annual Cumulative Rainfall Depth (in)	44

SUMMARY OF PROGRAM OUTPUT

Layer Label ID	Top	Bottom	
Layer Thickness (in)	2.1	3.8	
Effective Frequency (Hz) **	55.7	29.9	
Effective Temperature (oF)	107.5	82.8	
SPT Recom. Frequency (Hz)	25.00	25.00	
SPT Recom. Temperature (oF)	101.7	81.7	
Allowable Rut Depth (in)	**0.10**	**0.25**	
Allowable Layer E* (ksi)	**405.5**	**481.0**	
Predicted Rut Depth (in)	**0.14**	**0.22**	
Predicted Layer E* (ksi)	**289.5**	**603.1**	
Acceptable (Rut) ???	**NO**	**YES**	
Acceptable (E*) ???	**NO**	**YES**	

Space Provided for User Frequency Selection

Figure 3-21. Typical Mode 2 output.

A final feature of this program is its capability to refer the user to the appropriate output mode worksheet, if necessary. For example, if the user erroneously input Mode 3 instead of Mode 2, when the Mode 2 Worksheet is accessed, the program will provide a warning message and turn off all the output values in that worksheet, as shown in Figure 3-22. Under these conditions, either the user must return to the Welcome Worksheet and specify the appropriate mode or go directly to the appropriate mode output worksheet.

3.4.2 Mode 3

This mode provides data similar to those provided for Mode 2. However, there is a major difference in how the data are organized for the user. The following Mode 3 output values are provided (see Figure 3-23):

- Layer Label ID turned off and color-coded red for the layers not selected by the user,
- Layer thickness, input by the user,
- Allowable rut depth (layer RFC), subdivided as explained in Section 3.1.3,
- Allowable layer E*, calculated from the universal rut depth-E* relationships and the allowable rut depth,
- Effective frequency and temperature,
- SPT recommended frequency (SPT-Freq), input by the user, and
- SPT recommended temperature, computed from the SPT-Freq.

Knowing the SPT-Freq and temperature values, the user has the option to run (i.e., select) various E* tests from a database of asphalt mixes, and then perform the comparison to the critical (allowable) E* values provided above. This is shown in Figure 3-24 for a typical layer. The following data is input by the user:

- Trial Mix ID;
- Air Voids (%);
- Vbeff (%), Effective Binder Content; and
- Measured E* (ksi).

This measured E* is compared with the allowable E*, and then the program will provide the result of the deterministic comparison in the *Decision Yes or No?* column. The allowable E* value is a lower limit. If the measured or calculated E* value of the HMA is less than the allowable E*, the HMA mix design is not acceptable. If the HMA E* value is greater than the allowable E*, the HMA mix design is acceptable. In Figure 3-24, it can be seen that 7 out of 18 possible hypothetical mixes

WARNING!!!!

PROJECT GENERAL INPUT DATA

Project ID	Example 1
Project Location	Anytown, US
Date of Analysis	9/25/2005
Operator's Name	Andres Sotil

PROJECT TRAFFIC AND CLIMATIC CONDITIONS

Desired Speed (mph)	60
Desired Traffic (ESALs)	7,500,000
Mean Annual Air Temperature (oF)	48.1
Mean Monthly Air Temp St. Dev. (oF)	15
Mean Annual Wind Speed (mph)	5
Mean Annual Sunshine (%)	69
Annual Cumulative Rainfall Depth (in)	44

WARNING!!!!
CHECK APPROPRIATE MODE
OUTPUT YOU SELECTED
MODE NUMBER 3

SUMMARY OF PROGRAM OUTPUT

Layer Label ID			
Layer Thickness (in)			
Effective Frequency (Hz) **			
Effective Temperature (oF)			
SPT Recom. Frequency (Hz)			
SPT Recom. Temperature (oF)			
Allowable Rut Depth (in)			
Allowable Layer E* (ksi)			
Predicted Rut Depth (in)			
Predicted Layer E* (ksi)			
Acceptable (Rut) ???			
Acceptable (E*) ???			

Figure 3-22. Typical Mode 2 output warning message.

E* AS A SPT (SIMPLE PERFORMANCE TEST)

PROJECT GENERAL INPUT DATA

Project ID	Example 1
Project Location	Anytown, US
Date of Analysis	9/25/2005
Operator's Name	Andres Sotil

PROJECT TRAFFIC AND CLIMATIC CONDITIONS

Desired Speed (mph)	60
Desired Traffic (ESALs)	7,500,000
Mean Annual Air Temperature (oF)	48.1
Mean Monthly Air Temp St. Dev. (oF)	15
Mean Annual Wind Speed (mph)	5
Mean Annual Sunshine (%)	69
Annual Cumulative Rainfall Depth (in)	44

SUMMARY OF PROGRAM OUTPUT

Layer Label ID	Top	Bottom		FIRST LAYER
Layer Thickness (in)	2.1	3.8		
Allowable Rut Depth (in)	0.100	0.250		
Allowable Layer E* (ksi)	405.513	481.010		
Effective Frequency (Hz) **	55.68	29.86		SECOND LAYER
Effective Temperature (oF)	107.46	82.79		
SPT Recom. Frequency (Hz)	25.00	25.00		THIRD LAYER
SPT Recom. Temperature (oF)	101.70	81.67		

** The yellow spaces shown below are for your convenience. Equipment limitations sometimes do not allow the use of effective frequency. The default value is 25 Hz but you can change it to whatever value you need, and the corresponding effective temperature would be calculated below.

Figure 3-23. Typical Mode 3 output.

Top					
Trial Mix ID	Air Voids (%)	Vbeff (%)	Measured E* (ksi)	Allowable E* (ksi)	Decision Yes or No?
Trial 1	7	10	254	405.5	No
Trial 2	6	8.5	165	405.5	No
Trial 3 - Replicate 1	6.75	9.4	110	405.5	No
Trial 3 - Replicate 2	6.7	9.6	100	405.5	No
Trial 4 - Replicate 1	5.8	9.1	200	405.5	No
Trial 4 - Replicate 2	5.5	9.4	180	405.5	No
Trial 4 - Replicate 3	5.9	9.2	250	405.5	No

Figure 3-24. Typical Mode 3 output—typical layer comparison table.

are being compared with the allowable E* values. Different mixes can be compared, as well as different replicates within a given mix, but the final decision regarding which mix is most appropriate will also be guided by the user's (or agency's) expertise and experience.

Finally, similar to Mode 2, the program will indicate to the user the appropriate output mode if the selection is not Mode 3.

3.4.3 Mode 4

The final worksheet is that for Mode 4. This worksheet provides data that are similar to the Mode 2 and Mode 3 solutions. The difference lies in the specific scenario in which this program will be used. It is emphasized that the Mode 4 approach is directly associated with the QC/QA of the mix production. Considerations like the time and date of testing, as well as the in situ (actual) air voids, binder content, and aggregate gradation should be considered in this analysis mode. Thus, the tables in Figure 3-25 provide space for the user to make the appropriate decisions. Comparison by E*, as well as by predicted rut depth values, is performed. However, the final decision on whether a specific mixture is acceptable for the project must be made by the user. The tables in Figure 3-25 are provided for each HMA layer specified by the user.

This concludes the explanation of potential worksheets the user would encounter. The calculation worksheets are normally hidden from view.

However, the last section of this chapter briefly describes each of these calculation worksheets. Note that no changes should be made by the user to these worksheets since this will significantly impact the final solution.

3.5 Calculation Worksheets

3.5.1 Worksheet Names

The E* SPT Specification Criteria Program includes Excel worksheets used for a widely diverse set of calculations, interpolations, and iteration procedures. These worksheets are named General Calcs; Structure; 01, 02, 0275, 03, 04, 06, 08, 12, and 20; Interp; Layers; Distrib; Soft; Stiff; E Sum; E-Rut; Optim; A-E; A-Rut; EFF; and Break.

3.5.2 General Calcs and Structure Worksheets

The General Calcs Worksheet performs calculations that are not in the core of the rutting prediction procedure but provide appropriate data allowing for enhancements of models or for a more user-friendly interactive output. The worksheet itself is divided into six sections by color-coded tables.

The first section is designed to perform calculations and *if* statements for the title cells of the User Input, Option 1 and Option 2-3 Worksheets. These calculations are based on the alphanumeric code provided to the user for inputting the mode and option combination used in the analysis.

The second section is a line that states the maximum thickness of the total HMA layers that the program can handle. The current value is set at 30 inches of HMA.

The next section deals with the selection of an appropriate environmental site (from the 12 preselected sites) based only on the MAAT that is representative of the location of the project. Knowing this location, the program is capable of providing the user with a plot of the closest line of maximum rutting (LMR), as illustrated in Section 3.1.6. Figure 3-26 is

QA/QC E* DECISION BY LAYER **FIRST LAYER**

Layer Label ID	Top
Layer Thickness	2.1

SPT Recom. Frequency (Hz)	25
SPT Recom. Temperature (oF)	101.70

Allowable Layer Rut (in)	0.100
Allowable Layer E* (ksi)	405.5

Effective Frequency (Hz) **	55.68
Effective Temperature (oF)	107.46

Test Date	Test Time	Specimen ID	Actual AV (%)	Actual Vbeff (%)	Measured E* (ksi)	Target E* (ksi)	ACCEPT ? Yes or No ?
2/25/2005	4:00 PM	Section 1	7.1	11.2	250	405.5	No
2/26/2005	8:30 AM	Section 2-a	6.85	10.6	421	405.5	Yes
2/26/2005	10:30 AM	Section 2-b	6.5	10.25	610	405.5	Yes

Final Rutting Criteria (in)	Pred. Rutting based on E* (in)	ACCEPT? Yes or No?
0.10	0.16	No
0.10	0.09	Yes
0.10	0.06	Yes

Figure 3-25. Typical comparison table for Mode 4.

another example of such a plot, which can be drawn by the program for 24 conditions (12 sites and 2 mix types), entered in the Structure Worksheet.

The next section in the General Calcs Worksheet is quite relevant. It was stated earlier in this report that regional calibrations could be performed easily for this E* SPT Specification Criteria Program by changing the β_{r1} factor in the permanent deformation model developed by El-Basyouny (*3*). He found the national calibration value to be 0.509, and later in this study it was found that an ESAL-modified national calibration factor was equal to 0.623. This 0.623 value is indicated in the space provided in the User Input Worksheet.

However, it is critically important to recognize that if a regional calibration requires changing the values of β_{r2}, β_{r3}, or both in the underlying permanent deformation model, then a recalibration must be conducted with the entire rutting database used in this program (864 simulation scenarios).

With the β_{r3} value = 1.2 found by El-Basyouny (*3*), the coefficient on the traffic term in the permanent deformation

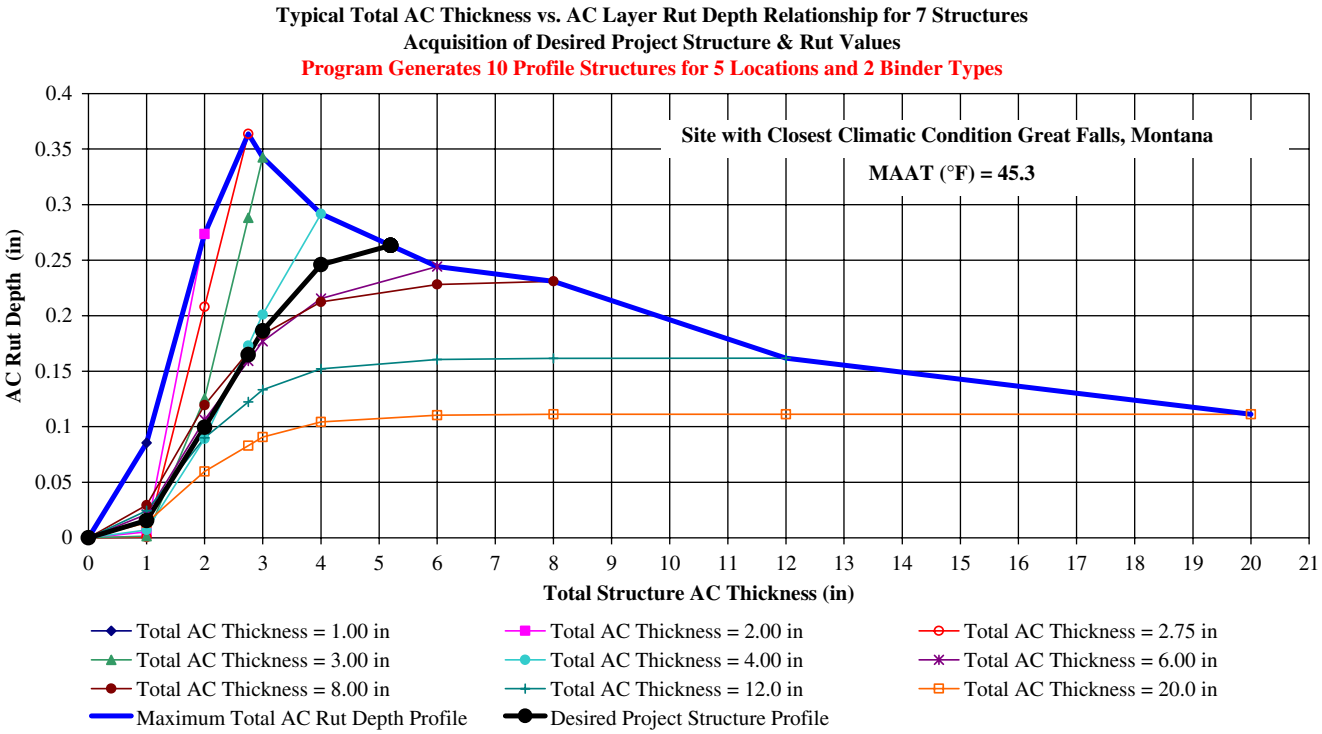

Figure 3-26. Typical Structure Worksheet.

model used in the *MEPDG* was equal to 0.479244, calculated as follows:

Previous Model Coefficient × β_{r3} (LTPP) = National CF
0.39937 × 1.2 = 0.479244

This value was used for the reduction of required runs due to different traffic levels, expressed in Equation 3.2 of Reference 2. However, if β_{r3} is changed, the value of the coefficient also changes from 0.479244. In the E* SPT Specification Criteria Program, the user has the option to input a new β_{r3} value if a recalibration is conducted.

The next section deals with input data required for the different equations used in the program solution. For example, if future changes are made to the model coefficients WPE; the user has the capability of updating the E* SPT Specification Criteria Program with them. However, if the WPE changes its format, then it would be necessary to undertake major program changes.

Similarly, the user has the ability to change the mix and volumetric properties of the two standard mixes used in this program. If new runs are necessary and other mixes are used, these new properties can be updated in future enhancements of the program.

In the iteration procedure, there are several assumed values such as tire force, pressure, and radius. Tire force is assumed to be 9,000 lb since an 18-kip ESAL is run in the MEPDG, and the pressure is assumed to be a standard 120 psi. These values are considered conventional but the user may change them if necessary.

Finally, the worksheet deals with the effective temperature and temperature factor regression coefficients. This worksheet contains the temperature factors for the 12 standard environmental sites as well as those of the project site.

3.5.3 Raw Data Worksheets

The next worksheets that are available in the E* SPT Specification Criteria Program are those related to the rutting database and the calculations performed to reduce them by the project traffic characteristics. There are nine worksheets, corresponding to the following HMA thicknesses: 1 inch, 2 inches, 2.75 inches, 3 inches, 4 inches, 6 inches, 8 inches, 12 inches, and 20 inches.

In each worksheet, there are tables containing 96 typical rows for the standard combinations of 12 sites, 2 mix types, and 4 traffic speeds, as well as a varying number of rutting columns, depending on the HMA thickness

Each worksheet performs the same calculations, using Equations 3.3 and 3.4 to reduce the database by the traffic speed and traffic number of repetitions, respectively.

$$RUT_{SP} = A\ Speed^{B} \quad (3\text{-}3)$$

where

Speed = average traffic speed (mph),

RUT_{SP} = desired rutting prediction at stated average traffic speed, and

A, *B* = Regression coefficients dependent on the environmental site, binder type, and HMA layer within given pavement structure.

$$RUT_X = RUT_{ST} * 10^{0.479244 (\log X - \log ST)} \quad (3\text{-}4)$$

where

RUT_X = desired rutting prediction at *X* number of traffic repetitions (inches) and

RUT_{ST} = rutting prediction at standard *ST* number of traffic repetitions (inches).

In order to appropriately implement Equation 3.3, a linear regression must be performed on the log-log scale. Once the regression coefficients *A* and *B* are available for each site-mix type combination using the project average traffic speed, the rutting is calculated. Then, using the project traffic number of repetitions and Equation 3.4, the database is reduced to the project traffic conditions.

Several additional calculations are performed in these worksheets that relate to some exceptions and limitations in the linear regressions performed. When the database contained extreme conditions; the MEPDG predicted rut depths may become equal to the layer thickness. This was especially true at a speed of 0.5 mph, or for low-stiffness mixes or hot environmental sites. The example in Figure 3-27 illustrates the additional calculations performed. When a calculated rut depth equals the HMA thickness, the datapoint is not considered in the calculations and the regression analysis is performed with three or two points instead of the original four points (from the traffic speed Equation 3.3).

Similarly, if Equation 3.4 yields a rut depth that exceeds the HMA thickness (for example, at high traffic levels), the rut depth is equated to the HMA thickness.

3.5.4 Interp, Layers, and Distrib Worksheets

In the Interp Worksheet, the program performs all the calculations necessary to output a summary table containing the reduction of the database to the traffic project conditions and the user-defined HMA thickness, following the sublayering scheme used when running the MEPDG.

Simultaneously, the Layers Worksheet performs the layer subdivision for the project structural design. That is, it divides the user input layers into the required sublayers to perform accurate E* and rut depth predictions. In addition, the layer RFC provided by the user is subdivided into the sublayer RFC.

Using the rutting values obtained in the Interp Worksheet and the layer subdivision from the Layers Worksheet, the rutting values at the user-defined sublayers are calculated in the Distrib (distribution of rutting) Worksheet, using simple linear interpolations.

3.5.5 Soft, Stiff, and E Sum Worksheets

The E* SPT Specification Criteria Program has two parts, the HMA rut depth part and the E* part. The HMA rut depth is calculated on the Distrib Worksheet. The Soft, Stiff, and E Sum Worksheets deal with the E* part.

The Soft and Stiff Worksheets carry out the E*, temperature, and frequency calculations for soft and stiff HMA mixes, respectively. Both worksheets are interconnected with the

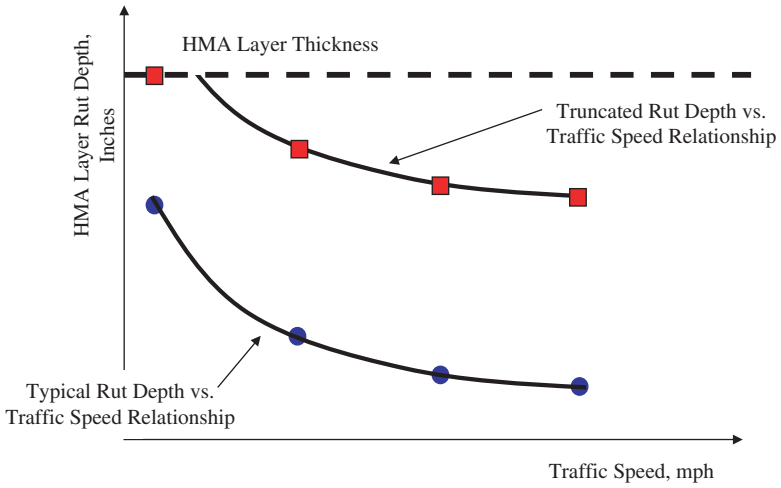

Figure 3-27. Comparison of typical versus truncated rut depth versus traffic speed relationships due to HMA thickness equal to rut depth.

Solver Worksheet for the required iteration sequence. The summary of results of these two worksheets is presented in the E Sum Worksheet.

3.5.6 E-Rut Worksheet

The calculations required to reduce the database to the final E* versus rut depth universal relationships are performed in this worksheet. The E*, effective temperature, and frequency values summarized in the E Sum Worksheet are interrelated with the HMA rut depth values shown in the Distrib Worksheet. For each sublayer, 12 effective temperatures and 12 rutting values are regressed. Using the project site effective temperature, the predicted rutting per sublayer is obtained for mix type. With this rutting prediction and the E* value also available in the E Sum Worksheet for the project site, the universal relationship is obtained for each HMA sublayer. These relationships are then used, along with the RFC and the E* provided for the proposed mix, for the comparisons performed in the different modes available. The next worksheets are used for the comparison calculations for the different modes, the handling of the user-proposed mix, and the development of user-friendly output worksheets.

3.5.7 Optim Worksheet

This worksheet develops the E* master curve from the measured E* data provided in the Option 1 Worksheet for the three HMA layers available. Sigmoidal master curve plots are available so the user, if desired, can assess how well the E* data are processed.

3.5.8 A-E and A-Rut

The program, using the RFC, calculates a critical E* value. The E-Rut Worksheet performs this calculation; the output represents the program system demand. For the system capacity part of the problem, A-E (actual E*) and A-Rut (actual rut depth) Worksheets perform the appropriate calculations.

In the A-E Worksheet, the program receives the input from the user for the material characteristics of the project. If Option 1 (E* from laboratory tests) is used, then the sigmoidal coefficients and second-order polynomial coefficients obtained in the Optim Worksheet are used. If Option 2 or Option 3 is selected, the necessary data are directly provided by the user in the Option 2-3 Worksheet. If Option 4 is selected, the program will separate the layers and sublayers accordingly, using a combination of *if* statements and commands.

The final output of this A-E Worksheet is the E* value per sublayer using the material characteristics provided by the user. With these E* values, the A-Rut Worksheet predicts the HMA rut depth for the project. These two values represent the system capacity, which is compared with the system demand in the Break Worksheet.

3.5.9 EFF Worksheet

Before explaining the Break Worksheet, it is necessary to comment on the EFF (effective temperature and frequency) Worksheet, in which the SPT recommended combination is calculated. As stated previously, the computed effective frequency may be higher than the 25-Hz limit selected in the overall program. In order to overcome this limitation; the SPT recommended temperature and frequency values are calculated from the WPE (for Option 3), the sigmoidal and second-order polynomial coefficients calculated in the Optim Worksheet (Option 1), provided directly by the user (Option 2), or a combination of the three sources (Option 4).

3.5.10 Break Worksheet

The last of the calculation worksheets to be described is the one developed to first select the critical sublayer within a layer (i.e., to break the sublayers output into user layers). Once the critical sublayers are defined, the worksheet recognizes the layer RFC (Layers), the predicted layer rut depth (A-Rut), the critical E* (E-Rut), the actual E* (A-E), and then performs the deterministic comparison that is provided in the output mode worksheets.

CHAPTER 4

Summary of Findings

A major research effort was conducted between 1995 and 2006, and first performed under an FHWA contract (1995–1999) and then under NCHRP Project 9-19 (1999–2006). The purpose of this research was to develop an SPT for permanent deformation (rutting) based on measurement of HMA dynamic modulus (E*). The function of the SPT is to provide a measure of the rutting response of an HMA mix design under realistic loading and temperature conditions. This report describes a key product of that research, the E* SPT Specification Criteria Program.

The E* SPT is explained in detail in *NCHRP Report 465, Simple Performance Test for Superpave Mix Design* and *NCHRP Report 547, Simple Performance Tests: Summary of Recommended Methods and Database*. NCHRP Project 9-29 developed practical, cost-effective equipment (the Simple Performance Tester) to accurately and precisely carry out the E* SPT, including first-article and production units, as well as a performance-type purchase specification. A proposed standard test method for determining the dynamic modulus and flow number for HMA using the simple performance test system is under review by AASHTO's member states.

4.1 The E* SPT Specification Criteria Program

The E* SPT Specification Criteria Program is software available as an Excel spreadsheet and a C++ program that converts measured or calculated HMA E* values to rut depth predictions. The program incorporates a database of pavement design scenarios pre-solved with the *Mechanistic-Empirical Pavement Design Guide* developed in NCHRP Projects 1-37A and 1-40. Using this database, interpolative estimates of potential rutting may be obtained for any HMA mix design under project-specific traffic (loading), environmental, and multi-layer structural conditions.

The program compares rutting estimates with rut depth limits established on a statewide or project-by-project basis. The rutting estimate is based upon the E* of the HMA, measured with the SPT or calculated with either the Witczak predictive equation (WPE) or a four-coefficient sigmoidal function derived from historical measured E* results.

4.2 Validation of the E* SPT Specification Criteria Program

Validation of predictive tools like the E* SPT Specification Criteria Program is necessary to build confidence in their use in day-to-day agency operations.

The purpose of validation is to determine whether a model is a reasonable representation of a real-world system and if the desired accuracy or correspondence exists between the model and the real world.

This report described the validation of the E* SPT Specification Criteria Program with materials and performance data from LTPP, WesTrack, MnRoad, the NCAT test track, and ALF, as well as 20 randomly simulated test sections built into the program database. Overall, the program had (1) a good coefficient of determination, equal to 0.835, (2) a standard error of 0.067 inches of rutting, (3) a coefficient of variation equal to 22%, and (4) a slight underprediction (bias) between predicted and measured rut depths ($y = 0.9926\ x$). In addition, the program provided good predictions of results obtained with the MEPDG.

These good-to-excellent validation statistics are evidence that the level of predictive accuracy achievable with the E* SPT Specification Criteria Program is satisfactory for implementation of the E* SPT methodology in HMA mix design and quality control.

References

1. Witczak, M.W., Kaloush, K.E., Pellinen, T., El-Basyouny, M., and Von Quintus, H. *NCHRP Report 465: Simple Performance Test for Superpave Mix Design*. Transportation Research Board, National Research Council, Washington, D.C., 2002.
2. Witczak, M.W. *Use of the Dynamic Modulus (E*) Test as a Simple Performance Test for Asphalt Pavement Systems (AC Permanent Deformation Distress): Volume I of IV* Preliminary Draft Final Report, NCHRP Project 9-19: Superpave Support and Performance Models Management. Arizona State University, Tempe, October 2005.
3. El-Basyouny, M.M. *Calibration and Validation of Asphalt Concrete Pavements Distress Models for 2002 Design Guide*. Ph.D. dissertation, Department of Civil and Environmental Engineering, Arizona Sate University, Tempe, 2004.
4. Witczak, M.W., Bari, J., Zapata, C.E., Pellinen, T., Kaloush, K., Sullivan, B., Quayum, M. M., Zborowski, A.J., and Sotil, A. *Material and Mix Properties, Construction Information and Performance Data Report. Part 6. FHWA-ALF Test Sections.* Superpave Support and Performance Models Management NCHRP Project 9-19 in conjunction to NCHRP Project 9-30 . Subtask C4 through C6. Arizona State University, Tempe, July 2003.

VOLUME II

Flow Number and Flow Time

CONTENTS

CHAPTER 1

Literature Review and Theoretical Background

1.1 Permanent Deformation of Asphalt Mixtures

Conceptual development of the Superpave mix design method was completed as part of the Strategic Highway Research Program (SHRP). The SHRP-A-003A Project, "Permanent Deformation Response of Asphalt Aggregate Mixes," described an innovative design and analysis system to evaluate the resistance of hot mix asphalt (HMA) mixes to permanent deformation. The system provided an effective methodology to define the effect of asphalt-aggregate interactions on pavement rutting. It also combined HMA testing with traffic loading (repetitions, wheel loads, and tire pressures), environmental conditions (temperature), and the pavement cross-section to ensure that permanent deformation in the form of longitudinal pavement ruts will not exceed acceptable limits.

The test program at the University of California at Berkeley (UCB) developed the Superpave simple shear test. A recommendation was made to use this test for measuring the permanent deformation characteristics of HMA mixes. Mixture response parameters for the simple shear test were slope and intercept of the accumulated permanent deformation, total shear strain, plastic to resilient strain ratio, resilient shear modulus (total and instantaneous), plastic and resilient shear strains, and number of cycles to plastic flow (*1*). The test is executed at the critical pavement temperature defined as the 7-day maximum pavement temperature at 2-in. depth. The analysis procedure was derived from data obtained from 40 general pavement studies sections throughout North America. The fundamental link between the laboratory tests and field performance was derived by determining a relationship between the number of cycles in the repetitive simple shear test at constant height (RSST-CH) to reach a given permanent shear strain and the number of ESALs to cause the same permanent shear strain in the pavement section.

It is worth mentioning that an advantage of the RSST-CH test is the ability to test specimens prepared from field cores. Also, empirical guidelines currently exist to correlate field and lab results. The disadvantage of this test is that the guidelines may be difficult (and not fundamental) to define for structural models used in the *Mechanistic-Empirical Pavement Design Guide* (MEPDG).

In the MEPDG approach, the permanent deformation characteristics of HMA are obtained from a triaxial, repeated dynamic load test for several thousand repetitions and the cumulative permanent deformation is recorded as a function of the number of cycles (repetitions) over the test period. Typical permanent deformation parameters, which are obtained and analyzed from the repeated load permanent deformation test, include the intercept (a, μ) and slope (b, α) parameters. The permanent deformation properties (α, μ) have been used as input for predictive design procedures (*2*). All four of the parameters noted (α, μ, b, a) are regression constants of a statistical model that is only based upon the "linear" secondary phase of the plastic strain—repetition curve. Additional mixture response parameters of the repeated load test are the number of cycles to failure, total and instantaneous resilient modulus, plastic strain, slope, and intercept of accumulated permanent and total strains (*1*). Two types of models are included in the MEPDG to ensure that the pavement structure will not exhibit more than a specified level of rut depth. These two types of models are typically referred to as subgrade strain and permanent deformation models. The permanent deformation models estimate the amount of permanent strain, deformation, or both within each pavement layer. These models define the vertical plastic deformation in each layer and accumulate all permanent strain values to estimate the total rutting at the surface of the pavement structure.

1.2 Fundamental Permanent Deformation Properties

The Distress Identification Manual for the Long-Term Pavement Performance Project defines a rut as "a longitudinal

surface depression in the wheel path [that] may have associated transverse displacement." Some amount of rutting occurs in nearly all flexible pavements.

Permanent deformation in an HMA layer is caused by a combination of densification (volume change) and shear deformation (no volume change) from the repetitive application of traffic loads. Shear deformation of properly constructed (compacted) pavements—caused primarily by large shear stresses in the upper portions of the HMA layer(s)—is dominant.

1.2.1 Types of Rutting

Rutting is categorized into three types and defined by the cause and layers in which the rutting occurs. Each type or category is summarized below.

1.2.1.1 One-Dimensional Densification or Vertical Compression

A rut depth caused by material densification is a depression near the center of the wheel path without an accompanying hump on either side of the depression. Densification of materials is generally caused by excessive air voids or inadequate compaction after placement of the HMA mat, thereby allowing the mat or underlying layers to compact when subjected to traffic loads. This type of rut depth usually results in a low-to-moderately-severe level of rutting.

1.2.1.2 Lateral Flow or Plastic Movement

A rut depth caused by the lateral flow of material is a depression near the center of the wheel path with humps on either side of the depression. This type of rut depth usually results in a moderate-to-highly-severe level of rutting. Lateral flow or displacement of materials will occur in those mixtures with inadequate shear strength or an insufficient amount of total voids in the HMA layer. Voids of an HMA mixture in the range of 3% or less after construction can be susceptible to lateral flow because the low voids allow the asphalt to act as a lubricant rather than a binder during hot weather. Overdensification of the HMA layer by heavy wheel loads can also result in bleeding or flushing on the pavement surface. This type of rutting is most difficult to predict.

1.2.1.3 Mechanical Deformation

A third type of rutting is consolidation, densification, and/or lateral movement of the unbound materials below the HMA surface. This type of rutting has been referred to as *mechanical deformation*. Mechanical deformation is a result of subsistence in the base, subbase, and/or subgrade and is usually accompanied by a longitudinal cracking pattern at the pavement's surface when the HMA mixture is too stiff (i.e., high elastic modulus). These longitudinal cracks generally occur in the center and along the outside edges of the ruts.

1.2.2 Mechanisms of Rutting

Surface distortion is caused by inelastic or permanent deformation from wheel loads in one or more layers. Inelastic deformations are defined as plastic deformations that are not recoverable after the load is removed—permanent deformations. When a wheel load is applied to the pavement surface, the HMA and other pavement layer deform in an amount that is proportional to the modulus and thickness of the individual layers at the temperature and speed of loading. When the load is removed, not all of the deformation under the load is recovered—a residual amount remains in one or more layers. Repeated wheel loads cause the residual deformations to accumulate, increasing the amount of permanent deformation and rutting.

The mechanisms for distortion, and specifically for rutting, can be subdivided into two types: (1) one-dimensional vertical inelastic displacements (densification), and (2) two-dimensional inelastic displacements (such as vertical and lateral flow). Densification involves a decrease in material volume; lateral or shear deformations involve the plastic flow of material with or without volume change. Each is discussed in more detail in the following paragraphs.

1.2.2.1 One-Dimensional Inelastic Deformations

Vertical inelastic deformation can be the result of additional densification of HMA and other pavement layers or the consolidation of unbound materials and soils. Densification is the continued, gradual reduction of air voids from repeated traffic applications that occur in pavement layers after initial compaction. Densification is the result of vertical inelastic deformations under load. HMA layers are susceptible to some additional densification because the compressive stresses from wheel loads and temperatures are much higher near the surface. The higher the temperature, the softer the asphalt, and the more susceptible the HMA is to densification under wheel loads.

Another, but much less common, rutting mechanism is the consolidation of supporting layers—primarily fine-grained materials and soils that have high levels of moisture. Pressures applied to the pavement's surface are transmitted to the unbound layers and subgrade. Consolidation is a slowly developing process that is dependent upon the amount of fines and moisture present in the soil.

1.2.2.2 Two-Dimensional Inelastic Deformations

The longitudinal or lateral distortion of HMA mixtures is caused by the localized shear failure in the mixture resulting from over stressing the mixture with high tire pressures.

Mixtures with low shear strength demonstrate this type of rutting. Most models developed to date, with the exception of the WesTrack models, use one-dimensional compression tests. Rutting caused by lateral flow is difficult to accurately predict with repeated load triaxial testing equipment, especially when the HMA mixture is highly anisotropic—properties vary by direction.

Yoder and Witczak (*3*) defined shear deformation as the plastic flow of the pavement layers without volume change. The shear deformation is resisted by the shear modulus of the material, G. The value of G, as well as elastic modulus, for viscoelastic, isotropic materials depends on the rate of load application as well as temperature. For viscoelastic material, such as HMA, the length of loading time affects the amount of deformation that occurs in the material. Thus, distortions will be less on highways with higher speeds than on highways with slower speeds, given the same truckloads.

1.2.3 Factors Affecting Rutting of HMA Mixes

Permanent deformation of asphalt aggregate mixes is a complex phenomenon where aggregate, asphalt, and aggregate-asphalt interface properties control the overall performance. Furthermore, over time, these properties (as well as their relative contribution) change until the mix reaches the end of its useful life (i.e., failure occurs due to excessive permanent deformation or crack development). HMA mixes have a rate and temperature dependent behavior, they dilate, exhibit different properties in tension and compression, and their behavior is strongly dependent on air void contents. When aged, they lose fluidity, which can play an important role in the development of permanent deformation. In some mixes, moisture damage also plays an important role in the development of permanent deformation. Different factors that influence permanent deformation and the effect of changing factors are shown in Table 1-1 and discussed in the following section.

1.3 Selection of Test System for Permanent Deformation

In order to select a standard testing procedure, special emphasis was placed on the ability of each test to represent in situ stress states and, to a somewhat lesser extent, on its simplicity (*4*). Two major criteria designed in the development of the process to measure permanent deformation were as follows:

1. Field simulation, including
   - Repeated dynamic loading (with stress reversal) to simulate approximate in situ traffic loading,
   - A state of stress representative of the shear stresses causing permanent deformation in the field, and
   - Supplemental data to use in mechanistic analysis.
2. Simplicity, meaning
   - Ease of specimen fabrication,
   - Minimum quantities of materials required for fabricating specimens in the laboratory,
   - Compatibility with equipment currently available in material laboratories, and
   - Minimal cost of new equipment or supplemental devices required to adapt existing equipment.

1.4 Repetitive Simple Shear Test at Constant Height

The primary objectives of SHRP-A-003A included the development of a series of accelerated performance-related tests for asphalt aggregate mixes and methods for analyzing asphalt aggregate interactions that significantly affect pavement performance (*4*). For permanent deformation evaluation, test methods used the simple shear test developed as a part of the SHRP-A-003A program.

1.4.1 Test Selection

Several reasons lead to the selection of the simple shear test at constant height, as follows:

- No change in volume—the volume of the specimen remains constant during the test. The height of the specimen is maintained constant, and gluing the top and the bottom of the specimens prevents lateral movement of the specimens.
- Specimen geometry—obtaining a 6-in. diameter by 2-in. high specimen from any pavement section by coring, or from any compaction method proposed by SHRP (i.e., gyratory or rolling wheel compaction), is easy.
- Rotation of principal axes—it is the simplest test that permits controlled rotation of the principal axes of strain and stress, which is important in a rutting study.
- Repetitive applied loads—studies indicate that application of repetitive loads is required to capture the rutting phenomenon.
- Dilation—dilation is one of the most important aspects of controlling the stability of a mix. Under shear strains, densely compacted mixtures tend to dilute. If dilation is constrained, then confining stresses are generated. It is in part due to the development of these confining stresses that a mix derives its stability against shear strains.

1.4.2 Equipment Description

The original testing system used for the simple shear permanent deformation test was developed by James Cox & Sons, Inc., and has been presented by Sousa, Tayebali, et al. (*5*).

Table 1-1. Factors affecting rutting of HMA mixes (*4*).

	Factor	Change in Factor	Effect of Change Factor on Rutting Resistance
Aggregate	Surface texture	Smooth to rough	Increase
	Gradation	Gap to continuous	Increase
	Shape	Rounded to angular	Increase
	Size	Increase in maximum size	Increase
Binder	Stiffness[a]	Increase	Increase
Mix	Binder content	Increase	Decrease
	Air void content[b]	Increase	Decrease
	VMA[c]	Increase	Decrease
	Method of compaction	—[d]	—[d]
Test or field conditions	Temperature	Increase	Decrease
	State of stress/strain	Increase in tire contact pressure	Decrease
	Load repetitions	Increase	Decrease
	Water	Dry to wet	Decrease if mix is water sensitive

NOTE:
[a]Refers to stiffness at temperature at which rutting propensity is being determined. Modifiers may be utilized to increase stiffness at critical temperatures, thereby reducing rutting potential.

[b]When air void contents are less than about 3%, the rutting potential of mixes increases.

[c]It is argued that very low (i.e., less than 10%) voids in mineral aggregate (VMA) should be avoided.

[d]The method of compaction, whether laboratory or field, may influence the structure of the system and therefore the propensity for rutting.

1.4.3 Specimen Preparation and Setup

A series of specimens is prepared using different air-void and asphalt content. In order to initiate testing, vertical and horizontal linear variable differential transformers (LVDTs) are attached to the specimen. The vertical LVDT is used to measure changes in specimen height as represented by changes in the distance between the top and bottom platens. The horizontal LVDTs measure the difference in horizontal displacement between two points on the specimen separated by 37.5 mm.

1.4.4 Test Procedure

In repetitive simple shear tests at constant height (RSST-CH), the vertical actuator maintains the height of the specimen and an LVDT measures the relative displacement between the specimen caps. In this manner, the height of the specimen is maintained constant. The horizontal actuator, which is under the control of the shear load cell, applies haversine loads corresponding to a 10 psi (69 kPa) shear stress magnitude with a 0.1 s loading time and 0.6 s rest period. An LVDT mounted directly on the specimen measures the shear deformation of the sample. Figure 1-1 shows the specimen loading condition in the simple shear test.

A wide range of testing at different temperatures and stress levels demonstrated that the 10 psi (69 kPa) shear stress magnitude was a reasonable level, and at this level of stress good mixtures would exhibit some permanent deformation while poor mixtures would not fail excessively fast.

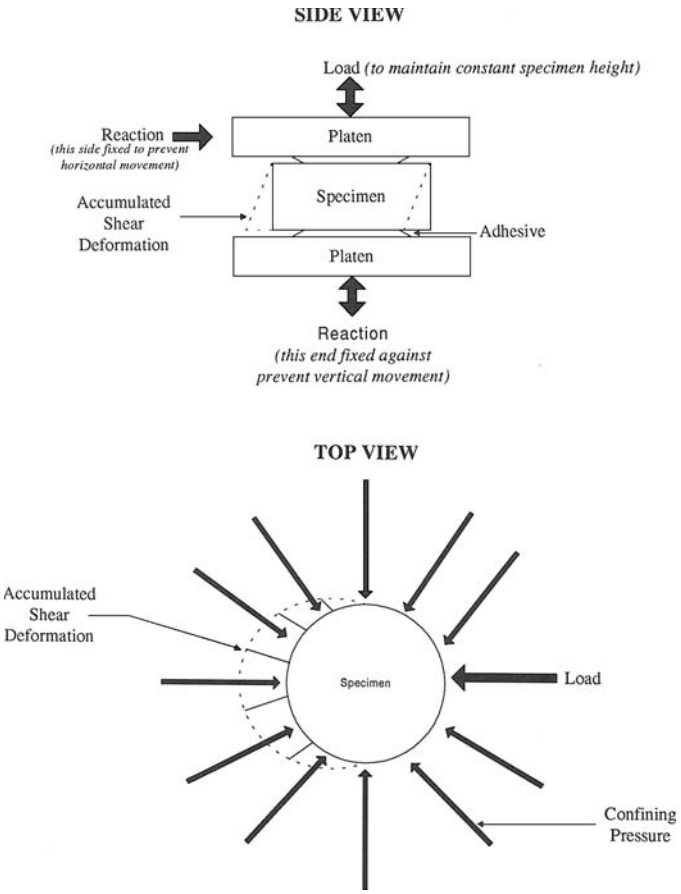

Figure 1-1. Specimen loading conditions (8).

Tests are typically executed until 5% shear strain level occurs. This value was selected because finite element studies (*6*) have shown that at that level of permanent strain, rut depths of about 0.5 in. (13 mm) can be expected. In RSST-CH, mix design study tests were executed until 5% shear strain level was reached or up to 5,000 cycles (*7*). Prior to testing, specimens are usually conditioned with 100 cycles of a 1 psi (7 kPa) haversine loading with a 0.1 s loading and 0.6 s rest period. The major purpose of this preconditioning is to set up the instrumentation. Tests can be executed at any temperature.

1.4.5 Test Parameters

The following test parameters are recorded for the simple shear test (*8*):

- Axial load (*P*),
- Shear load (*V*),
- Vertical displacement of the specimen (δ_v), and
- Horizontal displacement of the specimen (δ_h),

The following engineering quantities are calculated:

σ_{11} = P/A; axial stress where *A* is the cross-sectional area of the specimen;
τ_{12} = V/A; shear stress; and
$\varepsilon_{12} = \delta_v/h$; shear strain where *h* is the height of the specimen.

1.4.6 Maximum Permanent Shear Strain versus Rut Depth

To establish a relationship between the maximum permanent shear strain and rut depth, Sousa used finite element simulations of a standard, full depth, 15-in. thick HMA pavement section, and 14 mixes were used to obtain material constants. Sousa found that for all 14 mixes, a unique relationship appears to exist between maximum permanent shear strain and rut depth. The relationship was given by

$$\text{rut depth (in.)} = \text{slope}^* \text{maximum permanent shear strain} \quad (1\text{-}1)$$

where slope = 11.

It was also of interest to investigate whether that relationship was affected by the thickness of the HMA layer. For selected mixes, analyses were made for pavements with asphalt concrete layers of 4-, 6-, and 8-in. (102-, 152-, 203-mm) thicknesses. The subgrade modulus was changed to correspond to realistic pavement section conditions. The results indicated that the slope of the relationship between maximum permanent shear strain and rut depth was dependent on thickness and given by

$$\text{slope} = 0.74^* \text{thickness (in.)} \quad (1\text{-}2)$$

1.4.6.1 Relationship between Number of Load Cycles in RSST-CH and Equivalent Single Axle Load (ESAL)

Typical results from repeated shear tests on LTPP general pavement studies specimens were used by Sousa and Solaimanian (*9*) to determine the number of shear cycles required to reach the level of maximum shear strain determined for each site from the reported rut depth. Then the number of laboratory cycles to reach this value of shear strain was determined and correlated with the traffic level (ESALs) producing the reported rut depth.

The following type of relationship was obtained for pavements less than 10 years old:

$$\log(\text{Cycles}) = -4.36 + 1.24\log(\text{ESAL}) \quad (1\text{-}3)$$

This relationship was obtained with an $R^2 = 0.80$.

1.4.7 The Procedure to Estimate Permanent Deformation

A procedure to estimate the permanent deformation of HMA pavement based on the RSST-CH was presented by Sousa and Solaimanian (*9*). Figure 1-2 diagrams a nomograph

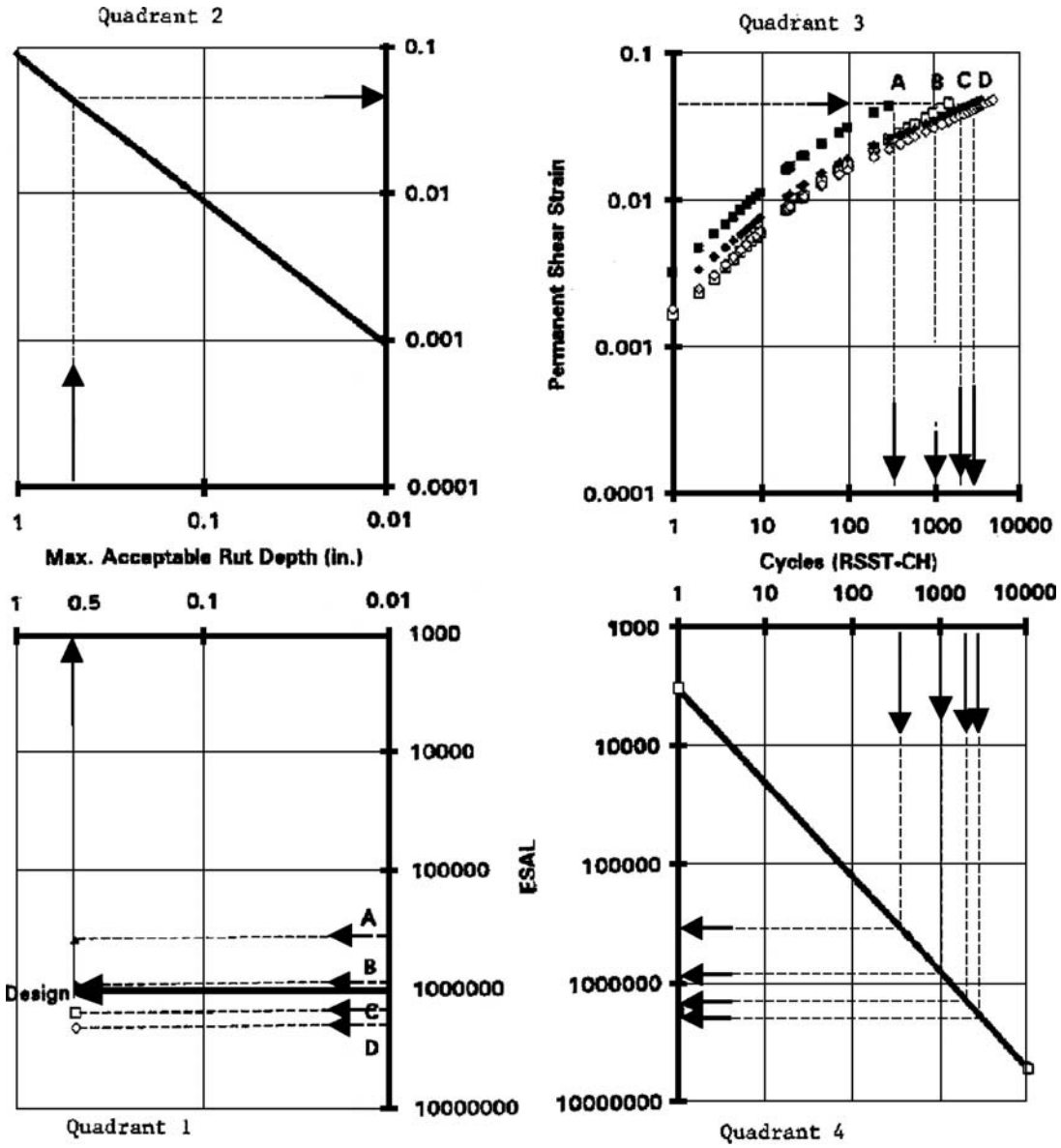

Figure 1-2. Schematic diagram of the abridged procedure for permanent deformation.

of the procedure. It is composed of four quadrants and should be followed clockwise starting in Quadrant 1.

In Quadrant 1, where the plot provides ESALs versus rut depth, two steps are involved as follows:

Step 1—Determine number of ESALs for design life and
Step 2—Select maximum allowable rut depth.

To facilitate the explanation of the procedure, assume that one wanted to design one pavement that would be designed to carry 1 million ESALs in the design life. The design criteria would impose a 0.5-in. (13-mm) rut depth as the maximum acceptable rut depth.

In the example, a 1 million ESAL design life was selected. The maximum acceptable rut depth was selected to be 0.5 in. (13 mm).

In Quadrant 2, where the plot provides rut depth versus permanent strain, one step is required as follows:

Step 3—Using the maximum allowable rut depth, the maximum allowable permanent shear strain is determined based on a relationship between depth and maximum shear strain.

In Quadrant 3, where the plot provides permanent shear strain versus cycles, three steps are required as follows:

Step 4—Determine mean highest 7-day pavement temperature at the site at 2-in. (51-mm) pavement depth,
Step 5—Execute RSST-CH at 10 psi (69 kPa) at that temperature, and
Step 6—The number of cycles in RSST-CH is determined to yield maximum allowable shear strain based on the relationship between shear strain and number of cycles obtained from RSST-CH.

SHRP binder/mixture specifications are developed based on maximum and minimum pavement temperatures. Maximum pavement temperature was defined as the average maximum

temperature for seven consecutive days. It is believed that rutting correlates better with this temperature than with mean monthly maximum or average yearly maximum temperatures.

Once the maximum pavement temperature at the surface was found, the maximum pavement temperature for any depth less than 8 in. (203 mm) is found through the following empirical formula (*10*).

$$T_d = T_s(1\text{-}0.063d + 0.007d^2 – 0.0004d^3) \quad (1\text{-}4)$$

where

d = depth in inches,
T_s = maximum pavement temperature (°F) at the surface, and
T_d = maximum pavement temperature (°F) at depth d.

Four typical graphs of the permanent shear strain obtained from the simple shear test at constant height executed at 10 psi (69 kPa) stress amplitude (with 0.1 s loading time and with 0.6 s rest period) and at the mean highest 7-day maximum weekly pavement temperature encountered at 2-in. (51-mm) depth versus number of cycles obtained for some of the mixes are presented in Quadrant 3. These relationships were obtained for dense-graded mixes at different asphalt contents (Mix A with higher asphalt content than Mix D).

This graph permits the determination of the number of cycles in RSST-CH required to reach a given permanent shear strain level (in this case, shear strain is rut depth divided by slope, or 0.5/11, which equals 0.04545). We can see that Mix D performs better than Mix A.

In Quadrant 4, where the plot provides cycles (RSST-CH) versus ESAL, the final step is as follows:

Step 7—The number of ESALs that can be carried by that mix before the desired rut depth (0.5 in. [13 mm]) is reached is determined using the relationship between ESALs and RSST-CH number of cycles.

With the results obtained from the analysis, we can identify which of the mixes would satisfy the design conditions. In the example, only Mixes C and D satisfy the requirements. Considerations should be given to reliability, and adjustments may be required. Depending on the level of reliability, Mix D might be the only one to satisfy the requirements.

1.5 MEPDG Approach for Permanent Deformation

1.5.1 MEPDG Distress Prediction Methodology

The MEPDG is an analysis guide and not a design procedure. In other words, the answer for a problem is *how much distress over time*, rather than *how thick does each layer need to be to limit the amount of distress to a specific value*. The general logic of the pavement prediction system being implemented in the MEPDG is a combination of four basic modules: a material characterization module, a pavement structural response module, a climatic module, and a distress/performance prediction module, which are common to most M-E prediction methodologies. Each is briefly defined below.

1.5.1.1 Material Characterization

The material characterization models describe how the various materials in the pavement system respond to traffic loading and environmental changes. Different material characterization models are required for the different categories of materials in the pavement system (e.g., HMA, unbound materials, stabilized layers, etc.). The major material characterization models for flexible pavements incorporated in the MEPDG are as follows:

- HMA—loading rate, temperature, and aging-dependent linearly elastic material as characterized by the complex modulus (E^*), phase angle (ϕ), and Poisson's ratio (ν);
- Unbound materials (base/subbase/subgrade)—either a linearly elastic material characterized by E and ν or a stress-dependent nonlinearly elastic material characterized by stress-sensitivity parameters k_1, k_2, k_3, Poisson's ratio (ν), and a tension cut-off criterion; and
- Stabilized materials (base/subbase)—a stiffness-degrading linearly elastic material characterized by E and ν and a stiffness degradation function.

Material characterization is considered to be the more important module to the performance predictions because it affects, to some degree, all components of the system.

1.5.1.2 Pavement Response

The pavement response model determines the structural response of the pavement system (i.e., stresses, strains, and deflections) due to traffic loads and environmental influences. Environmental influences may be direct (e.g., strains due to thermal expansion and/or contraction) or indirect via effects on material properties (e.g., changes in stiffness due to temperature and/or moisture effects). The MEPDG contains two pavement response models for flexible pavements. The JULEA multilayer elastic theory (MLET) program is used in cases where all of the unbound layers in the pavement are treated as linearly elastic. The DSC2D nonlinear finite element (FE) program is used in cases where stress dependency of the unbound material stiffness is to be considered in the performance or distress calculations. It is expected that the JULEA program will be used to complete most pavement analysis.

1.5.1.3 Environmental Effects

The environmental effects module predicts the spatial and temporal variations of temperature and moisture content/phases within the pavement structure and subgrade. The environmental effects model embedded in the MEPDG is the Enhanced Integrated Climatic Model (EICM) developed by the University of Illinois.

1.5.1.4 Distress/Performance Predictions

The MEPDG includes mechanistic-empirical models for distortion (rutting), load-related cracking, non-load-related cracking, and smoothness. The rut depth and load-related cracking models are based upon empirical relations between distress quantity and a mechanistically computed critical stress or strain in the pavement structure and subgrade. The thermal cracking distress model is based on an enhanced version of the mechanistic model developed under the SHRP Program (*11*). Smoothness, as measured by the International Roughness Index (IRI), is calculated from these predicted, and other, distresses. Reflection cracking is not included in the MEPDG because no model was judged suitable for implementation in the MEPDG based on the scope of work and ground rules established by NCHRP.

The final output from the performance prediction system is predicted magnitudes of pavement deterioration versus time. Pavement deterioration can be quantified in terms of individual distresses (rutting/fatigue cracking/thermal cracking), and in terms of roughness or ride quality.

1.5.2 MEPDG Calibration

The field calibration of the distress prediction methodology must be determined from comparisons of predicted performance to measured field observations. All of the performance models in the MEPDG are being calibrated (on a national level) to observed field performance at a representative spectrum of pavement test sites.

The highest quality calibration of the prediction models, however, requires testing of the HMA, unbound pavement materials, and subgrade soils at selected field sites. No laboratory testing was completed as a part of NCHRP Project 1-37A—it was assumed that the material properties and other inputs needed for the calibration process would be available from existing databases. The LTPP test sections were used extensively in the calibration-validation process, because of the consistency in the monitored data over time and the number of test sections spread throughout North America. However, some of the required material properties and site feature inputs were unavailable from the LTPP database. Because of the inevitably limited number of pavement test sites, minimal testing of selected properties, calculated properties from regression equations, and the national scope of the calibration, the predictions from the calibrated models have a relatively high level of uncertainty.

Tighter calibration of the models based upon measured material properties, design and construction practices, and performance histories from a more localized region should yield better predictive accuracy. More importantly, there is a need to obtain consistent data that are being used for multiple outcomes—the calibration-validation of HMA mixture and structural design procedures, performance-related specifications, and management of flexible pavements. Thus, the experimental plan being developed under NCHRP Project 9-30 to confirm and validate the distress prediction equations for mixture and structural design should be applicable to other uses and models to reduce the amount of duplication and costs among projects.

1.5.3 Rutting Phenomena

Recent research efforts have identified permanent deformation behavior of pavement materials under a given set of material, load, and environmental conditions, in three distinct stages. This simplified, yet effective, approach is widely used. Figure 1-3 illustrates the three stages, which can be described as follows:

- Primary Stage—High initial level of rutting, with a decreasing rate of plastic deformations, predominantly associated with volumetric change;
- Secondary Stage—Small rate of rutting exhibiting a constant rate of rutting change that is also associated with volumetric changes; however, shear deformations increase at increasing rate; and

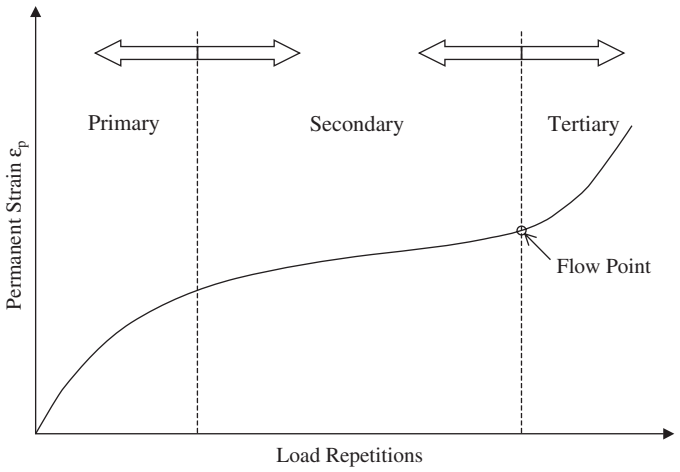

Figure 1-3. Typical repeated load permanent deformation behavior of pavement materials.

- Tertiary Stage—High level of rutting predominantly associated with plastic (shear) deformations under no volume change conditions.

The MEPDG utilizes an approach that models both the primary and secondary stages with two major simplifications. First, the primary stage is modeled using an extrapolation of the secondary stage trend. The second simplification is that the tertiary stage, although also very important, is not taken into account. Permanent deformation tests to reach this stage are extremely time-consuming and difficult to perform; therefore, very little research has been devoted to this type of analysis. Hence, it should be understood that true plastic shear deformations are not modeled within the system (in fact, few—if any—rutting prediction models incorporate this stage).

In addition to the above-mentioned limitation, it should be realized that the permanent deformation approach is not applicable for cementitiously stabilized, bedrock, or PCC fractured slab materials. These materials are assumed to have no contribution to the permanent deformation of the pavement because these materials normally are not very susceptible to this type of distress.

For overlay design, permanent deformation of existing HMA layers is not considered and is assumed to be zero. Although it is possible to start the analysis at the time these layers were placed, the total time to run the analysis will be significantly greater with little benefit. Normally, these layers will have little contribution to the total deformation because both the aging process is complete and the rate of deformation for an already consolidated layer is small. In addition, milling operations (or even rut filling operations) prior to overlay may restore the existing distorted surface back to a leveled (non-rutted) surface.

1.5.4 General Approach for Calculating Permanent Deformations

As mentioned earlier, the approach presented in the MEPDG is based upon incremental damage. The damage or rutting is estimated for each subseason defined and at the mid-depth of each sublayer within the pavement system. To estimate the permanent deformation of each individual sublayer, the system verifies the type of layer, applies the model corresponding to the material type of the sublayer, and computes for the plastic strain accumulated at the end of each subseason. The overall permanent deformation for a given season is the sum of permanent deformation for each individual layer and is mathematically expressed as

$$PD = \sum_{i=1}^{nsublayers} \varepsilon_p^i \times h^i \qquad (1\text{-}5)$$

where

PD = pavement permanent deformation,
$nsublayers$ = number of sublayers,
ε_p^i = total plastic strain in sublayer i, and
h^i = thickness of sublayer i.

The process is repeated for each load level, subseason, and month of the analysis period. Within the MEPDG, permanent deformation is only estimated for the asphalt bound and unbound layers. No permanent deformation is estimated for cementitiously stabilized materials. The estimation of permanent deformation for asphalt bound and unbound layers is discussed in the following paragraphs.

Permanent deformation (rutting) of asphalt mixtures is one of the most important distress types in flexible pavement systems. Major research efforts are now underway to ensure that this important characteristic of asphalt materials is considered in both the mixture design stage and the structural design aspects of flexible pavement performance. In fact, there is a strong possibility that a new fundamental simple performance test (SPT) will be developed that will also be linked directly to the permanent deformation properties developed in this project.

The MEPDG provides the user with the capability to predict rutting within all asphalt and unbound layer materials. The constitutive relationship used in the MEPDG will be based initially upon the statistical analysis of laboratory repeated load permanent deformation tests. This model form is

$$\frac{\varepsilon_p}{\varepsilon_r} = aN^b \qquad (1\text{-}6)$$

where

ε_p = accumulated plastic strain at N repetitions of load;
ε_r = resilient strain of the asphalt material as a function of mix properties, temperature, and time rate of loading;
N = number of load repetitions; and
a, b = non-linear regression coefficients.

While statistical relationships used for asphalt mixtures are reasonable, it is quite likely that a field adjustment factor, β_r, will be necessary and determined from the calibration-validation effort using the LTTP data. As a consequence, the most likely MEPDG equation will be of the following form:

$$\varepsilon_p = \beta_r \varepsilon_r a N^b \qquad (1\text{-}7)$$

Leahy conducted one of the original studies (*14*) utilizing this particular model form. This study utilized over 250 HMA mix specimens, evaluated for their repeated load permanent deformation behavior. A total of 2,860 permanent strain data points were calculated from these tests using the regressed coefficients a and b at various load repetitions. The resilient strain was assumed to be reasonably constant and independent of the number of load repetitions. The experimental

factorial included three HMA levels, three stress levels, two binder types, three temperatures, and two aggregate types. The model recommended by Leahy relating the ratio of cumulative plastic to elastic strain was

$$\log\left(\frac{\varepsilon_p}{\varepsilon_r}\right) = -6.631 + 0.435\log N + 2.767\log T + 0.110\log S + 0.118\log\eta + 0.930\log V_{beff} + 0.5011\log V_a \quad (1\text{-}8)$$
$$R^2 = 0.76$$

where

ε_p = accumulated permanent strain,
ε_r = resilient strain,
N = number of load repetitions,
T = mixing temperature (degrees F),
S = deviatoric stress (psi),
η = viscosity at 70°F (10^6 poise),
V_{beff} = effective asphalt content, percent by volume, and
V_a = air void content, percent.

A sensitivity analysis performed on the model showed that temperature was by far the most important variable. The model was less sensitive to loading conditions, material type, and mix parameters.

The Leahy model statistics of $R^2 = 0.76$ are considered quite good in any statistical modeling techniques. However, part of the accuracy of this model was achieved by incorporating several independent variables that, while increasing the R^2 value, limit the implementation usefulness of the model.

Ayres reanalyzed the original Leahy data, as well as additional laboratory data that had been developed at the University of Maryland. Ayres (*15*) recommended the following model:

$$\log\left(\frac{\varepsilon_p}{\varepsilon_r}\right) = -4.80661 + 2.58155\log T + 0.429561\log N \quad (1\text{-}9)$$
$$R^2 = 0.725$$

Ayres reported that this new model represented a small decrease in the explained variances of the original Leahy model ($R^2 = 0.725$ compared to $R^2 = 0.76$). He attributed this difference to the elimination of the four predictor variables from the original Leahy model. This appeared to be quite justified, as the Ayres model becomes quite direct to implement in systems modeling rutting behavior. This benefit is gained through a very small loss (3%) in the R^2 value.

Finally, the work conducted in NCHRP Project 9-19, "Superpave Support and Performance Models Management," completed in 2006 at Arizona State University yielded more HMA mixture data from repeated load permanent deformation testing.

These tests were conducted in the Special Geometry and Aggregate Size Study and Simple Performance Test of NCHRP Project 9-19 Task C. The mixtures, temperatures, and stress levels investigated by Kaloush (*12*) greatly expanded the data range of the variables introduced in the statistical modeling. Although this aspect is a direct benefit to any statistical regression techniques, one logical consequence of a broader database is to lower the correlation coefficient of the developed model.

The database examined by Kaloush used the original Leahy data in combination with the Superpave Models Task C findings. This resulted in a total database of 3,476 permanent strain data points being used in the regression analysis. Several models were developed by Kaloush, reflecting a differing number of independent variables used in the equation. They are as follows:

$$\log\left(\frac{\varepsilon_p}{\varepsilon_r}\right) = -3.15552 + 1.734\log T + 0.39937\log N$$

and (1-10)

$$R^2 = 0.644 \qquad S_e = 0.321 \qquad \frac{S_e}{S_y} = 0.597$$

$$\log\left(\frac{\varepsilon_p}{\varepsilon_r}\right) = 0.3082 + 0.3534\log N \quad (1\text{-}11)$$

$$R^2 = 0.550 \qquad S_e = .363 \qquad \frac{S_e}{S_y} = 0.675$$

The equation with the temperature term has approximately 10% greater R^2 than the equation without it. Because this is a significant improvement in overall model accuracy, this equation (using both the N and T terms) has been selected for use in the MEPDG. It is a relatively simple equation to use in the implementation process. Thus, the final lab expression that has been selected is

$$\frac{\varepsilon_p}{\varepsilon_r} = 10^{-3.15552} N^{0.39937} T^{1.734} \quad (1\text{-}12)$$

The field-calibrated form of this model that is used in the MEPDG is the following:

$$\frac{\varepsilon_p}{\varepsilon_r} = 10^{-3.15552*\beta_{1r}} N^{0.39937*\beta_{2r}} T^{1.734*\beta_{3r}} \quad (1\text{-}13)$$

The computational power and simplicity of this equation form needs to be clearly noted. Given a particular layered pavement cross section, the vertical resilient strain at any given depth (along a vertical axis, defined in the x, y plane) is defined by knowledge of the three-dimensional stress state and the elastic properties (modulus and Poisson's ratio) of the HMA layer in question from the following:

$$\varepsilon_{rz} = \frac{1}{E^*}(\sigma_z - \mu\sigma_x - \mu\sigma_y) \quad (1\text{-}14)$$

The complex moduli of asphalt mixtures are employed in the MEPDG via a master curve. Thus, E^* is expressed as a function of the mix properties, temperature, and time of load.

Knowledge of the vertical resilient strain at any point, along with the ε_p relationship, allows for the direct calculation

of the plastic strain, ε_p, at any given point within the asphalt layer after N repetitions of load to be computed.

The incremental rut depth at each depth, along the x, y axis, through the HMA layer can be found from

$$\Delta R_{d_i} = \varepsilon_{p_i} . \Delta h_i \quad (1\text{-}15)$$

Finally, by simply summing all incremental ΔR_d through the entire layer, one can obtain the total layer rut depth from

$$R_d = \sum_{i=1}^{n} \Delta R_{d_i} \quad (1\text{-}16)$$

1.5.5 Permanent Deformation Implementation—General Approach for Linear Elastic Analysis

Models for permanent deformation in the MEPDG system provide the plastic strain under specific pavement conditions for a total number of load repetitions. Because conditions vary from one season to another (e.g., temperature, resilient strain, moisture) and it is necessary to account for the total plastic deformation up to the specific season i, it is necessary to use a special approach.

For the general solution, permanent deformation is estimated for each layer and at each computational location using pavement responses calculated through JULEA at the mid-depth of each sublayer.

Computations of permanent deformations are done at locations defined by the analysis module for regular traffic. Alternatively, for special wheel configurations, the user is allowed to select the location points of interest for evaluation. In the ensuing models described, the equivalent number of load cycles for each subseason is found by solving the permanent deformation model for N with the accumulated deformation up to the subseason and the material properties and load conditions prevailing in the given subseason.

The approach is illustrated in Figure 1-4 with a model in the following form:

$$\varepsilon_p = f(\varepsilon_r, T, N) \quad (1\text{-}17)$$

where

ε_p = total plastic strain,
ε_r = resilient strain,
T = temperature, and
N = total number of load cycles.

The total plastic strain $\varepsilon_{p,i-1}$ at the end of subseason *i-1* corresponds to a total number of traffic repetitions Nt_{i-1} (point A). In the next subseason i, the layer temperature is T_1 and resilient strain for load and material conditions prevailing in i is $\varepsilon_{r,i}$.

At the beginning of the next subseason i (point B), there is an equivalent number of traffic repetitions $Nteq_i$ that is associated with the total deformation at the end of subseason *i-1* but under conditions prevailing in the new subseason (T_1, $\varepsilon_{r,i}$). The approach is necessary because models for permanent deformation provide an estimate of the total deformation rather than the increment in plastic strain due to a seasonal traffic.

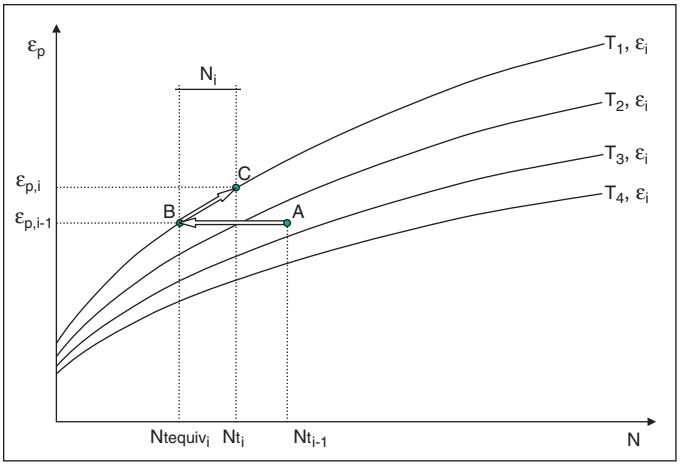

***Figure 1-4. Permanent deformation approach in the* MEPDG.**

By adding the number of traffic repetitions at season i (N_i) to the total equivalent number of repetitions $Nteq_i$, using the specific material model, it is possible to estimate point C, which corresponds to the total plastic strain at the end of subseason i.

1.6 WesTrack Approach

The WesTrack models were recently developed to determine the importance of different mixture properties and their variance as related to rutting in establishing performance-related specifications. Two models were developed from the study: Level I is an empirical model relating mix properties to rut depth, and Level II is based on M-E principles. For Level I, rut depth is a function of ESALs, air voids, asphalt content (percent by weight), and the percentage of aggregate finer than the No. 200 sieve. The Level II analysis consists of calculating the permanent shear strain (γ) at 2 in. (50 mm) below the surface, shear stress (τ), and compressive strain (ε_v) on top of the subgrade. Total rut depth measured at the surface is expressed as a function of the number of load repetitions by combining the rut depth predicted in the HMA layer and unbound layers.

In simple loading, permanent shear strain in the HMA was assumed to accumulate according to the following equation:

$$\gamma_p = ae^{(b\tau\gamma_e N^c)} \quad (1\text{-}18)$$

where

γ_p = plastic or inelastic shear strain at a depth of 2 in. (50 mm) below the surface,
γ_e = elastic shear strain at the same depth noted above,
N = number of axle load applications, and
a, b, c = regression constants.

The time-hardening principle was used to estimate the accumulation of the inelastic strains in the HMA under in situ conditions by the following equations:

$$a_t = ae^{(b\tau\gamma t,e)} \quad (1\text{-}19)$$

$$\gamma_{p,1} = a_1[\Delta N_1]^c \quad (1\text{-}20)$$

$$\gamma_{p,t} = a_t\left[\left(\frac{\gamma_{p,t-1}}{a_t}\right)^{\frac{1}{c}} + \Delta N_1\right]^c \quad (1\text{-}21)$$

where

ΔN_t = number of load applications during the t^{th} hour,
$\gamma_{e,t}$ = elastic shear strain at the t^{th} hour, and
t = the t^{th} hour of traffic applications.

The rutting that is estimated in the HMA layer due to the shear deformations is determined from the following equation where K equals a coefficient related to the thickness of the HMA layer (see Table 1-2).

$$RD_{HMA} = K\gamma_{p,t} \quad (1\text{-}22)$$

The rut depth contribution from all unbound materials or layers within the pavement structure is calculated by the following equation:

$$RD_{Unbound} = \frac{0.14}{\left[1.05x10^{-9}\left(\varepsilon_{v(Unbound)}\right)^{-4.484}\right]^{0.372}}(N)^{0.372} \quad (1\text{-}23)$$

The WesTrack procedure uses a similar time-hardening principle for the unbound materials, as used for the HMA and by the MEPDG. Rut depth accumulation can be expressed in the following form:

$$RD_{t(Unbound)} = d_t\left[\left(\frac{RD_{t-1(Unbound)}}{d_t}\right)^{\frac{1}{0.372}} + \Delta N_t\right]^{0.372} \quad (1\text{-}24)$$

where

$$d = \frac{0.14}{\left[1.05x10^{-9}(\varepsilon_{v(Unbound)})^{-4.484}\right]^{0.372}} \quad (1\text{-}25)$$

$\varepsilon_{v\ (Unbound)}$ = vertical compressive strain in an unbound aggregate base/subbase layer or subgrade soil.

The total rut depth measured at the surface of the pavement is simply the estimated rut depth from the HMA layers plus the rut depth from the unbound layers and subgrade soil, as shown below:

$$RD = RD_{HMA} + \sum_{i=1}^{I} RD_i \quad (1\text{-}26)$$

1.7 Evaluation of Flow Number

The repeated load flow number (F_n) test is a dynamic creep test where a haversine type of loading is applied with loading and rest periods between loadings. As shown in Figure 1-3, the typical results between the measured permanent strain and load cycle, the permanent strain, can be divided into three major zones. In the primary phase, the strain rate decreases; in the secondary phase, the permanent strain rate is constant; and in the tertiary phase the permanent strain rate dramatically increases. At low stress levels, the material may mainly exhibit primary and/or secondary permanent strain. In this case, the permanent strain rate may approach a value equal to zero as the total strain reaches a certain value. This also suggests that at this very low stress level the tertiary flow region may never appear within a reasonable amount of time. At higher stress levels, the constant secondary permanent strain rate phase depends on the stress level applied.

Ideally, the large increase in permanent strain generally occurs at a constant volume within the tertiary zone. The flow number is therefore defined as the postulated cycle when shear deformation, under constant volume, starts. This is the point when tertiary flow starts in the mixture. This is the point where the rate of change of permanent strain reaches the minimum value. So, the flow number can be viewed as the minimum point in the relationship of rate of change of permanent strain versus loading cycle. The approach used in this analysis to find the flow number was as follows.

Table 1-2. Suggested values of *K* as a function of HMA layer thickness.

HMA Thickness, Inches	*K* Value
5 to 7	5.5
7 to 9	7.0
9 to 12	8.5
>12	10.0

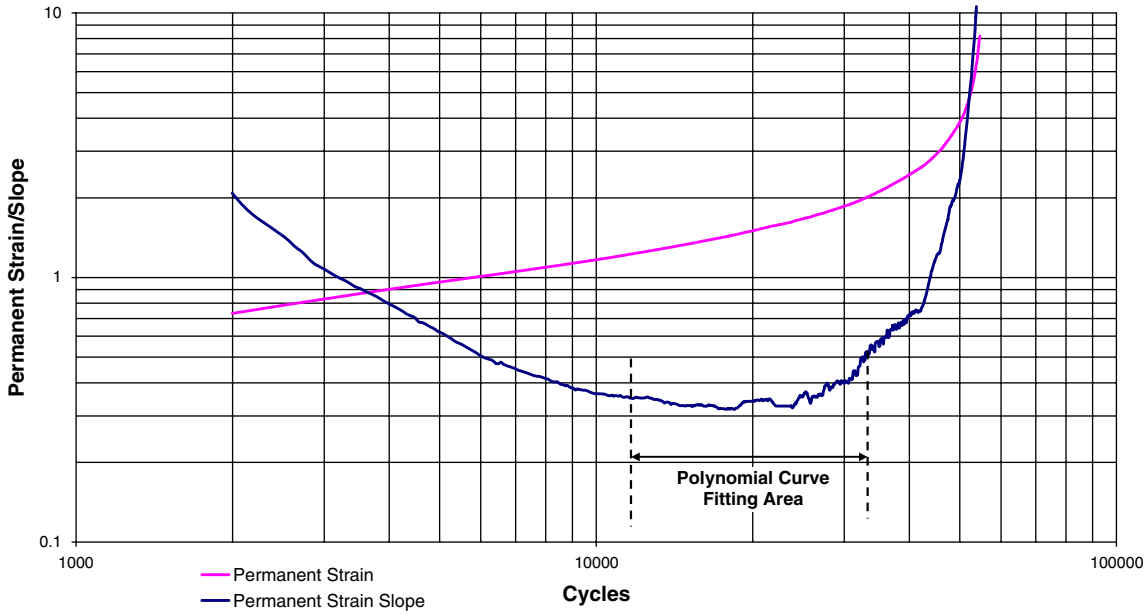

Figure 1-5. Repeated load flow number permanent strain/slope plot (13).

Figure 1-5 shows the accumulated strain and slope versus cycles in log-log domain. Around the secondary-tertiary zone, the slope curve seems to reach the minimum value and the slope curve can be described by a polynomial curve. The minimum slope point on the log scale unit of cycles is found n_i. Then, at a specific cycle n_i, a polynomial equation is fitted by a significant number of points, to define the polynomial. The form of this equation is

$$\varepsilon p(n)_i = a + bn + cn^2 \quad (1\text{-}27)$$

where

$\varepsilon p(n)_i$ = permanent strain at cycle n for n_i point evaluated,
n = loading cycle, and
a, b, c = regression coefficients.

By taking the derivative of the equation, one obtains the following:

$$\frac{d(\varepsilon p(n)_i)}{dn} = b + 2cn \quad (1\text{-}28)$$

Therefore, the rate of change in permanent strain at cycle n_i is equal to b plus $2cn_i$. For each datapoint selected one can obtain the rate of change in permanent strain by repeating the above procedure. Once all the rates of change in permanent strain are calculated, one can find the zero value of rate of change in permanent strain (i.e., the flow number). This is accomplished by another polynomial curve fitting using equal datapoints on both sides of the minimum value. Theoretically the flow number is the cycle corresponding to a rate of change of permanent strain equal to zero.

1.8 Evaluation of Flow Time

Figure 1-6 shows typical test results between the calculated total compliance and time in an unconfined state creep test. This figure shows that the total compliance can be divided into three major zones: the primary, secondary, and tertiary flow zones.

In general, the large increase in compliance generally occurs at a constant volume within the tertiary zone. The flow time (F_t) is therefore defined as the postulated time when shear deformation, under constant volume, starts. The flow time also is viewed as the minimum point in the relationship of rate of change of compliance versus loading time. This is the point at which tertiary flow starts in the mixture. This is the point where the rate of change of compliance reaches the minimum value. So, the flow time can be viewed as the minimum point in the relationship of rate of change of compliance versus

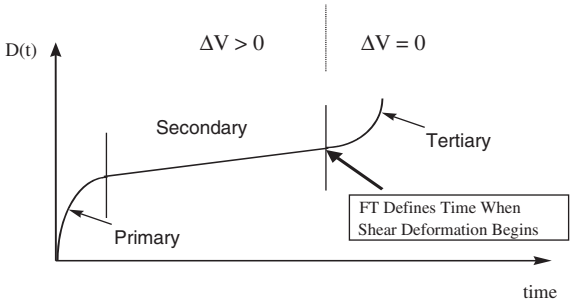

Figure 1-6. Typical test results for the calculated total compliance and time.

loading cycle. The approach used in this analysis to find the flow time was as follows.

The minimum slope point on the log scale unit of time is found time *t*. Then, at a specific time *t*, a polynomial equation is fitted by a significant number of points "*i*", to define the polynomial. The form of this equation is:

$$D(t) = a + bt + ct^2 \quad (1\text{-}29)$$

where:

$D(t)$ = compliance at time t for i point evaluated
t = time of loading
a, b, c = regression coefficients

By taking the derivative of the equation, one obtains the following:

$$\frac{d(D(t)_i)}{dt} = b + 2ct \quad (1\text{-}30)$$

Therefore, the rate of change in compliance at time t_i is equal to $b + 2ct_i$. For each data point selected one can obtain the rate of change in compliance by repeating the above procedure. Once all the rates of change in compliance are calculated, one can find the zero value of rate of change in compliance, i.e., the flow time. This is accomplished by another polynomial curve fitting, using equal data points on both sides of the minimum value. Theoretically the "flow time" is the time corresponding to a rate of compliance change equal to zero.

1.9 Correlation between Test Temperature and Stress Level on Flow

For the practical implementation of flow number or flow time as SPT and to develop the SPT criteria, the effects of temperature and stress were studied. The research done by Kaloush (*12*), and Hafez (*16*) showed the definite temperature and stress effect on flow number and flow time. In 2002, Kaloush (*12*), and Sullivan (*13*) made very good progress in the time-temperature superposition study. This study provided a very good guideline for the final test protocol for the simple performance test. If the principle of time-temperature superposition is valid for HMA at one or both of the flow number and flow time parameters and common (small strain linear based) time-temperature superposition factors apply, a significant reduction in the required laboratory testing requirements could be achieved. In asphalt mixture design and analysis, this would allow one to utilize shift factors achieved from E* testing and directly apply them to the flow parameters (F_n or F_t) determined at any test temperature to determine the response at any other temperature of interest. (*13*) Similarly, this stress shift concept would provide a good way of performing a simple performance test at a convenient stress level, which could then be converted to an effective stress level.

1.9.1 Time-Temperature Superposition

The NCHRP Project 9-19 research team has found that time-temperature superposition concepts may be valid in mixtures having a well-defined degree of damage. Kaloush (*12*) performed the primary study in which using dynamic modulus testing shift factors could be used to shift the values of flow number or flow time. Sullivan proved this correlation with two major objectives in mind. The first objective was to determine whether the time-temperature superposition holds for both flow number and flow time testing with damaged specimens until tertiary flow. The second was to compare the flow number/flow time shift factors to the E* shift factors. Sullivan used three test cells from MnRoad and four separate test temperatures with one constant stress level. The time-temperature superposition principle was then applied to the measured flow parameters F_t or F_n using the flow parameters as the time variable to determine the temperature shift factor $\alpha(T)$ by

$$F_{tR} \text{ or } F_{nR} = \frac{F_n \text{ or } F_n}{\alpha(T)} \quad (1\text{-}31)$$

where

F_n or F_t = measured flow parameter at any temperature and
F_{nr} and F_{tr} = flow parameter at the selected reference temperature.

Sullivan (*13*) conducted a temperature-shifting study on three MnRoad cells that had common aggregate gradation and used an AC120/150 binder. Both flow number and flow time testing was conducted at four separate temperatures (85, 100, 115, and 130°F) and one constant stress level of 25 psi (172 kPa). Then the shift factor was calculated by the above equation. The temperature shift factors from E* were taken from NCHRP Project 9-19 Phase II dynamic modulus testing. E* shift factors were changed from a reference temperature of 70°F to the flow number and flow time reference temperature of 100°F. The comparison between shift factors determined from E* and flow testing (flow number and flow time) showed smooth continuous curve for flow testing and indicated that flow number and flow time results are thermologically simple up until the tertiary region and that there would be a very good correlation between flow number and flow time.

1.9.2 Comparison of Temperature Shifting Results

Sullivan (*13*) compared E* shift factors to the shift factors from flow number and flow time tests. The shift factor relationship shows the existence of a high correlation between

the E* and flow shift factors, indicating that the shift factors obtained for E* can be applied to the results of flow number or flow time testing also.

1.9.3 Flow Number-Flow Time Stress Dependency Master Curve

The purpose of the formation of a flow number-flow time stress dependency master curve was to predict flow parameters incorporating test temperature and stress in one model. In this way it would be possible to do the testing at a convenient temperature and stress level. Then, using the master curve, the flow parameters can be calculated at the desired stress level. Sullivan (*13*) described the stress dependency master curve as a sigmoidal function in the log-log space as follows:

$$Log(\sigma) = \delta + \frac{\alpha}{1 + e^{\beta+\gamma(\log(F_{nr} or\ F_{tr}))}} \quad (1\text{-}32)$$

where

σ = applied stress,
$t_r = F_t$ or F_n at the reference temperature,
δ = minimum stress that will cause damage,
$\delta + \alpha$ = maximum stress that will cause instantaneous damage, and
β, γ = parameters describing the shape of the sigmoidal function.

To build up this model, Sullivan (*13*) used four mixes and two confining pressures using global values of fitting parameters (β and γ), with α being a linear function of δ. Using the linear optimization, Sullivan got the final model as follows:

$$\log(F_{nr}) = \frac{\ln\left(\frac{-1.30118(\delta) + 4.34383}{\log(\sigma_1) - \delta} - 1\right) + 0.71385}{0.289212} \quad (1\text{-}33)$$

1.9.4 Steps Undertaken to Produce Stress Dependency Master Curves

Sullivan presented the following steps to create stress dependency master curve. The list below shows all of the steps undertaken from the initial time-temperature superposition principle through to the determination of the sigmoidal fitting parameters from Sullivan's study (*13*).

- The first step is to determine the temperature "reduction" factor by using the time-temperature superposition principal. The purpose of which is to "reduce" the measured flow time or flow number recorded at any temperature other than the reference temperature to an equivalent flow time or flow number that would be found at the reference temperature and the tested stress level. This is undertaken by recording flow time or flow number at the same stress level (25 psi; 172 kPa) and four test temperatures (85, 100, 115, and 130°F). The shift factor ($\alpha(T)$) for each test temperature is then determined by

  $$\log(\alpha(T)) = \log({}^{Fn}/_{(Fn\ at\ reference\ temperature)})$$

  In this case, a reference temperature of 100°F was used.
- The $\log(\alpha(T))$ values where then plotted against the test temperature and by using a polynomial curve to fit the measured data the equation of $\log(\alpha(T))$ versus temperature was then determined for each mix.
- Using varying stress levels for each mix, the values of flow time or flow number were then measured at the varying stress levels.
- The measured F_t or F_n is then "reduced" to the reference temperature (100°F) (i.e., the measured values at a temperatures other than 100°F are reduced to the value that would be obtained at a test temperature of 100°F) by the temperature shift factor according to

  $$t_R = \frac{F_t\ or\ F_n}{\alpha(T)} \text{ or } \log(F_{nr} \text{or } F_{tr} = \log(F_{n/t}) - \log(\alpha(T)) \quad (1\text{-}34)$$

- F_{tr} or F_{nr} is then plotted against the applied stress and the fitting parameters (α, β, γ, and δ) of the sigmoidal function are then calculated by non-linear optimization methods such as the solver module in Excel.

1.10 SPT Criteria Development

As a part of the NCHRP Project 9-19, Kaloush showed the conceptual design for the simple performance test criteria by using the repeated load test. If the actual traffic loading patterns, magnitude and rate of deformation, and stress state in the field were considered, it was felt that the confined repeated load permanent deformation test would be the better laboratory test to simulate field conditions (*12*). Kaloush showed three laboratory test parameters from two tests (flow number and flow time) having good to excellent correlations with field rut depth. Those three parameters were the flow time from the static creep test, the flow number of the repeated load test, and the permanent strain (ε_p) from the repeated load permanent deformation test. Sullivan (*13*) suggested a combination of flow number and ε_{pf} can be used to define a unique point in deformation/time space and should be a good predictor of rut depth for standard traffic loadings.

1.10.1 Reduced Flow Number Shifting Concept

Sullivan (*13*) showed that the temperature-reduced flow number and rut depth measurements plotted in logarithmic coordinates are essentially parallel lines. Figure 1-7 shows the

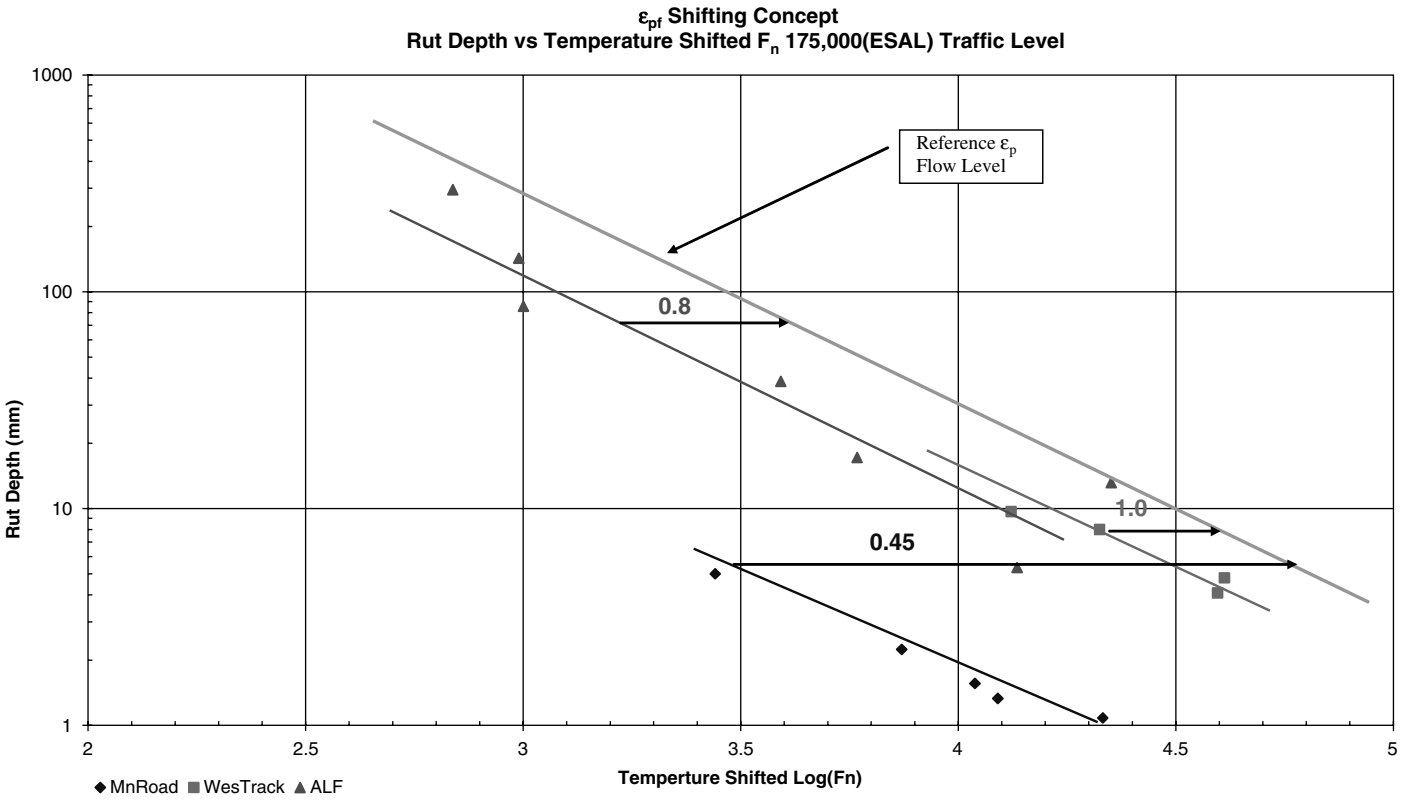

Figure 1-7. Temperature-shifted flow number versus field rut depth.

distance from any relative point to the right of the data decreases as the level of ε_{pf} increases. This figure shows that the flow number values can be shifted horizontally along the flow number axis relative to the level of ε_{pf}. On the other hand, relative to a level of ε_{pf} at some arbitrarily selected reference level, the rut depth measurements could be shifted vertically. This correlation shows that the shift function ($\alpha\varepsilon_{pf}$) appears to be a linear function in logarithmic coordinates as a function of ε_{pf} that is as follows:

$$\log(F_n((\varepsilon_{pf})) = \log(F_n) + a\log((\varepsilon_{pf}))$$

To test the validity of this concept, Sullivan (*13*) analyzed results for 16 mixes, including temperature, reduced flow number, $\varepsilon_{pf,}$ and 175,000-ESAL traffic level. This analysis showed that by using the level of ε_{pf}, the results of the flow number can be "normalized" to a constant level of failure and thus provide a very good indication of the rutting potential of asphalt mixtures.

1.10.2 Traffic-Shifting Concept

The ε_{pf}-reduced flow number is valid only for a constant traffic level. But since traffic levels are not constant, to be truly able to rate mixes as to their performance potential the actual level of traffic must be included. Analysis showed that the temperature-reduced flow number and rut depth plotted in logarithmic coordinates essentially form parallel lines for varying traffic levels. Therefore, the rut depths can be shifted vertically with increasing traffic levels.

This suggests that a shifting process can be incorporated in which the flow number is shifted horizontally along the flow number axis or, alternatively, is shifted vertically along the rut depth axis as a function of the relative traffic level. So, in the case of traffic shifting, the shift function (α_{Traff}) appears to be a linear function in logarithmic coordinates, that is, $\log(Rut(Traff)) = \log(Rut) + a\log((Traff)) + b$.

1.10.3 Determination of Rut Depth from Repeated Load Test Results

Sullivan (*13*) used three test site samples selected from NCHRP Project 9-19 to calibrate and optimize the proposed shifting procedure. FHWA-Accelerated Loading Facility (ALF), WesTrack, and ALF mixes were chosen to optimize the results both for confined and unconfined testing. For example, Sullivan suggested the following seven steps and associated equations to get field rut depth by using unconfined repeated load tests:

Step 1. Determine the effective field temperature (T_{eff} °F).

Step 2. Determine the flow number (F_n) and plastic strain at failure (ε_{pf}) at any temperature (T_t°F) and stress level (σ).

Step 3. Perform the stress shifting and determine the flow number in reference stress (F_{nr}) with the following equations:

$$\delta = \frac{(e^{\log(F_n)0.289212-0.71385)}+1)\mathrm{Log}(\sigma)-4.34383}{-1.30118+(e^{\log(F_n)0.289212-0.71385)}+1)} \quad (1\text{-}35)$$

and

$$\log(F_{nr}) = \frac{\ln\left(\frac{-1.30118(\delta)+4.34383}{\log(\sigma_1)-\delta}-1\right)+0.71385}{0.289212} \quad (1\text{-}36)$$

Here, the stress level should be the reference stress level used in criteria development.

Step 4. Perform temperature shifting and determine the reduced flow number at field temperature (F_{nR}). Using the E* testing results, the polynomial constants of the temperature shift equation are found where the equation form is

$(\alpha)T = aT^2 + bT + c$

Since the mixture was tested at T_t °F , the E* shift factors, which were determined at a reference temperature of 70°F, need to be further shifted to the reference temperature (i.e., 100°F) and a new equation determined at the reference temperature. The flow number shift factor is determined from the E* shift factor by the following equation:

$$\alpha(T)_{F_n} = 0.0423(\alpha(T))^2 + 0.8367\alpha(T) \quad (1\text{-}37)$$

Then the flow number (F_n) is converted to the reduced flow number at effective field temperature (F_{nR}) by the following equation:

$$t_R = \frac{F_n}{\alpha(T)} \text{ or } \log(\mathrm{F_{nR}}) = \log(F_n) - \log(\alpha(T)) \quad (1\text{-}38)$$

Step 5. Determine the ε_{pf}-reduced flow number ($F_{n\varepsilon}$) by the following equation:

$$\log(F_{n\varepsilon}) = \log(F_n) - 2.290(\log(\varepsilon_{pf})) \quad (1\text{-}39)$$

Step 6. Determine the rut depth at 1 million ESALs (corresponding to the ε_{pf}-reduced flow number) by the following equation:

$$\log(Rut_{1,000,000}) = -0.6523\log(F_{n\varepsilon}) + 3.9426 \quad (1\text{-}40)$$

Step 7. Determine the rut depth at any desired ESALs by the following equation:

$$\log(\mathrm{Rut}) = \log(\mathrm{Rut}_{1,000,000}) - 0.002(\log(\mathrm{ESAL}))^2 + 0.2815(\log(\mathrm{ESAL})) - 1.6079 \quad (1\text{-}41)$$

CHAPTER 2

Test Results and Analysis

2.1 Statistical Analysis of Flow Number and Flow Time Results

Efforts in this part of the study were directed on statistical analysis of the SPT parameters, flow number and flow time. Data from mixtures with varying material properties and testing conditions were included, yielding a total of 715 flow number tests and 374 flow time tests for analysis.

Statistical analysis was done to measure the variability or dispersion between replicates of flow number and flow time from the repeated load and static creep tests, respectively. Coefficient of variation and standard deviation were used as statistical tools to measure variability, to provide better measure of variability, or both. For every set of test results, mean, standard deviation, and coefficient of variation were calculated.

Confined and unconfined flow tests were analyzed separately as well as combined. A power model in log-log domain was used to find the relation of the standard deviation among the replicates to the mean flow values.

2.1.1 Repeated Load Flow Number Test Result Analysis

The results of the repeated load flow number tests at different stress levels, temperatures, and air void levels were statistically analyzed to determine means, standard deviations, and coefficients of variation between replicates.

Figure 2-1 is a plot of standard deviation and mean flow number for confined and unconfined tests analyzed separately. Two power models are shown on the plot where standard deviation and mean flow number are used as variables. The power model in log-log domain for the confined testing had a coefficient of determination of 0.72 and the model was as follows.

$$\sigma_d = 0.2212(F_n)^{1.0279} \quad (2\text{-}1)$$

The power model for the unconfined testing had a coefficient of determination of 0.76 and the model for the unconfined testing in log-log domain was as follows.

$$\sigma_d = 0.0858(F_n)^{1.1032} \quad (2\text{-}2)$$

Figure 2-1 demonstrates that at low flow numbers, the dispersion in confined testing is higher than unconfined testing. At higher flow numbers, the dispersion is lower. For both confined and unconfined testing, the standard deviation increases with increasing mean flow numbers. From the power model developed for confined and unconfined tests, it is observed that the coefficient of variation for confined testing is higher than that for unconfined testing.

Figure 2-2 is a plot of the standard deviation versus mean flow number for the combined confined and unconfined tests. The coefficient of determination is 0.73 and the data points are well distributed about the trend line. The power model for the combined data in log-log domain is as follows:

$$\sigma_d = 0.1441(F_n)^{1.0613} \quad (2\text{-}3)$$

Figure 2-3 shows the relationship between standard deviation and mean flow number in normal scale. A linear regression model was used to get the relationship. The coefficient of variation for this plot is 0.61. The linear model for the combined data in normal scale is as follows:

$$\sigma_d = 0.6104(F_n) \quad (2\text{-}4)$$

Figure 2-4 shows the relationship between the coefficient of variation and mean flow number in normal scale. No specific trend is observed especially because the number of data points varied.

2.1.2 Static Creep Flow Time Test Results

The results of static creep flow time tests at different stress levels, temperatures, and air void levels were statistically

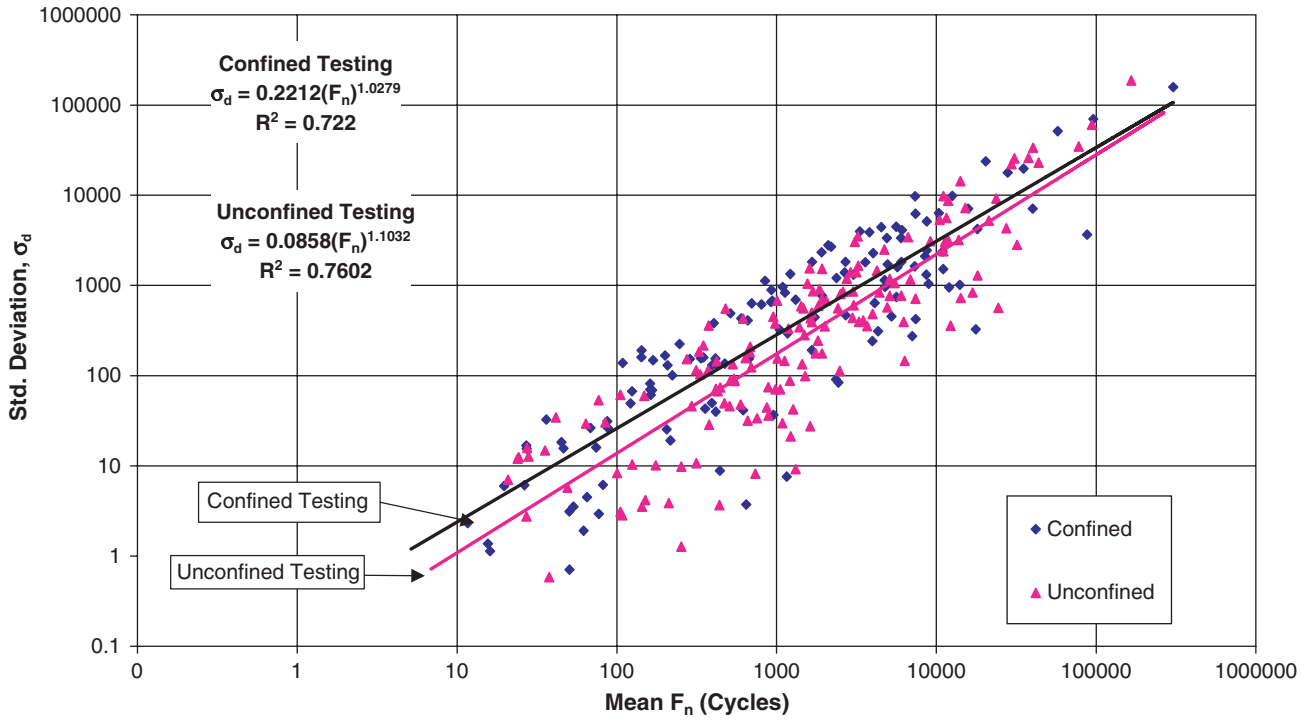

Figure 2-1. Mean flow number (confined and unconfined) versus standard deviation.

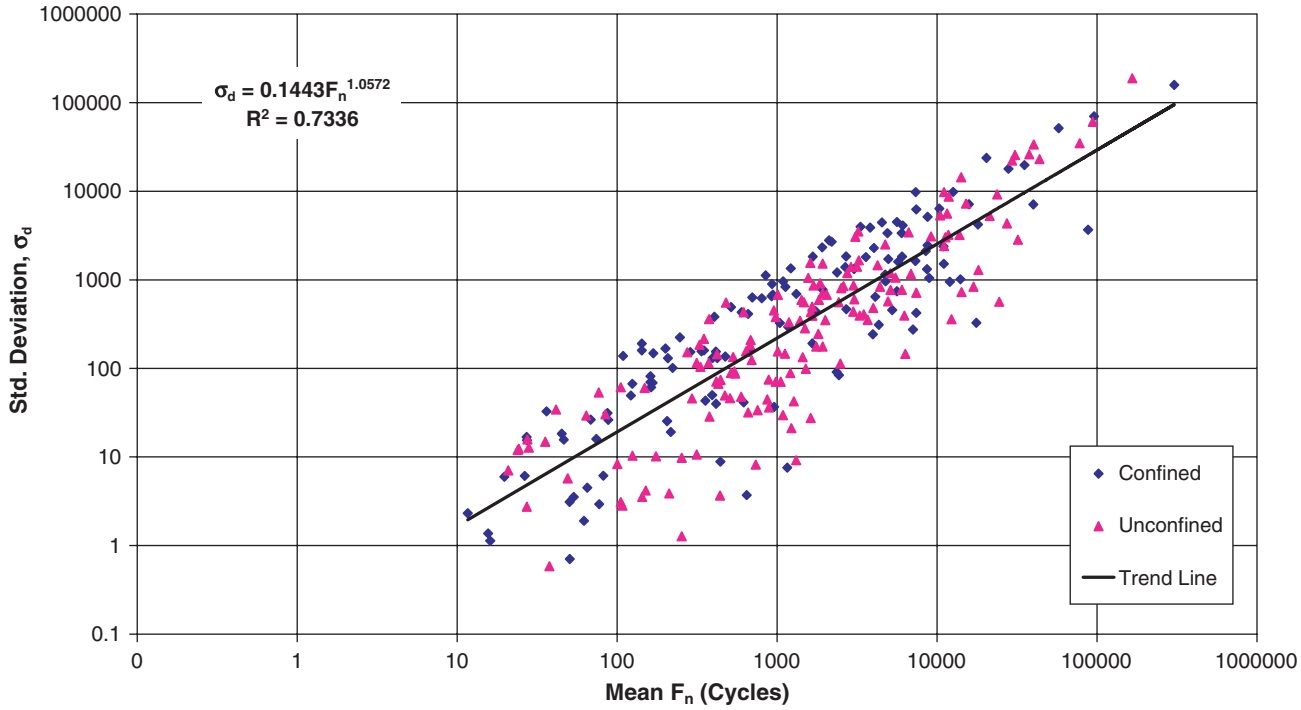

Figure 2-2. Mean flow number (confined and unconfined) versus standard deviation.

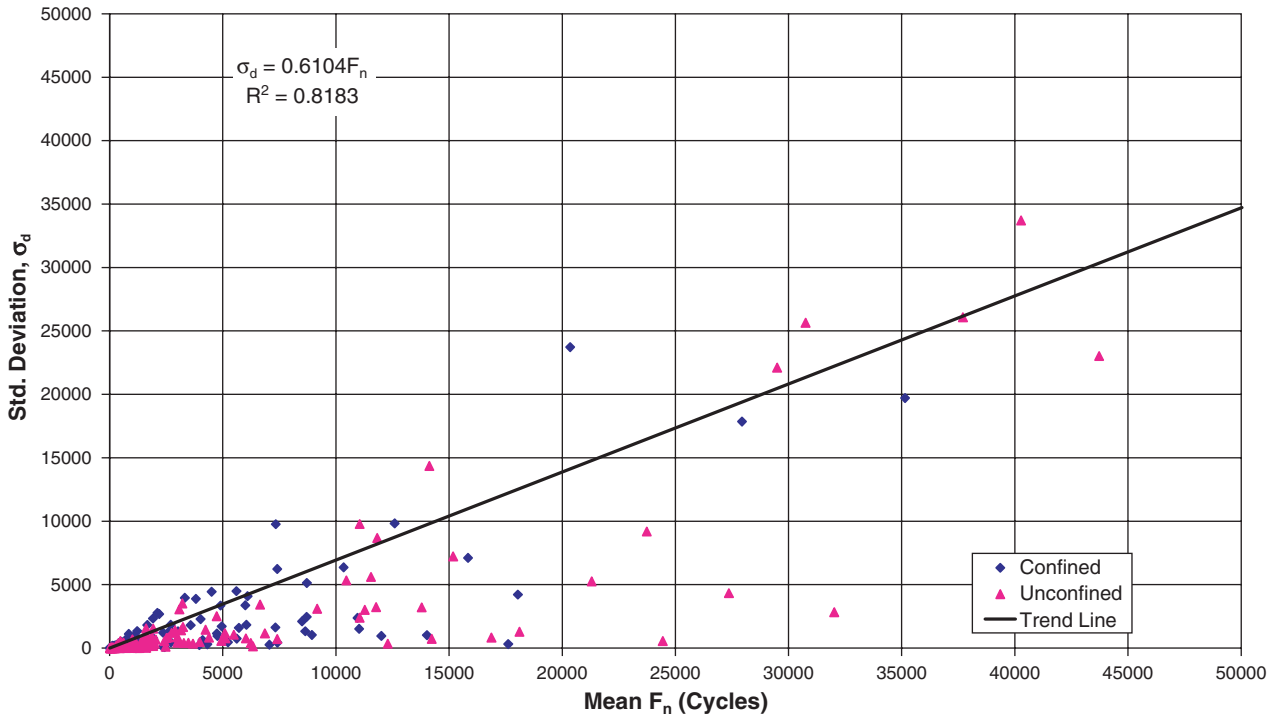

Figure 2-3. Mean flow number (confined and unconfined) versus standard deviation.

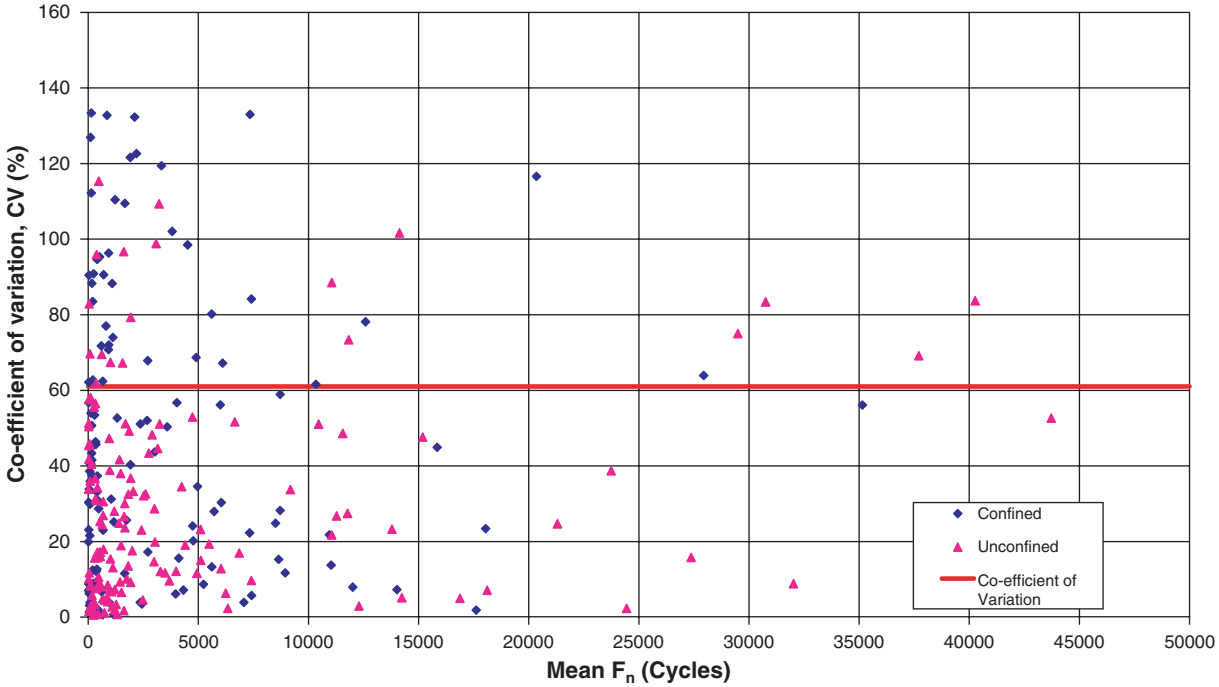

Figure 2-4. Mean flow number (confined and unconfined) and coefficient of variation.

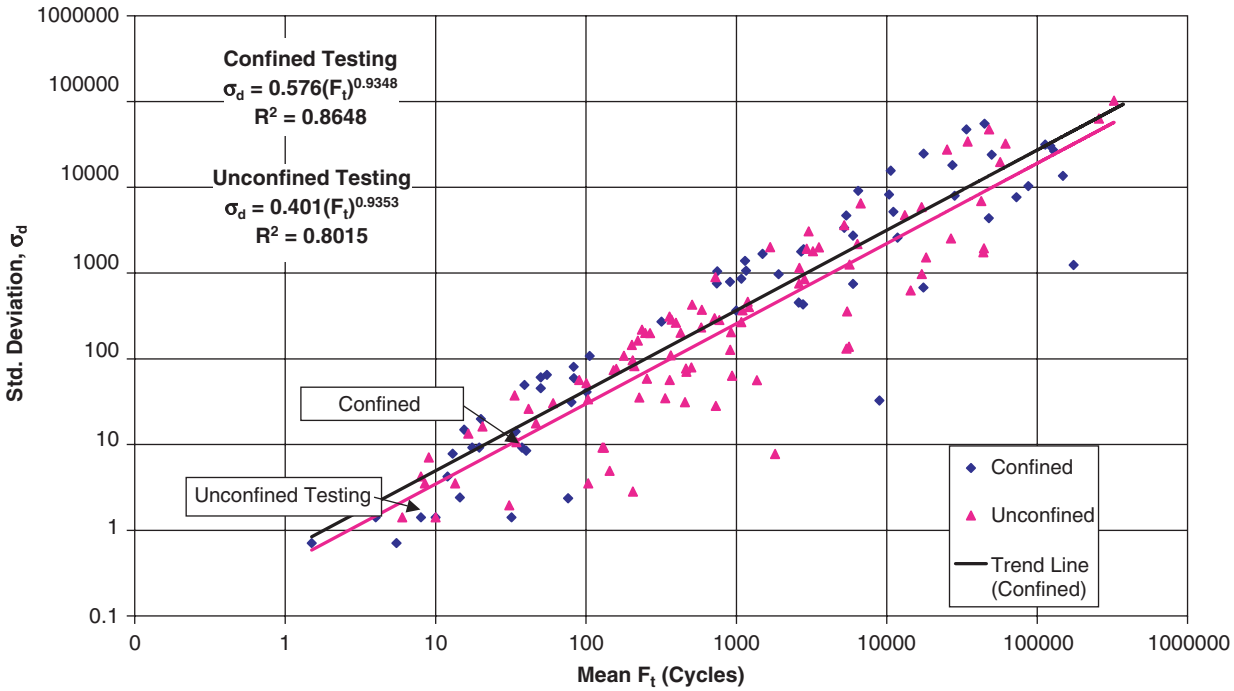

Figure 2-5. Mean flow time (confined and unconfined) versus standard deviation.

analyzed to determine means, standard deviations, and coefficients of variation between replicates.

Figure 2-5 is a plot of standard deviation and mean flow time for confined and unconfined tests analyzed separately. Two power models are shown on the plot where standard deviation and mean flow number are used as variables.

The power model in log-log domain for the confined testing had the coefficient of determination of 0.86 and the model was as follows.

$$\sigma_d = 0.5760(F_t)^{0.9348} \quad (2\text{-}5)$$

The power model for the unconfined testing had a coefficient of determination of 0.80 and the model for the unconfined testing in log-log domain was as follows:

$$\sigma_d = 0.4011(F_t)^{1.1032} \quad (2\text{-}6)$$

Figure 2-5 shows that for both confined and unconfined testing, the standard deviation increases with increasing mean flow times. From the power model developed for confined and unconfined tests, it is observed that the slope values for confined and unconfined testing are very close and they are almost parallel lines. The confined tests were more precise, thus the coefficient of determination was better for the confined than the unconfined tests.

Figure 2-6 is a plot of the standard deviation versus mean flow time for the combined confined and unconfined tests. The coefficient of determination is 0.83 and the data points are well distributed about the trend line. The power model for the combined data in log-log domain is as follows:

$$\sigma_d = 0.4630(F_t)^{0.9361} \quad (2\text{-}7)$$

Figure 2-7 shows the relationship between standard deviation and mean flow time in normal scale, with the relationship based on a linear regression model. The coefficient of variation from this plot is 0.25, which is better than that of the flow number relationship. The linear model for the combined data in normal scale is given by the following equation:

$$\sigma_d = 0.2541(F_t) \quad (2\text{-}8)$$

Figure 2-8 shows the relationship between coefficient of variation and mean flow time; no specific trend is observed.

2.2 Relationship between Flow Number and Flow Time

The objective of this part of the study was to conduct a comparison study to determine if any correlation exists between the measured flow number and flow time of repetitions obtained from the repeated load and static creep tests, respectively. This correlation would provide a practical link between the two flow parameter tests and would be of great benefit in criteria development. For a wide range of mixtures and testing conditions, this relationship would provide an important link between the prediction methodologies used to define rutting levels for a given flow time or flow number.

The initial study by Kaloush (*12*) in NCHRP Project 9-19 Phase I showed encouraging results for the relationship

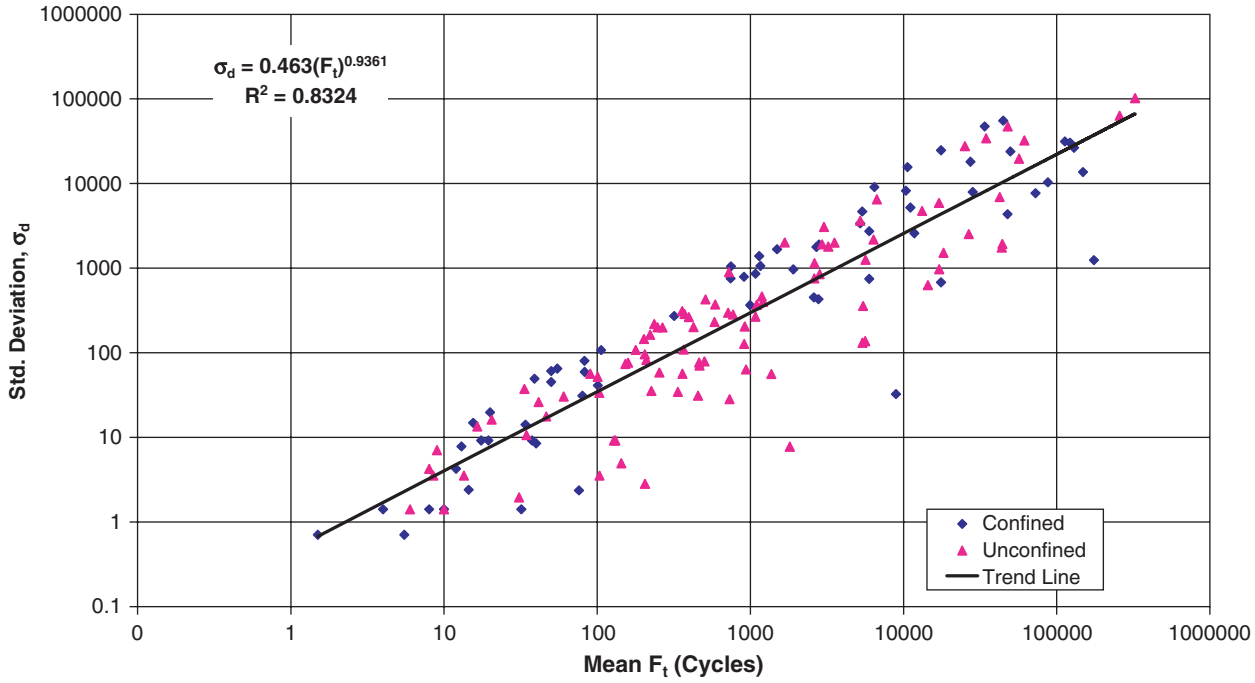

Figure 2-6. Mean flow number (confined and unconfined) versus standard deviation.

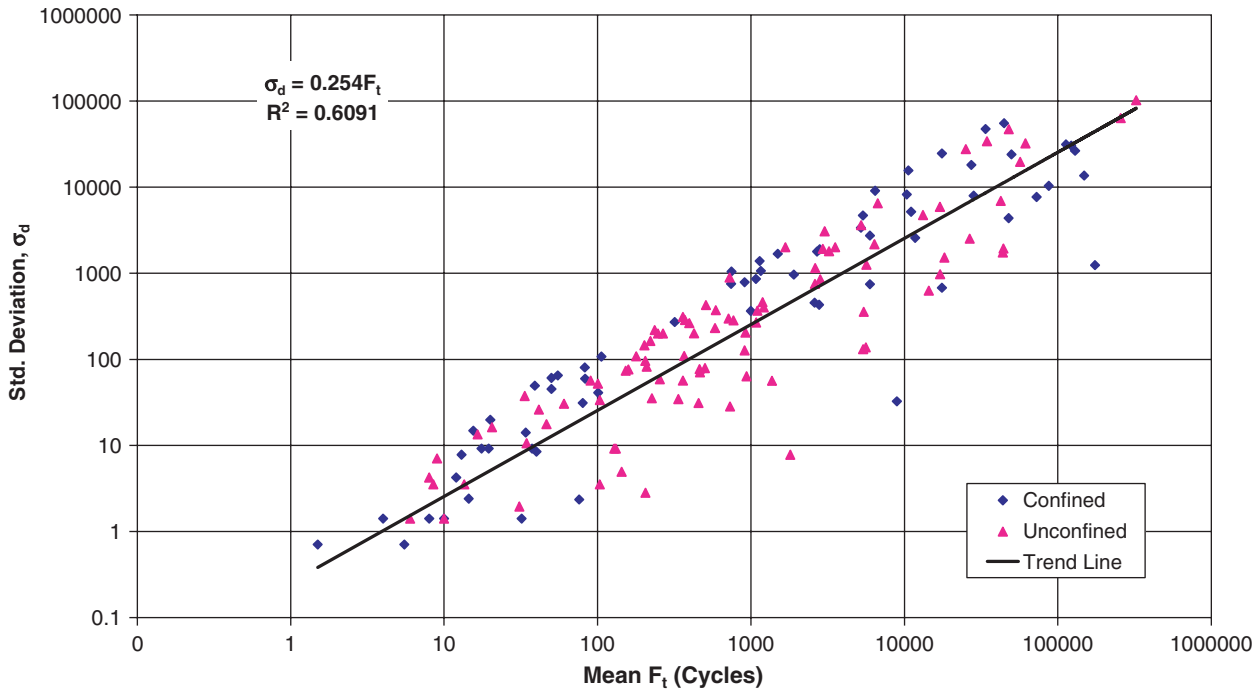

Figure 2-7. Mean flow time (confined and unconfined) versus standard deviation.

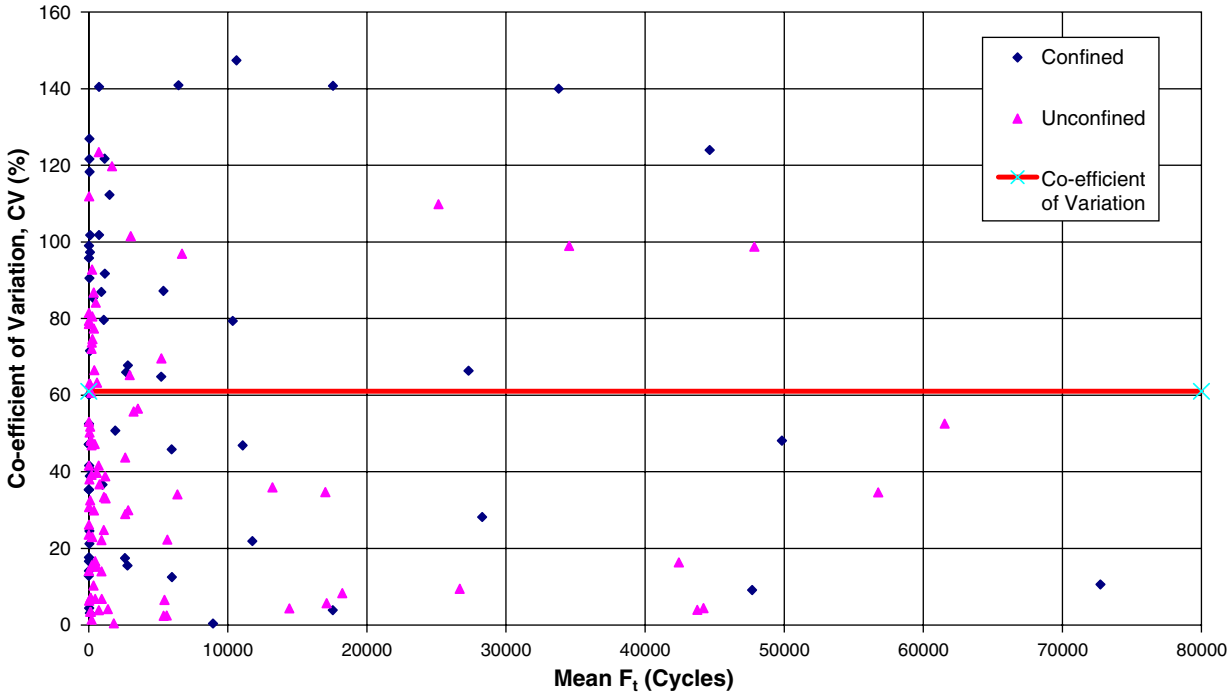

Figure 2-8. Mean flow number (confined and unconfined) and coefficient of variation.

between those two major SPT flow testing parameters (F_n and F_t). In the Phase I study, there were limitations to the total number of cycles (10,000 in the repeated load test). In Phase II, Sullivan (*13*) used over 60 different mixtures to do flow testing with an unlimited number of cycles and found very good correlation in log-log domain.

In addition to all previous flow number and flow time data, this study included more datapoints from ALF field cores and WesTrack plant mixes. The data used in this comparison analysis are shown in Table 2-1 and include results from over 64 different mixtures from different test sites and four different confinement levels. Table 2-1 shows average replicate flow number and flow time results for a specific mix and stress level. It represents all test sites and cells along with different stress levels and temperatures.

2.2.1 Relationship of Flow Number and Flow Time (Unconfined)

Kaloush (*12*) studied the flow number versus flow time relationship for unconfined testing. Unconfined tests were used as the repeated load confined tests generally did not yield tertiary flow within 10,000 load cycles. A total of 26 data points were used in the linear model, which had a coefficient of determination of 0.81.

Figure 2-9 shows the correlation between flow number and flow time for unconfined testing data (shown in Table 2-1) using a power model. A total of 101 datapoints from seven test sites were used in this model. The statistics of the model were very good as represented by the coefficient of determination of 0.81. The power relationship between flow number and flow time for unconfined testing was as follows:

$$\log(F_n) = 1.7828 Log(F_t)^{0.5644} \quad (2\text{-}9)$$

Based on the above relationship, it can be concluded that for unconfined flow testing there is a very good correlation between flow time and flow number.

2.2.2 Relationship of Flow Number and Flow Time (Confined)

Figure 2-10 shows the correlation between flow number and flow time for confined testing. A total of 16 datapoints from four test sites were used in the power model, which had a coefficient of determination of 0.13. Compared to the unconfined testing, this plot had fewer datapoints. Perhaps because of outliers, the statistics for the confined testing were not as good as those for the unconfined testing.

The power relationship between flow number and flow time for confined testing was as follows:

$$\log(F_n) = 3.1398 Log(F_t)^{0.1078} \quad (2\text{-}10)$$

Based on the limited confined testing in this study, it can be concluded that no good correlation between flow time and flow number existed. This is despite the fact that previous studies showed reasonable correlation.

Table 2-1. Comparison of flow number and flow time results.

Experiment	Cell	Confining Stress (psi)	Deviator Stress (psi)	Test Temperature, °F	Average Ft	Average Fn
FHWA-ALF	Cell 05	0	20	130	104	241
		0	10	130	715	1628
		20	120	130	8933	4901
	Cell 07	0	20	130	2611	6028
		0	10	130	13208	7761
	Cell 08	0	20	130	3542	6651
	Cell 09	0	20	130	202	376
		0	10	130	205	981
		20	120	130	5374	2109
	Cell 10	0	20	130	153	531
		0	10	130	1190	1658
		20	120	130	11765	4741
	Cell 11	0	20	130	425	1271
		0	10	130	17105	7481
		20	120	130	28277	4741
	Cell 12	0	20	130	1079	1391
		0	25	130	1369	692
		10	300	130	6	164
		20	120	130	112900	19055
Indiana	4A 64-28 S(rap)	0	25	130	2251	14791
	4B 64-28 I(rap)	0	25	130	25150	15060
	6A 64-16 S	0	25	130	209	1857
	6B 64-16 I	0	25	130	589	3159
MnRoad	Cell 01	0	10	130	26	89
		0	25	130	6	27
		0	15	130	26	77
		0	25	115	16	96
		0	25	100	226	683
	Cell 03	0	25	130	6	49
		0	25	100	267	416
	Cell 04	0	25	130	21	54
		0	25	115	42	314
		0	25	100	371	754
	Cell 14	0	25	130	4	12
		0	25	100	221	887
	Cell 15	0	25	130	33	68
		0	25	100	366	2001
	Cell 16	0	10	130	360	444
		0	30	100	730	2041
		20	100	130	1141	7601
	Cell 17	0	10	130	129	514
		0	30	100	360	2481
		20	100	130	83	1413
	Cell 18	0	10	130	121	1011
		0	30	100	935	2991
		20	100	130	3276	5001
	Cell 19	0	25	130	10	36
		0	25	100	584	954
	Cell 20	0	10	130	14	144
		0	30	100	236	659
		20	100	130	77	1258
	Cell 21	0	25	130	9	36
		0	25	100	336	548
	Cell 22	0	10	130	90	349
		0	30	100	770	1511

Table 2-1. (Continued).

Experiment	Cell	Confining Stress (psi)	Deviator Stress (psi)	Test Temperature, °F	Average Ft	Average Fn
NCAT	E06	0	25	130	455	1926
		0	25	100	1807	12289
	N02	0	25	130	3023	6860
		0	25	100	31953	23181
	N03	0	25	130	102	1211
		0	25	100	110000	22563
	N05	0	25	130	17009	3682
	N07	0	149	130	21	407
		0	25	148	6794	21306
		0	25	130	26676	22203
		0	149	100	500	7762
	N11	0	25	148	509	867
		0	25	130	2576	23310
	N12	0	25	100	43763	29605
		0	25	130	18230	39000
	N13	0	25	148	396	1185
	S02	0	40	148	4525	16483
	S13	0	40	148	2465	2432
		0	25	148	44200	35523
Nevada	Hv 64-22 B	0	76	130	10	199
		0	25	130	1675	1494
		0	25	100	47851	29497
	Hv 64-22 T	0	25	130	205	541
	Hv Ac-20P B	0	25	130	61	1009
	Hv Ac-20P T	0	25	130	143	1857
	Hv Ac-20P T	0	25	100	5603	3071
	SP 64-22 B	0	25	130	5649	4531
		10	149	149	85	90
	SP 64-22 T	0	25	130	47	148
		0	25	100	1210	22050
	SP AC-20P B	0	76	100	132	4365
		0	25	130	3227	31623
	SP AC-20P T	0	25	130	159	1087
Sub C4b Sensitivity	3.9%-01%	0	10	130	43190	4777
	3.9%-04%	0	10	130	3479	1767
	3.9%-07%	0	10	130	584	240
	3.9%-10%	0	10	130	60	137
	4.55%-01%	0	10	130	65500	11477
	4.55%-04%	0	10	130	3734	3175
	4.55%-10%	0	10	130	74	383
	5.2%-01%	0	10	130	2096	11328
	5.2%-04%	0	10	130	216	1035
	5.2%-07%	0	10	130	16	232
	5.2%-10%	0	10	130	28	202
	5.9%-01%	0	10	130	1246	3249
	5.9%-04%	0	10	130	171	1129
	5.9%-07%	0	10	130	56	156
	5.9%-10%	0	10	130	20	103
WesTrack	Cell 03	0	75	100	725	1610
		10	200	100	15	4515
	Cell 04	0	10	130	5216	3281
	Cell 07	0	10	130	501	1051
		20	120	130	17540	5321
	Cell 09	0	75	100	254	1689
		10	250	100	60	1720
	Cell 14	0	75	100	31	374
		10	250	100	76	8504
	Cell 23	0	10	130	5390	5491
	Cell 24	0	50	100	2937	13789
		0	10	130	910	1756
		10	200	100	106	60169

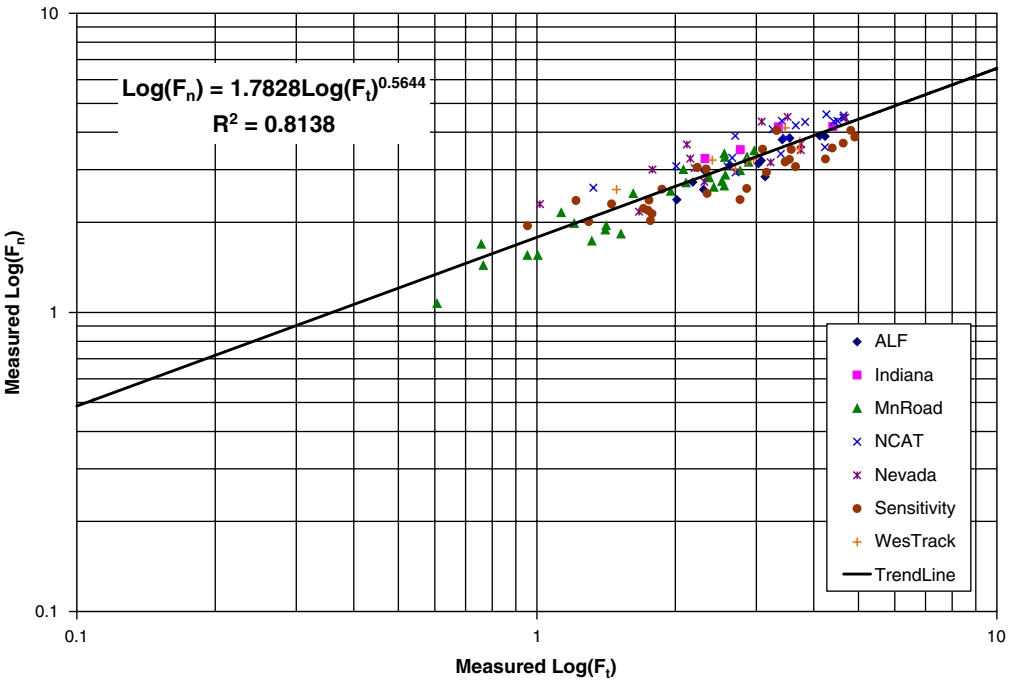

Figure 2-9. Relationship of flow number and flow time (unconfined testing).

2.2.3 Relationship of Flow Number and Flow Time (Confined and Unconfined)

Combined confined and unconfined testing data were used to get final correlation between flow number and flow time. A total of 117 datapoints from seven test sites were used in the power model, which had a coefficient of determination of 0.58. The power relationship between flow number and flow time for combined confined and unconfined testing was as follows:

$$\log(F_n) = 2.0654\,Log(F_t)^{0.4294} \quad (2\text{-}11)$$

In this analysis it was found that one datapoint was an outlier. Figure 2-11 shows the relationship without the outlier

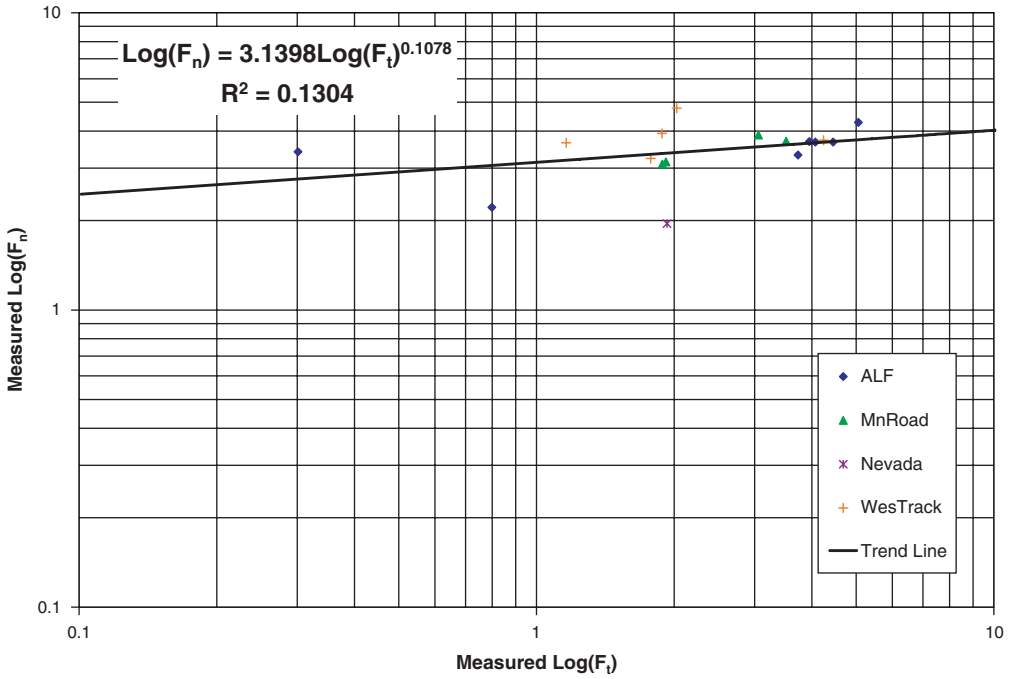

Figure 2-10. Relationship of flow number and flow time (confined testing).

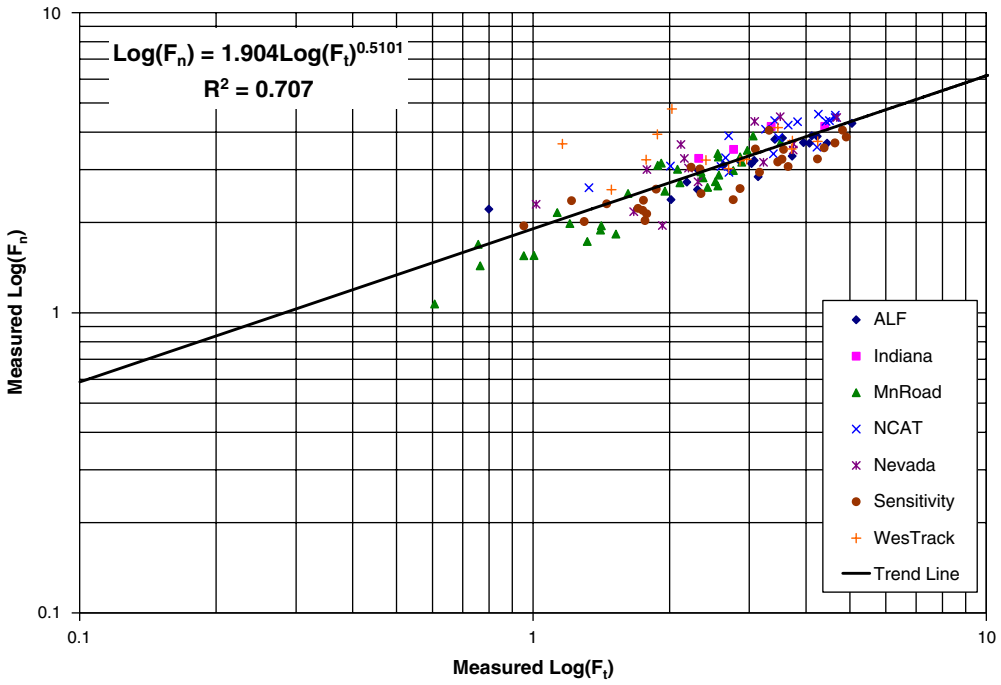

Figure 2-11. Relationship of flow number and flow time (unconfined and confined testing).

data with a coefficient of determination of 0.71. A total of 116 datapoints were used in the power model.

The power relationship between flow number and flow time for combined confined and unconfined testing results without one outlier point is as follows:

$$\log(F_n) = 1.904 Log(F_t)^{0.5101} \quad (2\text{-}12)$$

2.3 Factors Affecting Strain Failure Zones

The objective of this effort was to investigate the effect of mix and loading variables on three material strain parameters at flow. Three unique parameters that were investigated are total compliance at flow time ($D(t)_f$) for the static creep flow time test, the plastic strain at the flow number (ε_{pf}) for the repeated load flow time test, and the ratio of plastic to resilient strain at the flow number ($\varepsilon_{pf}/\varepsilon_r$) for the repeated load flow number test.

2.3.1 Accumulated Plastic Strain (ε_{pf}) at Flow Number

Plastic strain at tertiary flow is defined as the total cumulative permanent (unrecoverable) strain at failure obtained from the repeated load permanent deformation flow number test. If this parameter was found to be somewhat constant for all mixtures, it would provide a practical link between field rut depth and the laboratory-measured flow parameter (F_n).

In order to test the effect of the mix and loading variables on the potential ε_{pf}, the distribution of the results for six variables were evaluated. The six different variables are confinement level, temperature, mix type, binder type, binder content, and air void level. The distributions were made both separately and combined for the unconfined and confined tests. In addition, the distributions also were evaluated separately for lab blend, plant mix, or field core test specimens. A master summary table of distributions, relationships, statistical significance and their influences by mix variables and testing conditions is shown in Table 2-2.

These results show that confinement level, mix type, and air void level affect both the confined and unconfined ε_{pf} results for lab blend mixes, plant mixes, and field cores. Temperature and binder type have no effect on unconfined $\varepsilon_{pf,}$ whereas temperature has an effect on confined plant mix flow number, and binder type has an effect on both lab blend and plant mixes. Binder content has an effect on ε_{pf} for confined and unconfined lab blend mixes. Arizona Department of Transportation (ADOT) sensitivity study tests were analyzed for possible effects of binder content. In the sensitivity study, different binder contents had the same air void level, loading conditions, and test temperature.

Table 2-2. Factors affecting stain failure zones—summary of statistical analysis.

Factors	ε_{pf} (F_n Test)				$\varepsilon_{pf}/\varepsilon_r$ (F_n Test)				$D(t)_f$ (F_t Test)			
	Unconfined		Confined		Unconfined		Confined		Unconfined		Confined	
	Plant Mix	Lab Blend	Plant Mix	Lab Blend	Plant Mix	Lab Blend	Plant Mix	Lab Blend	Plant Mix	Lab Blend	Plant Mix	Lab Blend
Confinement Level	Y	Y	Y	Y	Y	Y	Y	Y	Y	Y	Y	Y
Temperature	N	N	Y	X	N	Y	N	X	N	N	N	N
Mix Type	Y	Y	Y	Y	Y	Y	Y	Y	Y	Y	Y	Y
Binder Type	N	N	Y	Y	Y	Y	Y	Y	Y	Y	Y	Y
Binder Content	X	Y	X	Y	X	N	X	Y	X	Y	X	Y
Air Void	Y	Y	Y	Y	N	Y	Y	Y	Y	Y	N	Y

NOTE: Y = yes, effect is significant; N = no, effect in not significant; X = no evaluation was conducted or no data were available.

2.3.2 Plastic to Resilient Strain Ratio ($\varepsilon_{pf}/\varepsilon_r$) at Flow Number

The ratio of the plastic to resilient strain is defined as the ratio of total cumulative permanent strain at tertiary flow and the average resilient strain within the secondary zone, which is assumed to be constant in that zone. If this ratio was found to be constant or reasonably consistent, the rutting in the field may be directly correlated to laboratory-measured permanent strain or flow number of repetitions.

In order to investigate the effect of the mix and loading variables on the potential plastic to resilient strain ratio at flow, the distribution of the results was done for six variables: confinement level, temperature, mix type, binder type, binder content, and air void level. All distributions were made both separately and combined for unconfined and confined testing, as well as by mix type (i.e., lab blend, plant mix, or field core). Table 2-2 also shows a master summary of the results concluded from the plot distributions and statistical analysis.

Confinement level, mix type, and binder type were found to affect both confined and unconfined flow number results for lab blend mixes, plant mixes, and field cores. Temperature had no effect on plant mixes for both unconfined and confined flow numbers, but it had an effect on unconfined lab blend mix flow number. Binder content had an effect on confined lab blend mixes but no effect on unconfined lab blend mixes. Air void content had an effect on all mixes except for unconfined plant mixes.

2.3.3 Total Compliance at Flow ($D(t)_f$)

The total compliance at flow is defined as the total strain at failure in the flow time tests. In flow time tests, the total compliance is calculated using the addition of elastic, viscoelastic, and viscoplastic strains. If this parameter were found to be constant or reasonably consistent, the rutting in the field may be directly correlated to laboratory-measured flow time or compliance values.

In order to investigate the effect of the mix and loading variables on the potential ($D(t)_f$), the distribution of test results was made for six variables: confinement level, temperature, mix type, binder type, binder content, and air void content. All distributions were made both separately and combined for unconfined and confined testing, as well as for the mix type (i.e., lab blend, plant mix, or field core). Table 2-2 provides a master summary of the results developed from distributions and statistical analysis.

Confinement level, mix type, and binder type affected both confined and unconfined flow time results for lab blend mixes, plant mixes, and field cores. Temperature had no effect on ($D(t)_f$) at flow time. Binder content had an effect on confined and unconfined lab blend mixes. Air void content affected all mixes except confined plant mixes.

CHAPTER 3

Development of SPT Failure Criteria

3.1 Scope

This chapter describes the investigation of the relationships among three variables: the laboratory-measured flow number, field rut depth, and traffic level. In general, the relationships of interest were how HMA rut depth in the field correlates to the reduced flow number obtained in the laboratory and what impact traffic levels have.

These relationships were investigated separately for the mixes discussed in Chapter 2.

3.2 Reduced Flow Number versus HMA Rut Depth at Different Traffic Levels

One important goal of this study was to find the relationship between the reduced flow number and field rut depth at a specific traffic level. Lab-measured flow numbers were reduced by global temperature shifting for simplicity and ease of manipulation. All the flow numbers were reduced to 100°F and 25 psi (172 kPa) for unconfined testing. For confined testing, a stress level of 150 psi (1034 kPa) was chosen, except for the WesTrack site where 200 psi (1379 kPa) was considered, both at 100°F. These stress levels were selected primarily to ensure tertiary flow failure of the mixes. Mainly, lab and field data from three of the NCHRP Project 9-19 test sites (ALF, WesTrack, and MnRoad) were analyzed.

The first step was to find whether any relationship exits between HMA rut depth to reduced flow number at a given traffic level. Generally, power models in log-log domain were used to evaluate the correlation. Next, the slope and intercept of the models at different traffic levels were analyzed.

Temperature-reduced flow numbers were calculated with the following equation:

$$\log(F_{nr}) = \frac{\ln\left(\frac{\alpha}{\log(\sigma)-\delta}-1\right)-\beta}{\gamma} \qquad (3\text{-}1)$$

The parameters in the equation were defined in Chapter 2 and were determined from a global temperature shifted master curve analysis.

3.2.1 ALF

Lab blend mixes and field core samples were used from the ALF experiment. For the lab blend mix, only unconfined testing was done in NCHRP Project 9-19 Phase I. For the field cores, both confined and unconfined testing was conducted. In ALF pavement testing, one-half of a single rear truck axle load is applied to a pavement section at a speed of 11.2 mph. The number of ALF passes was used to represent traffic and was correlated with HMA rut depth.

Table 3-1 shows the rut depth in different ALF cells at different numbers of passes for all mixes. Testing condition, applied stress, and temperature-reduced flow numbers are also shown in Table 3-1. For the reference temperature of 100°F, all of the reduced flow numbers were calculated at a 25 psi (172 kPa) deviatoric stress for unconfined testing and 150 psi (1034 kPa) for confined testing. Rut depths were calculated at 10, 100, 1,000, and 4,000 passes. Field data indicated that the number of passes just before the tertiary flow region was about 4,000 passes.

3.2.1.1 ALF—Field Cores Unconfined Flow Number

Figure 3-1 shows the relationship between reduced flow number and rut depth at different passes. In this plot, three of five lanes were used. Two cells (Lanes 8 and 11) were determined by the research team to be outliers and were not considered in this analysis. Power model relationships are shown on the plot for different ALF passes. It is observed that the model intercept values were increasing and the slope values were decreasing with increasing traffic. Here, passes represented traffic.

Figure 3-2 shows the relationship between intercept and passes in log-log domain. It presents a perfectly linear

Table 3-1. Reduced flow number and rut depth for different ALF passes.

Phase	Site	Cell	C/UC	Stress	Log(Fn)	Pred Fn	Rd at Different Passes			
							10	100	1000	4000
FHWA-ALF (Lab Blended) / Unconfined										
Phase1	FHWA_ALF	Cell 5	U	25	3.0050257	1011.64	0.1096	0.2598	0.6161	1.0361
Phase1	FHWA_ALF	Cell 9	U	25	3.3411975	2193.80	0.1360	0.2868	0.6047	0.9476
Phase1	FHWA_ALF	Cell11	U	25	3.6888635	4884.99	0.1028	0.2004	0.3907	0.5840
Phase1	FHWA_ALF	Cell12	U	25	4.0216908	10512.13	0.1522	0.2374	0.3702	0.4838
Phase1	FHWA_ALF	Cell 8	U	25	4.185859	15341.19	0.1470	0.2116	0.3044	0.3789
Phase1	FHWA_ALF	Cell 7	U	25	4.5671429	36909.90	0.0738	0.1292	0.2261	0.3167
Phase1	FHWA_ALF	Cell10	U	25	4.6429267	43946.74	0.1421	0.2933	0.6105	0.9532
FHWA-ALF (Field Cores) / Unconfined										
Phase2	FHWA_ALF	Cell 5-S2	U	25	4.0547926	11344.69	0.1096	0.2598	0.6161	1.03613
Phase2	FHWA_ALF	Cell10-S1&2	U	25	4.4013741	25198.46	0.1421	0.2933	0.6105	0.95324
Phase2	FHWA_ALF	Cell 8-S1	U	25	5.1561795	143277.99	0.147	0.2116	0.3044	0.37895
Phase2	FHWA_ALF	Cell 7-S2	U	25	5.3753155	237309.71	0.0738	0.1292	0.2261	0.31667
Phase2	FHWA_ALF	Cell11-S1&2	U	25	5.9829653	961535.53	0.0953	0.1859	0.3625	0.54188
FHWA-ALF (Field Cores) /Confined										
Phase2	FHWA_ALF	Cell11-S1&2	C	150	5.0902583	123100.07	0.1102	0.2148	0.4188	0.6261
Phase2	FHWA_ALF	Cell 9-S2	C	150	5.4440444	277999.75	0.136	0.2868	0.6047	0.9476
Phase2	FHWA_ALF	Cell 5-S2	C	150	5.4479372	280502.79	0.1096	0.2598	0.6161	1.03613
Phase2	FHWA_ALF	Cell10-S1&2	C	150	5.6569935	453934.85	0.1622	0.3076	0.5834	0.85771
Phase2	FHWA_ALF	Cell12-S1	C	150	5.817304	656604.67	0.1522	0.2374	0.3702	0.48378

NOTE: U = unconfined testing; C = confined testing.

relationship between intercept and passes with a coefficient of determination of 1.0.

Figure 3-3 shows the relationship between slope and log of traffic. It also shows that there is linear relationship between intercept and passes with a coefficient of determination of 1.0. It shows that slope value was decreasing with increasing number of ALF passes (i.e., *N*).

3.2.1.2 ALF—Field Cores Confined Flow Number

Figure 3-4 shows the relationship between confined reduced flow number and rut depth at different passes. Four of five lanes were used. Lane 11 was determined to be an outlier and its data were not included in this analysis. Power model relationships are shown on the plot for different ALF passes. The model intercept values increased and the slope values decreased with increasing traffic.

Figure 3-5 shows the relationship between intercept and passes in log-log domain. It presents a perfectly linear relationship between intercept and passes with a coefficient of determination of 1.0.

Figure 3-6 shows the relationship between slope and log of traffic. It also shows that there is a linear relationship between intercept and passes with a coefficient of determination of

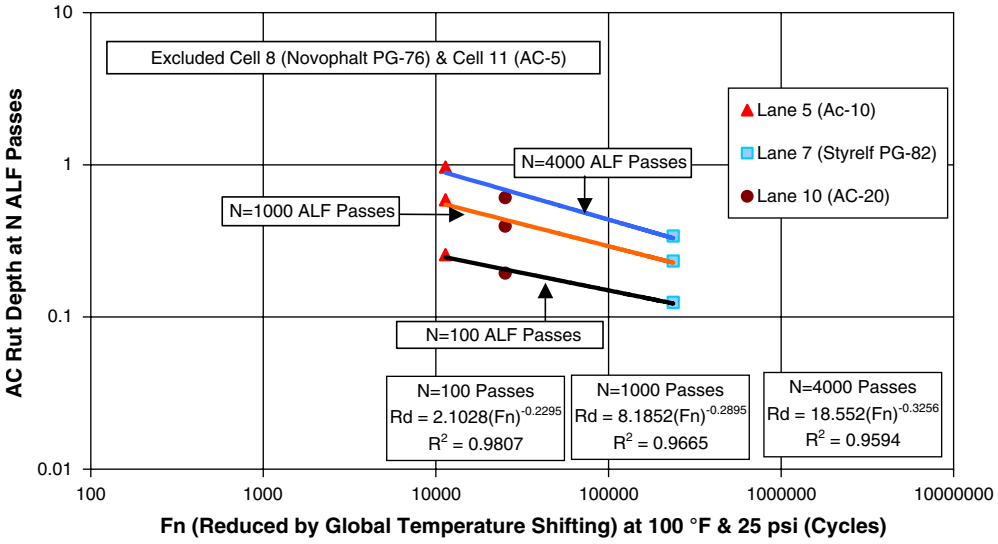

Figure 3-1. Flow number (reduced by global temperature shifting) at 100° F and 25 psi (172 kPa) versus rut depth at N ALF passes and 136.4° F for ALF field cores (unconfined).

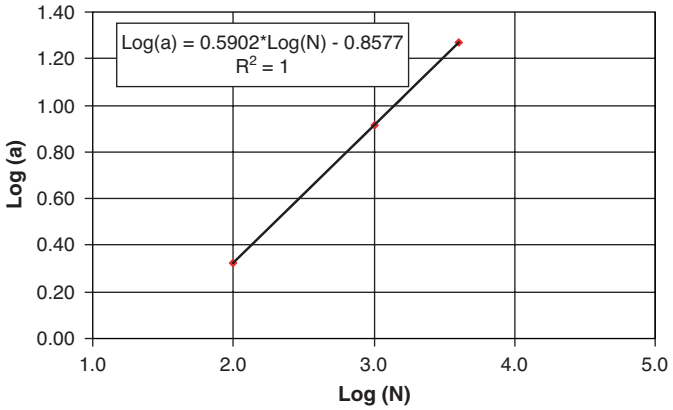

Figure 3-2. Log(intercept) versus log(cycles) for ALF field cores unconfined samples.

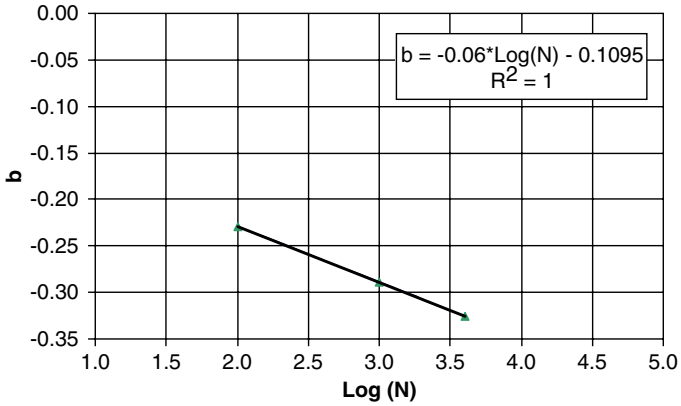

Figure 3-3. Slope versus log(cycles) for ALF field cores (unconfined).

1.0. It shows that slope value was decreasing with increasing number of *N* (i.e., ALF passes).

3.2.1.3 ALF—Lab Blend Unconfined Flow Number

ALF lab blend mixes were used to find the relationship between reduced flow number and HMA rut depth at different traffic levels. Figure 3-7 shows the relationship between reduced flow number and rut depth at different passes. Four of seven lanes were used. The data from three lanes (Lanes 8, 9, and 10) were determined to be outliers and were not included in this analysis. Power model relationships are shown on Figure 3-7 for different ALF passes. It is observed from power relationships that the intercept values were increasing and the slope values were decreasing with increasing traffic.

Figure 3-8 shows the relationship between intercept and passes in log-log domain. It presents a perfectly linear relationship between intercept and passes with coefficient of determination of 1.0.

Figure 3-9 shows the relationship between slope and log of traffic. It also shows that there is a linear relationship between intercept and passes with coefficient of determination of 1.0.

It shows that slope value was decreasing with increasing number of ALF passes (i.e., *N*).

3.2.2 MnRoad

MnRoad plant mixes were used to perform flow number testing for validation of the SPT study and those testing results were used to find the relationship between HMA field

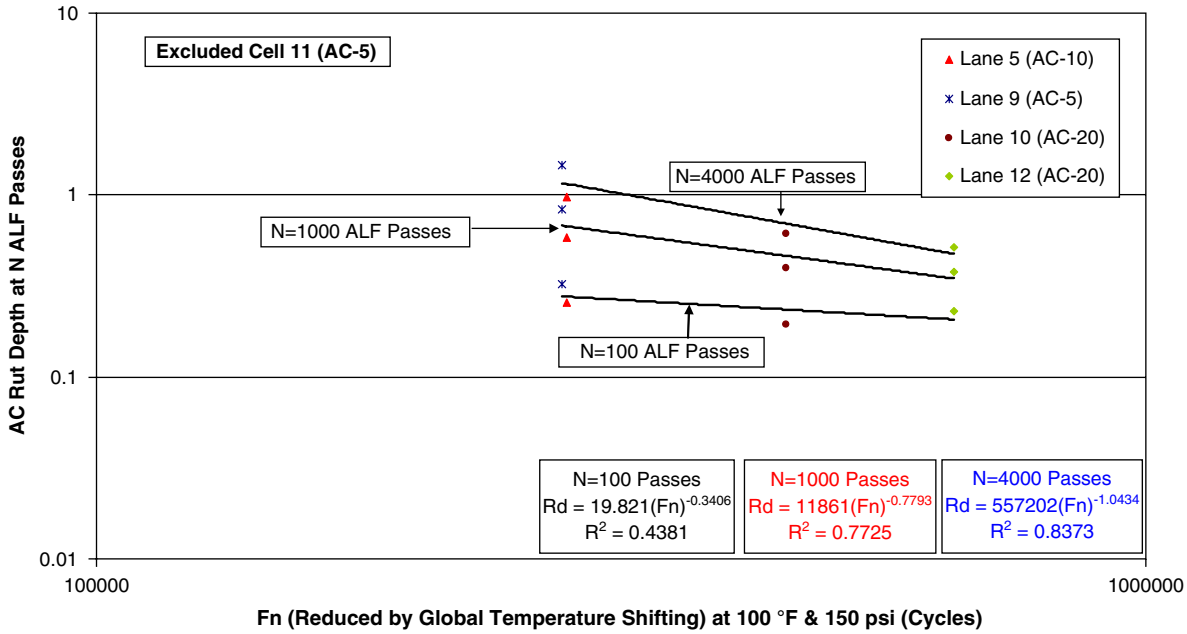

Figure 3-4 Flow number (reduced by global temperature shifting) at 100° F and 150 psi (1034kPa) versus rut depth at N *ALF passes and 136.4° F for ALF field cores (confined).*

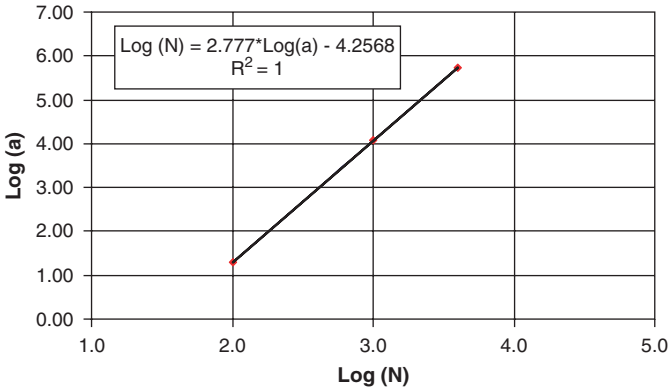

Figure 3-5. Log(intercept) versus log(cycles) for ALF field cores (confined).

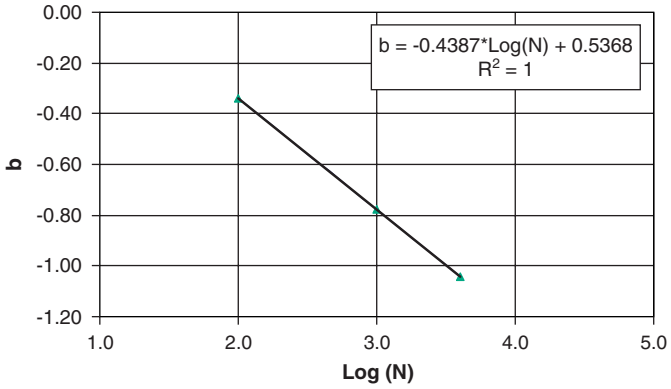

Figure 3-6. Slope versus log(cycles) for ALF field cores (confined).

rut depth versus reduced flow number. Confined and unconfined tests were analyzed separately. All rut depths for different traffic levels were collected from MnRoad ESALs versus HMA rut depth relationship.

Table 3-2 shows the rut depth in different MnRoad cells for different ESALs. All different types of MnRoad mixes are shown in the table. In Table 3-2, testing condition, applied stress, and temperature-reduced flow numbers are also shown. With a reference temperature of 100°F, all of the reduced flow numbers were calculated by taking 25 psi (172 kPa) deviatoric stress for unconfined testing and 150 psi (1034 kPa) for confined testing. Rut depths were calculated for 100,000, 500,000, 1,000,000, and 4,000,000 ESALs. It was seen in field data analysis that 1 million ESALs was the highest number of ESALs in the tertiary region.

3.2.2.1 MnRoad—Unconfined Flow Number

Figure 3-10 shows the relationship between reduced flow number and rut depth at different traffic levels. In this plot, six of seven MnRoad cells were used. One cell (Cell 1) was determined by the research team to be an outlier and was not considered in this analysis. Power model relationships are shown on the plot for different ESALs. It is observed that the model intercept values were decreasing and the slope values were increasing with increasing traffic.

Figure 3-11 shows the relationship between intercept and passes in log-log domain. It showed that there was a linear relationship between intercept and passes with a coefficient of determination of 1.0. From the relationship, it was found

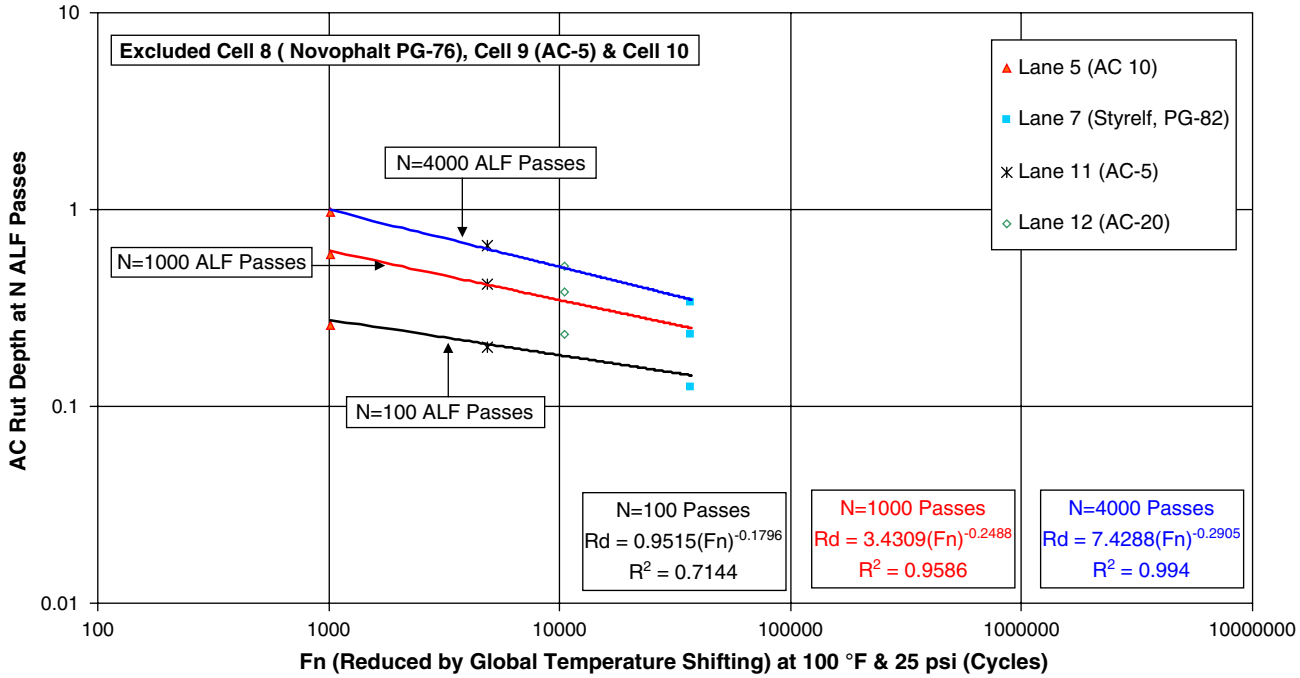

Figure 3-7. Flow number (reduced by global temperature shifting) at 100° F and 25 psi (172 kPa) versus rut depth at N ALF passes and 136.4°F for ALF lab blend (unconfined).

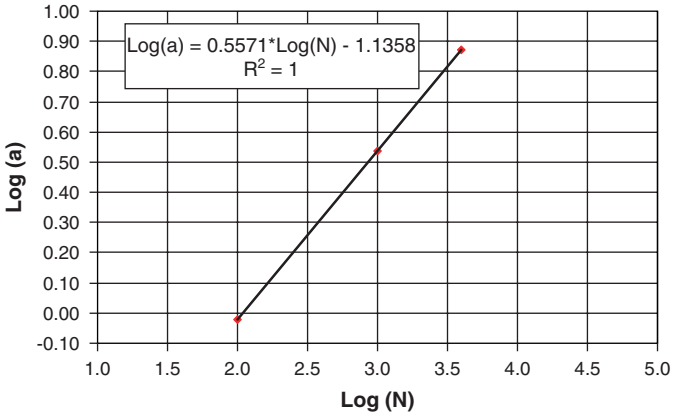

Figure 3-8. Log(intercept) versus log(cycles) for ALF lab blend (unconfined).

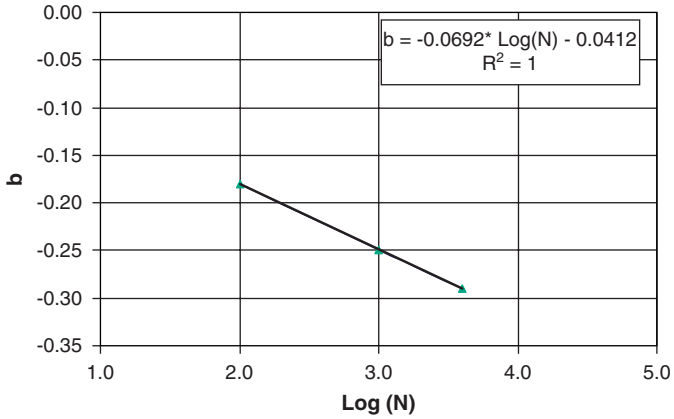

Figure 3-9. Slope versus log(cycles) for ALF lab blend (unconfined).

that unlike ALF mixes, intercept values were decreasing with increasing traffic.

Figure 3-12 shows the relationship between slope and log of traffic. It showed that there was a linear relationship between intercept and passes with a coefficient of determination of 1.0. It showed that slope value was increasing with increasing traffic (i.e., ESALs).

3.2.2.2 MnRoad—Confined Flow Number

All of the cells from the MnRoad plant mixes were analyzed to determine the relationship, shown in Figure 3-13, between reduced flow number and rut depth at different traffic levels. Data from six MnRoad cells were used to determine the power relationship. The model intercept values decrease and the slope values increase with increasing traffic.

Figure 3-14 shows the relationship between intercept and passes in log-log domain. It presents an excellent linear relationship between intercept and number of passes with a coefficient of determination of 1.0. From the relationship it is found that like unconfined MnRoad mixes, intercept values were decreasing with increasing traffic.

Figure 3-15 show the relationships between the log of traffic and the log of the intercept and the slope, respectively. Both relationships are linear with coefficients of determination of 1.0. The log (intercept) decreases and the slope increases with an increasing number of ESALs (i.e., *N*).

3.2.3 WesTrack

Repeated load flow number testing was done for WesTrack plant mixes. Both confined and unconfined testing was conducted.

Table 3-2. Reduced flow number and rut depth in MnRoad at different ESALs.

Phase	Site	Cell	C/UC	Stress	Log(Fn)	Pred Fn	Rd at Different ESALs			
							10^5	5*10^5	10^6	4*10^6
MnRoad (Plant Mix) / Unconfined										
Phase2	MnRoad	Cell4	U	25	2.5624243	365.11	0.10957	0.1985	0.2564	0.42772
Phase2	MnRoad	Cell14	U	25	2.7853567	610.04	0.05303	0.1251	0.1811	0.37931
Phase2	MnRoad	Cell1	U	25	2.8133257	650.62	0.03786	0.0929	0.1367	0.29604
Phase2	MnRoad	Cell21	U	25	2.8333245	681.28	0.04187	0.1199	0.1887	0.46715
Phase2	MnRoad	Cell3	U	25	2.8515741	710.52	0.0537	0.1072	0.1444	0.26196
Phase2	MnRoad	Cell19	U	25	3.0364196	1087.48	0.03666	0.1018	0.158	0.3807
Phase2	MnRoad	Cell15	U	25	3.1117598	1293.48	0.04119	0.0967	0.1396	0.29112
MnRoad (Plant Mix) / Confined										
Phase2	MnRoad	Cell3	C	150	2.3347762	216.16	0.0537	0.1072	0.1444	0.26196
Phase2	MnRoad	Cell15	C	150	2.5801733	380.34	0.04119	0.0967	0.1396	0.29112
Phase2	MnRoad	Cell14	C	150	2.6377734	434.28	0.05303	0.1251	0.1811	0.37931
Phase2	MnRoad	Cell1	C	150	2.6518762	448.62	0.03786	0.0929	0.1367	0.29604
Phase2	MnRoad	Cell19	C	150	2.8792148	757.21	0.03666	0.1018	0.158	0.3807
Phase2	MnRoad	Cell21	C	150	2.8792148	757.21	0.04187	0.1199	0.1887	0.46715

NOTE: U = unconfined testing; C = confined testing.

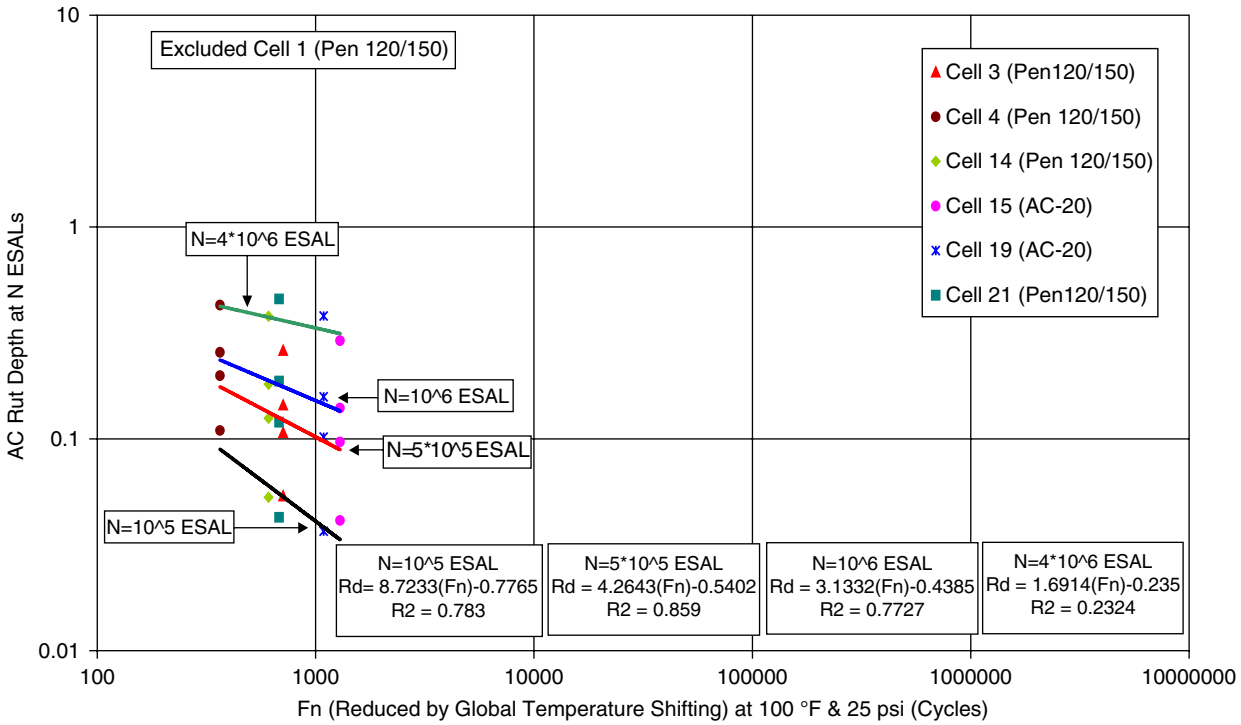

Figure 3-10. Flow number (reduced by global temperature shifting) at 100° F and 150 psi (1034 kPa) versus rut depth at N ESALs for MnRoad plant mixes (unconfined).

Table 3-3 shows the rut depth in different WesTrack cells at various ESALs for all mixes. Testing condition, applied stress, and temperature-reduced flow numbers are also shown in the table. For the reference temperature of 100°F, all of the reduced flow numbers were calculated at 25 psi (172 kPa) deviatoric stress for unconfined testing and 200 psi (1379 kPa) for confined testing. Rut depths were calculated at 5,000, 10,000, 100,000, and 500,000 ESALs. Field data indicated that 500,000 ESALs was the approximate number where tertiary behavior began.

3.2.3.1 *WesTrack—Plant Mixes Unconfined Flow Number*

Figure 3-16 shows the relationship between reduced flow number and field rut depth at different ESAL levels. In this plot, eight of nine WesTrack cells were used. The data for Cell 6 were determined to be outliers and were excluded from the analysis. Power model relationships are shown on Figure 3-16 for different ESAL levels. Both the model intercept and slope values increase with increasing traffic.

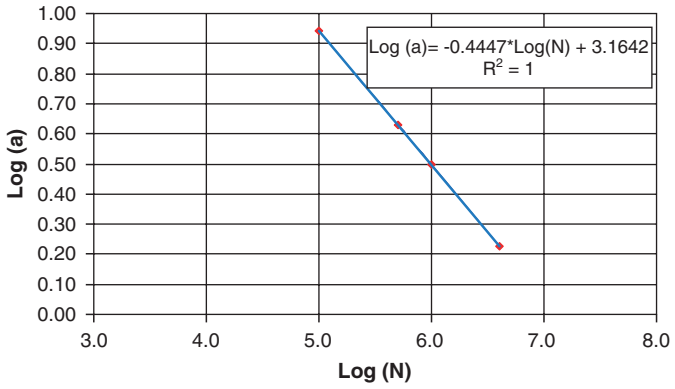

Figure 3-11. Log(intercept) versus log(cycles) for MnRoad plant mixes (unconfined).

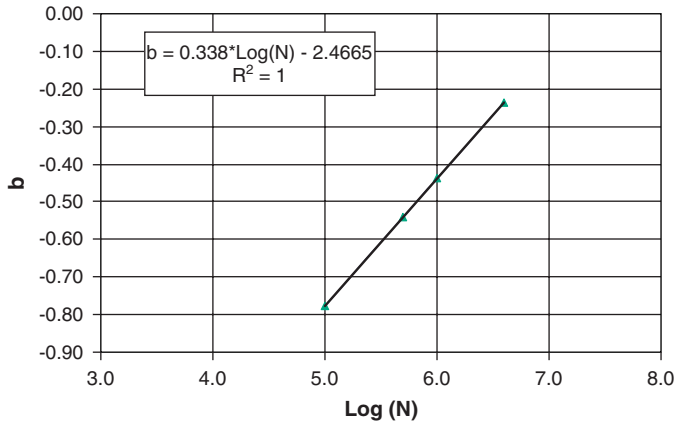

Figure 3-12. Slope versus log(cycles) for MnRoad plant mixes (unconfined).

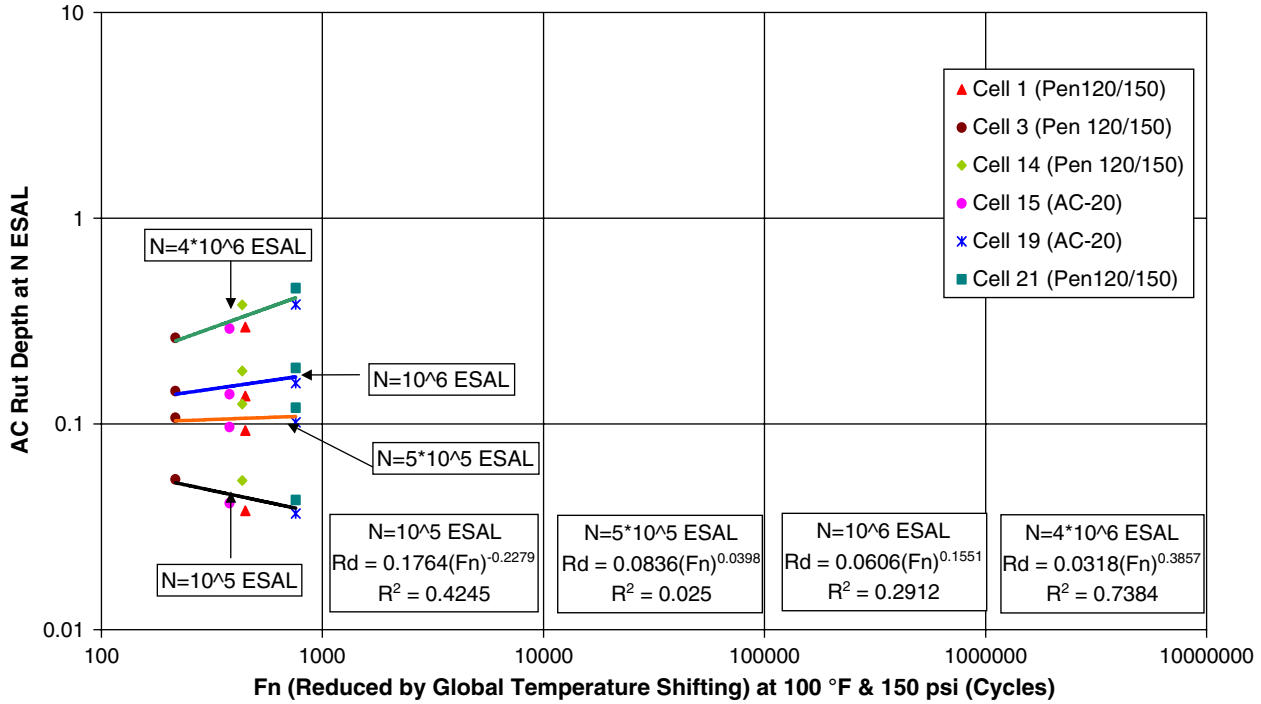

Figure 3-13. Flow number (reduced by global temperature shifting) at 100° F and 150 psi (1034 kPa) versus rut depth at N ESALs for MnRoad plant mixes (confined).

Figure 3-17 shows the relationship between intercept and ESALs in log-log domain. The relationship is linear with a coefficient of determination of 1.0. Figure 3-18 shows the relationship between slope and log of traffic. There is also a linear relationship between intercept and ESALs with a coefficient of determination of 1.0. Both intercept and slope values increase with increasing ESALs.

3.2.3.2 WesTrack—Plant Mixes Confined Flow Number

Figure 3-19 shows the relationship between confined reduced flow number and field rut depth at different ESALs for WesTrack. In this plot, 9 of 12 WesTrack cells were used. Three cells (Cells 9, 11, and 18) were determined by the research team to be outliers and were not considered in this analysis. Power model relationships are shown on the figure for different ESALs. It is observed that the model intercept values were increasing and the slope values were decreasing with increasing traffic.

Figure 3-20 shows the relationship between intercept and passes in log-log domain. It presents a perfectly linear relationship between intercept and ESALs with a coefficient of determination of 1.0.

Figure 3-21 shows the relationship between slope and log of traffic. It also shows that there is a linear relationship

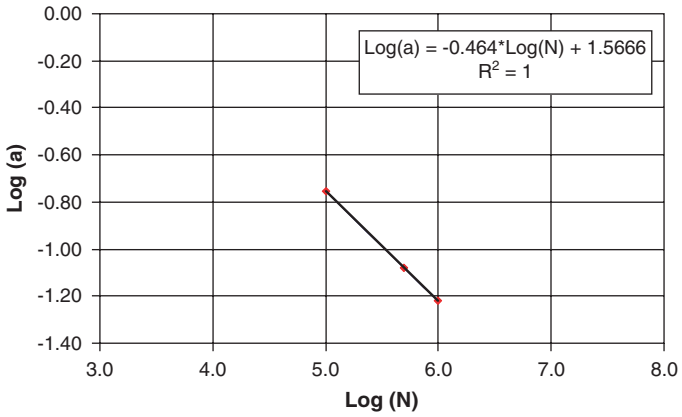

Figure 3-14. Log(intercept) versus log(cycles) for MnRoad plant mixes (confined).

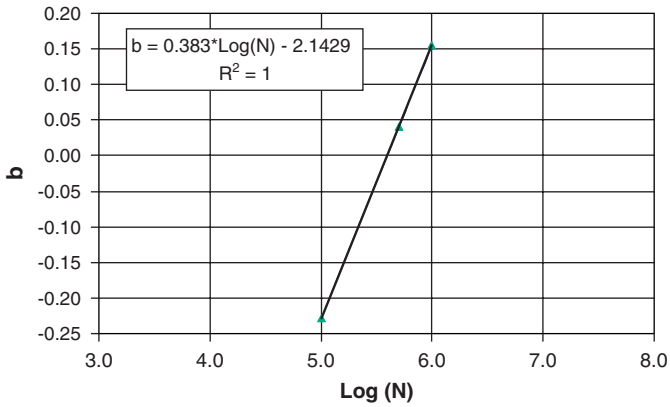

Figure 3-15. Slope versus log(cycles) for MnRoad plant mixes (confined).

Table 3-3. Reduced flow number and rut depth in WesTrack for different ESAL levels.

Phase	Site	Cell	C/UC	Stress	Log(Fn)	Pred Fn	Rd at Different ESALs			
							5000	10^4	10^5	5*10^5
WesTrack (Plant Mix) / Unconfined										
Phase2	Westrack	Cell5	U	25	4.12000	13182.65	0.0571	0.0729	0.1647	0.2912
Phase2	Westrack	Cell10	U	25	4.38534	24285.01	0.0337	0.0476	0.1510	0.3382
Phase2	Westrack	Cell21	U	25	4.40034	25138.36	0.0512	0.0652	0.1459	0.2562
Phase2	Westrack	Cell23	U	25	4.55741	36091.92	0.0340	0.0469	0.1368	0.2890
Phase2	Westrack	Cell19	U	25	4.61986	41673.33	0.0675	0.0841	0.1747	0.2913
Phase2	Westrack	Cell20	U	25	5.10646	127777.86	0.0755	0.0964	0.2170	0.3826
Phase2	Westrack	Cell4	U	25	5.24219	174660.48	0.0617	0.0745	0.1397	0.2167
Phase2	Westrack	Cell6	U	25	5.41726	261374.30	0.0482	0.0690	0.2273	0.5228
Phase2	Westrack	Cell8	U	25	5.86015	724681.86	0.0573	0.0733	0.1657	0.2931
Phase2	Westrack	Cell17	U	25	6.21898	1655685.57	0.0389	0.0533	0.1509	0.3124
Phase2	Westrack	Cell11	U	25	7.33700	21727250.75	0.0309	0.0410	0.1050	0.2028
WesTrack (Plant Mix) / Confined										
Phase2	Westrack	Cell6	C	200	3.07799	1196.72	0.0482	0.0690	0.2273	0.5228
Phase2	Westrack	Cell20	C	200	3.60814	4056.37	0.0755	0.0964	0.2170	0.3826
Phase2	Westrack	Cell9	C	200	3.61167	4089.48	0.0813	0.0923	0.1411	0.1897
Phase2	Westrack	Cell11	C	200	4.33325	21540.40	0.0309	0.0410	0.1050	0.2028
Phase2	Westrack	Cell7	C	200	4.38515	24274.67	0.0760	0.0956	0.2051	0.3497
Phase2	Westrack	Cell17	C	200	4.48409	30485.13	0.0389	0.0533	0.1509	0.3124
Phase2	Westrack	Cell16	C	200	4.49774	31458.31	0.0926	0.1085	0.1838	0.2656
Phase2	Westrack	Cell1	C	200	4.67110	46892.49	0.0779	0.0941	0.1759	0.2724
Phase2	Westrack	Cell18	C	200	4.78095	60388.51	0.0357	0.0452	0.0991	0.1715
Phase2	Westrack	Cell12	C	200	5.01247	102913.10	0.0492	0.0620	0.1340	0.2295
Phase2	Westrack	Cell5	C	200	5.15826	143965.95	0.0571	0.0729	0.1647	0.2912
Phase2	Westrack	Cell23	C	200	5.59595	394410.14	0.0340	0.0469	0.1368	0.2890

NOTE: U = unconfined testing; C = confined testing.

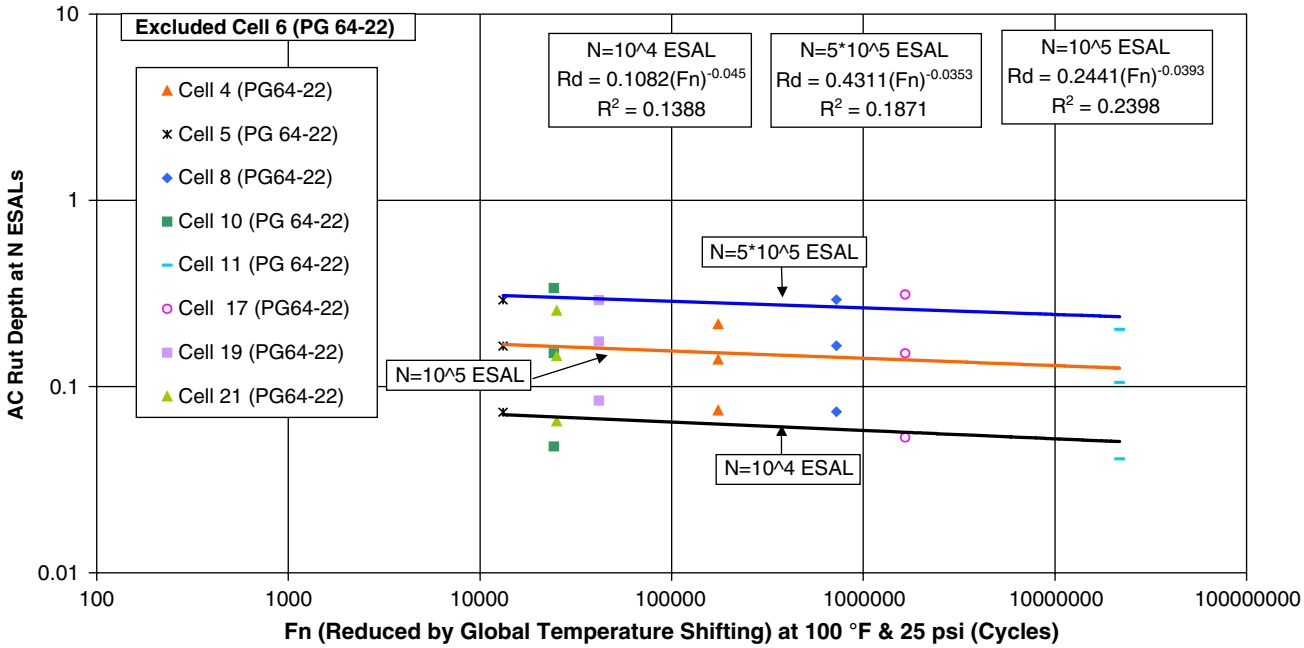

Figure 3-16. Flow number (reduced by global temperature shifting) at 100° F and 150 psi (1034kPa) versus rut depth at N ESALs for WesTrack plant mixes (unconfined).

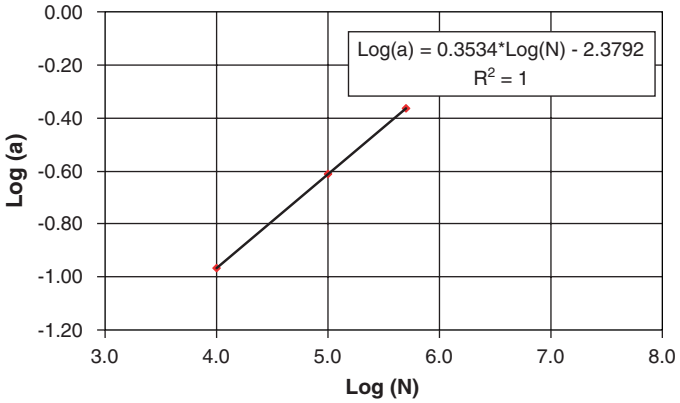

Figure 3-17. Log(intercept) versus log(cycles) for WesTrack plant mixes (unconfined).

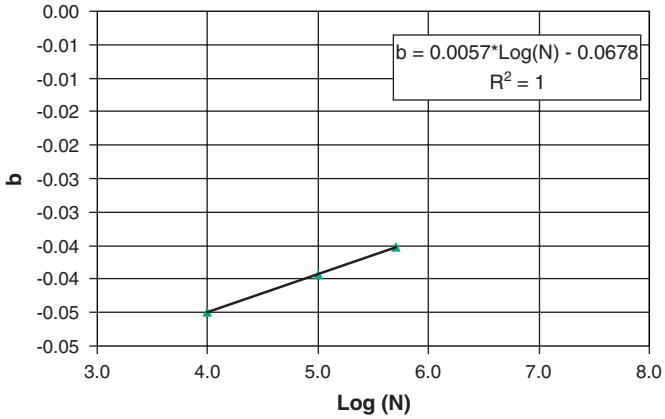

Figure 3-18. Slope versus log(cycles) for WesTrack plant mixes (unconfined).

between intercept and passes with a coefficient of determination of 1.0. It shows that slope value was decreasing with an increasing number of *N*.

3.3 Model Development for Flow Number, Field Rut Depth, and Traffic

The effort of this section was devoted to developing a model for predicting field rut depth using laboratory-measured flow number and traffic level. From the previous analysis of field rut depth and flow number at various traffic levels, it was shown that the intercept and slope values were well related to traffic. The relationship between the rut depth and flow number was as follows:

$$R_d = a(F_n)^b \quad (3\text{-}2)$$

where

R_d = rut depth,
F_{nr} = reduced flow number at the reference temperature,
a = intercept, and
b = slope.

The relationship between intercept (a) with traffic (N) in log-log domain where k equals slope and l is a constant was as follows:

$$\text{Log}(a) = l - k * \text{Log}(N) \quad (3\text{-}3)$$

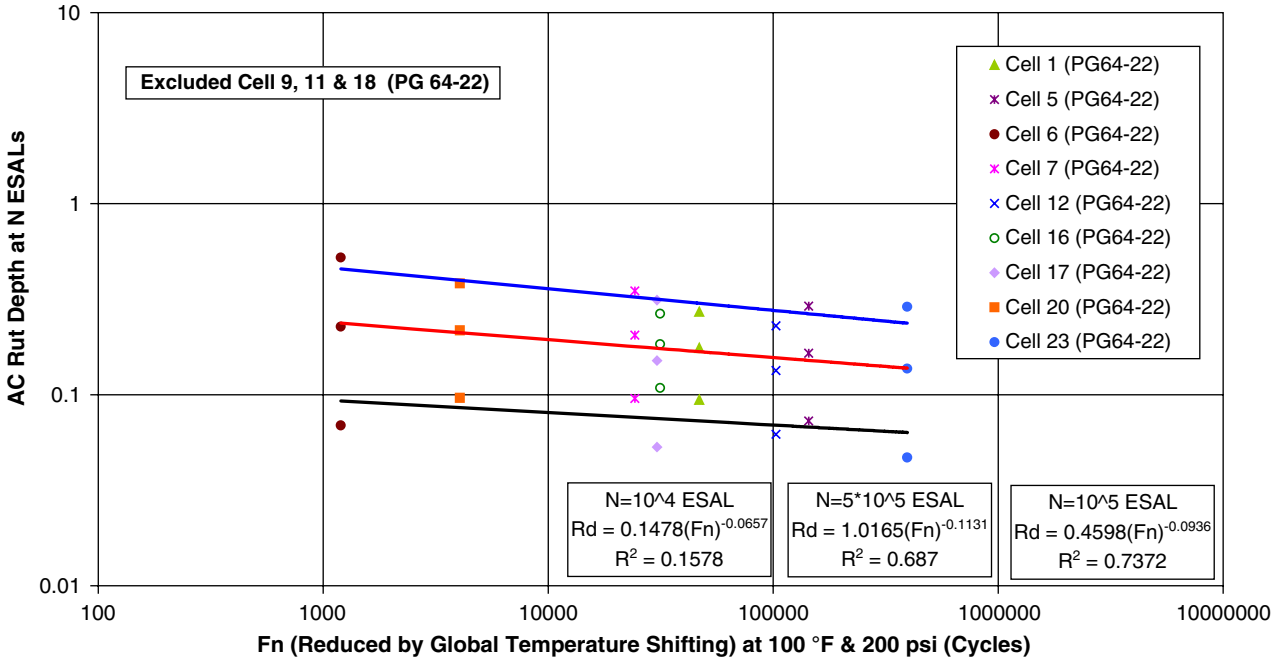

Figure 3-19. Flow number (reduced by global temperature shifting) at 100° F and 200 psi (1379 kPa) versus rut depth at N ESALs for WesTrack plant mixes (confined).

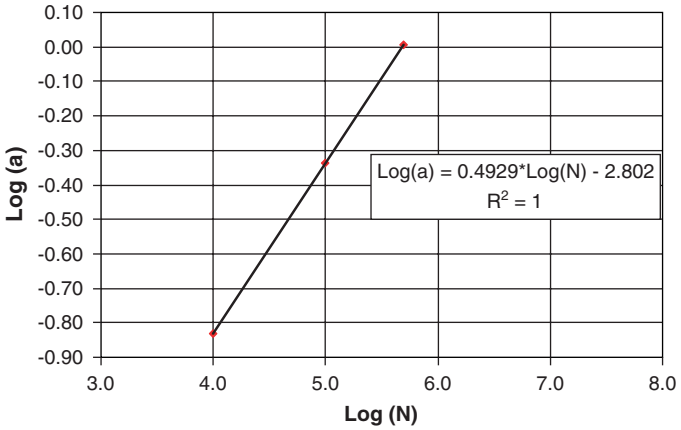

Figure 3-20. Log(intercept) versus log(cycles) for WesTrack plant mixes (confined).

The relationship between intercept (a) with traffic (N) in log-log domain was changed to the following form:

$a = i_1 * (\mathrm{N})^{-\mathrm{m2}}$
$i_1 = e^I$
$m_2 = k$

The relationship between slope (b) with Log(N) where m_1 equals slope and l_0 is a constant was as follows:

$$b = m_1 * \mathrm{Log}(N) - l_0 \quad (3\text{-}4)$$

By substituting the a and b values in Equation 3.1 the following relationship is obtained for R_d, F_n, and N:

$$R_d = i_1 * (N)^{-m_2} * (F_m)^{m_1 * \mathrm{Log}(N) - l_0} \quad (3\text{-}5)$$

This model was used to get the predictive rut depth for a particular traffic level and flow number. Three NCHRP Project 9-19 test sites ALF, MnRoad, and WesTrack were investigated here for predicted and measured rut depth for particular traffic levels. All of the models were statistically evaluated for their accuracy and rationality. The statistics that were applied to measure the model accuracy are coefficient of determination (R^2), standard error of estimate (S_e), and relative accuracy (S_e/S_y).

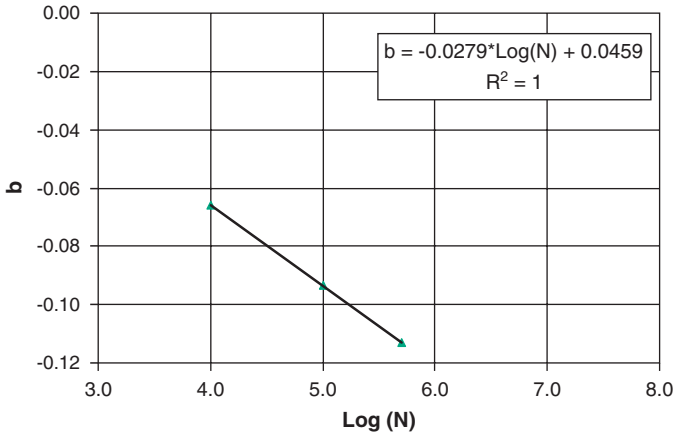

Figure 3-21. Slope versus log(cycles) for WesTrack plant mixes (confined).

3.3.1 ALF

ALF lab blend and field core test data (flow number and field rut depth) were used for developing the rutting model. For lab blend mix only, unconfined testing was done in NCHRP Project 9-19 Phase I, and for field cores, both confined and unconfined testing was done in NCHRP Project 9-19 Phase II. All of these test conditions were analyzed separately.

ALF passes at 100, 1,000, and 4,000 with their corresponding field rut depths data were used to get the model for predicted rut depth. Reduced flow numbers were calculated by using the global temperature shifted master curve parameters and the model presented in Equation 3.1.

3.3.1.1 ALF—Field Cores Unconfined Flow Number

For obtaining the relationship of rut depth, ESALs (traffic), and flow number, two different analyses were conducted. In the previous section, the relationships for field rut depth and reduced flow number were shown without the outliers. The first analysis in this section includes the outliers to get the relationship. Five ALF lane unconfined tests were used in this analysis. By using the non-linear optimization model in Equation 3.5 the following model parameters were determined:

$$R_d = 0.05696 * (N)^{0.59404} * (Fn)^{-0.05848 * \mathrm{Log}(N) - 0.02973} \quad (3\text{-}6)$$

where

R_d = predictive rut depth,
N = traffic (expressed in ESALs/passes), and
F_{nr} = reduced flow number using global temperature shift.

Figure 3-22 shows the results of the linear optimization performed on the five mixes. The figure shows fair correlation between the measured and predictive rut depth. Cells 8 and 11 (outliers) contributed to the low coefficient of determination (R^2 of 0.60 and S_e/S_y of 0.71).

The model found without the two outlier datapoints was as follows:

$$R_d = 1.0989 * (N)^{0.3848} * (Fn)^{-0.0115 * \mathrm{Log}(N) - 0.3201} \quad (3\text{-}7)$$

Figure 3-23 shows the results of this model, where good correlation between the measured and predictive rut depth was obtained. Excellent statistical measures are shown with an R^2 of 0.97 and an S_e/S_y value of 0.20.

3.3.1.2 ALF—Field Cores Confined Flow Number

Five ALF lane confined flow number tests were used to get the rut depth model. By using the non-linear optimization from Equation 3.5, the following model parameters were determined:

$$R_d = 0.02662 * (N)^{0.61689} * (Fn)^{-0.05026 * \mathrm{Log}(N) - 0.04932} \quad (3\text{-}8)$$

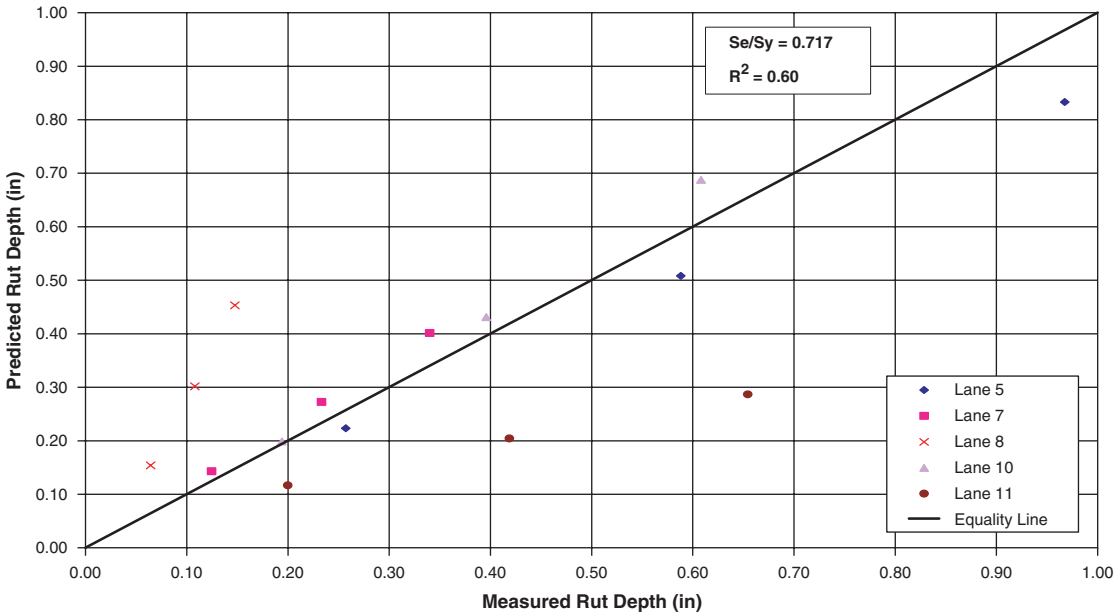

Figure 3-22. Measured versus predicted rut depth for ALF field cores (unconfined) using all cells.

Figure 3-24 shows the results of the linear optimization performed on the five mixes. The statistics show a fair correlation between the measured and predictive rut depth, with an R^2 of 0.56 and an S_e/S_y value of 0.75.

The data for Cell 11 were determined to be outliers and the analysis was repeated with the outlier data excluded as shown in Figure 3.25.

By using the non-linear optimization model in Equation 3.5, the following model parameters were determined:

$$R_d = 1.2552 * (N)^{1.6972} * (Fn)^{-02429 * Log(N) - 0.25154} \quad (3\text{-}9)$$

Figure 3-25 shows the results of this model, where good correlation between the measured and predictive rut depth was obtained, with an R^2 of 0.89 and an S_e/S_y of 0.40. The S_e for the model evaluated was small, which indicates good model accuracy.

3.3.1.3 ALF—Lab Blend Unconfined Flow Number

The rut depth model for ALF lab blend mixes was determined from the data for seven ALF lane tests. Lab blend flow number tests were performed only in NCHRP Project 9-19 Phase I.

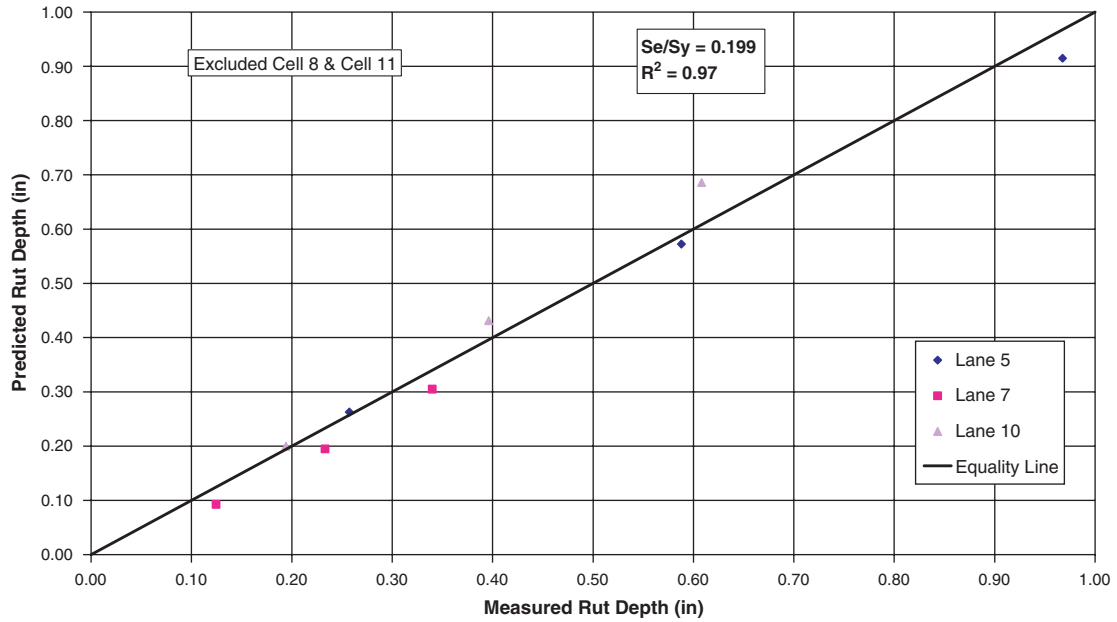

Figure 3-23. Measured versus predicted rut depth for ALF field cores (unconfined).

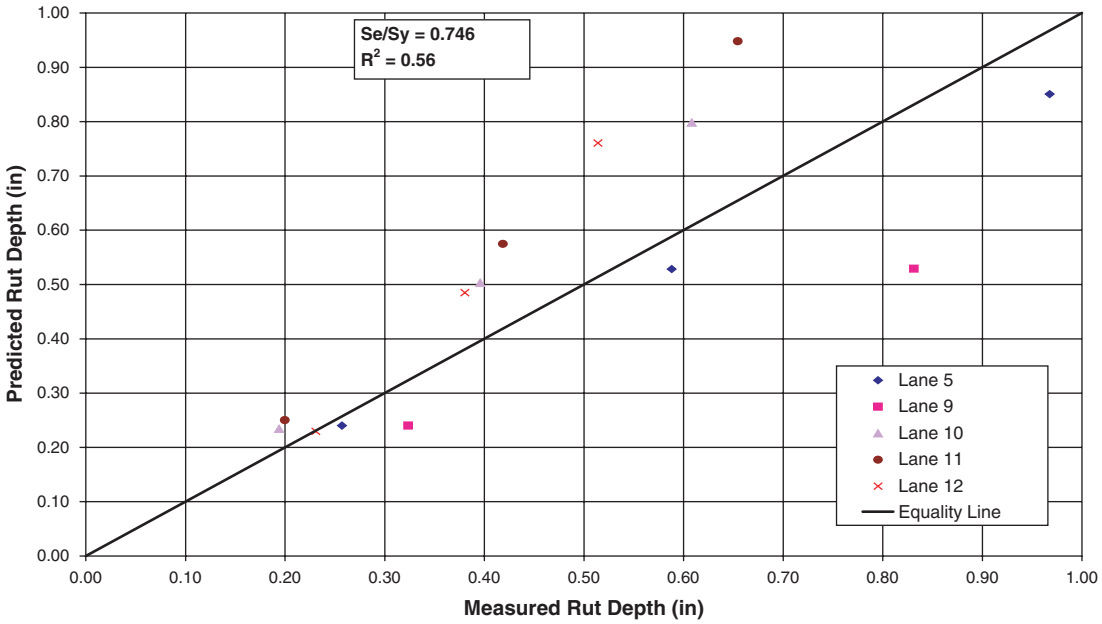

Figure 3-24. Measured versus predicted rut depth for ALF field cores (confined) using all data.

The model parameters determined by using the non-linear optimization model in Equation 3.5 were as follows:

$$R_d = 0.07173 * (N)^{0.60868} * (Fn)^{-0.07455 * Log(N) - 0.05257} \quad (3\text{-}10)$$

Figure 3-26 shows the results of the linear optimization performed on the seven lab blend mixes. The statistics show a fair correlation between the measured and predictive rut depth. A fair data fit was shown with an R^2 of 0.69. The S_e of 0.20 for the model evaluated was small compared to the mean rut depth. The 0.60 S_e/S_y value for the power model indicates a fair relative accuracy of the model.

One of the ALF lab blend mixture cells was determined to be an outlier as in the previous section. The model found without the outlier datapoint was as follows:

$$R_d = 1.4646 * (N)^{0.2718} * (Fn)^{0.1885 * Log(N) - 0.4629} \quad (3\text{-}11)$$

Figure 3-27 shows the results of this model, where fair correlation between the measured and predictive rut depth was obtained. Fair statistical measure was shown with an R^2 of 0.56. Although the S_e for the model evaluated is small compared to the mean rut depth, the 0.78 S_e/S_y value for the power model indicates poor relative model accuracy. So, excluding

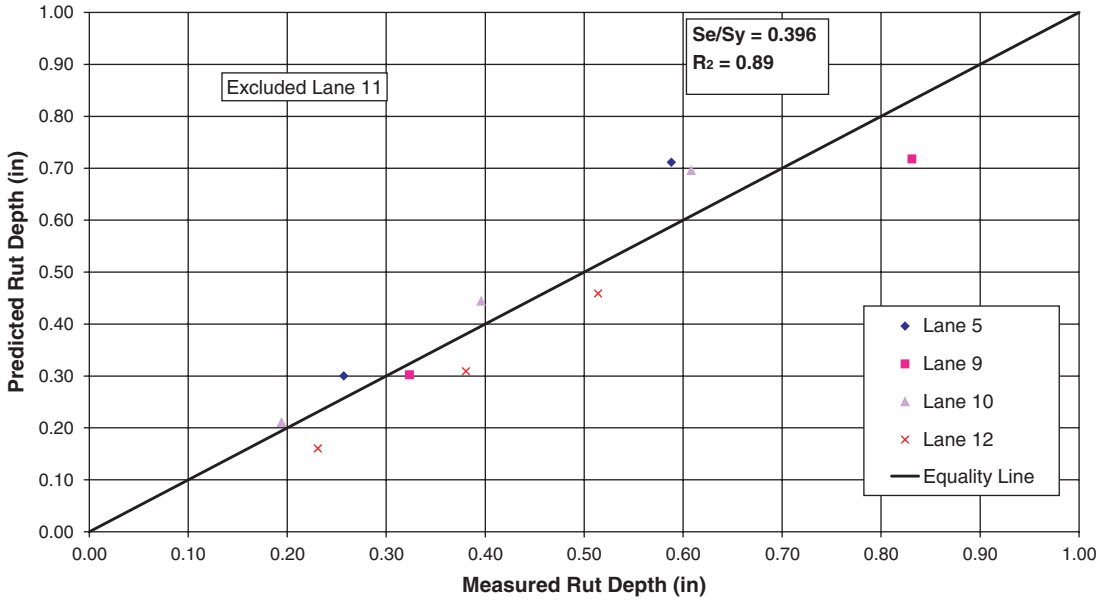

Figure 3-25. Measured versus predicted rut depth for ALF field cores (confined).

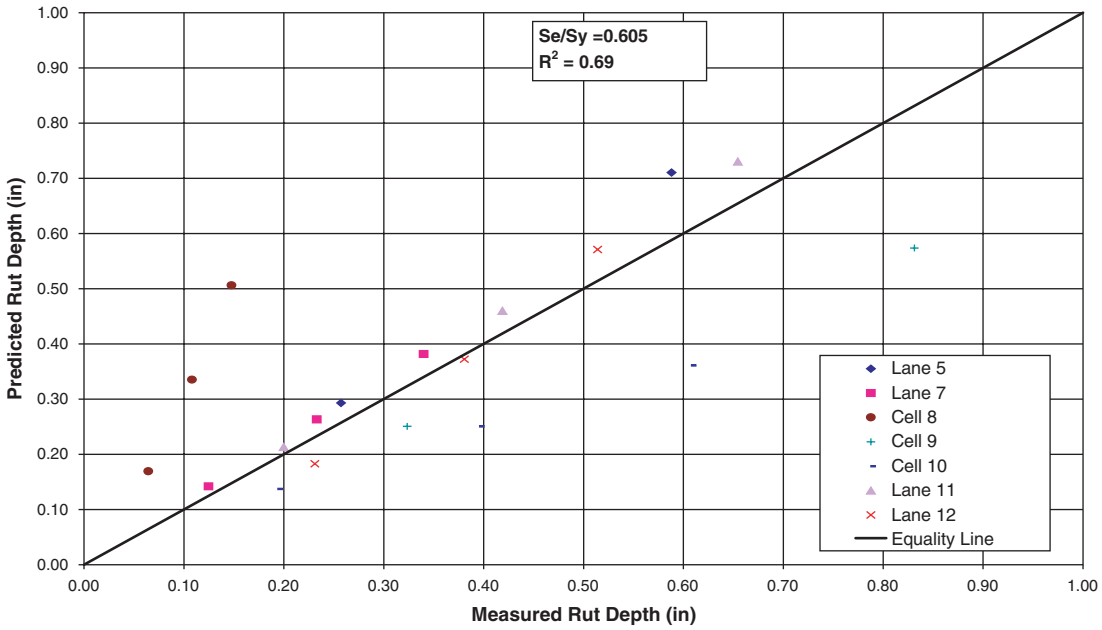

Figure 3-26. Measured versus predicted rut depth for ALF lab blend (unconfined) using all data.

the outlier does not show good model accuracy for ALF lab blend mixes.

3.3.2 MnRoad

Plant mix samples were used from the MnRoad experiment. Reduced flow numbers from MnRoad plant mixes and field rut depth were used for developing the rutting model. Four traffic levels were used to develop this model. All test conditions were analyzed separately.

Rut depths at 100,000, 500,000, 1,000,000, and 5,000,000 ESALs were used to get the model for measured and predicted rut depth. Reduced flow numbers were calculated by using the global temperature shifted master curve parameters and the model presented in Equation 3.1.

3.3.2.1 MnRoad—Plant Mixes Unconfined Flow Number

Seven MnRoad lane unconfined tests were used in this analysis. By using the non-linear optimization model in Equation 3.5 the following model parameters were determined:

$$R_d = 43.15246 * (N)^{-0.19937} * (Fn)^{0.25272 * Log(N) - 1.93811} \quad (3\text{-}12)$$

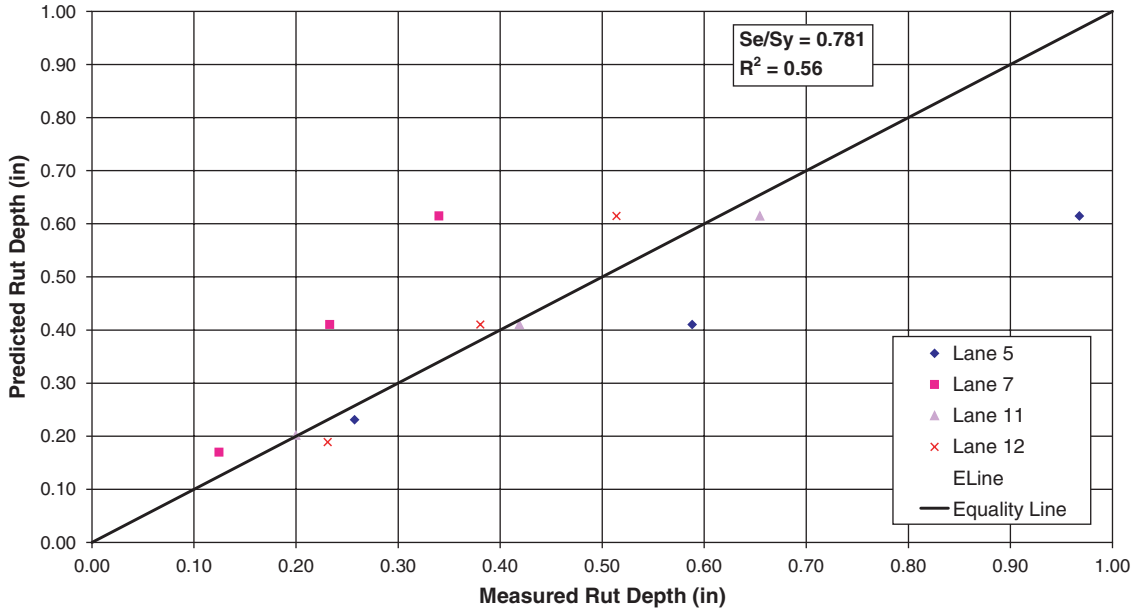

Figure 3-27. Measured versus predicted rut depth for ALF lab blend (unconfined).

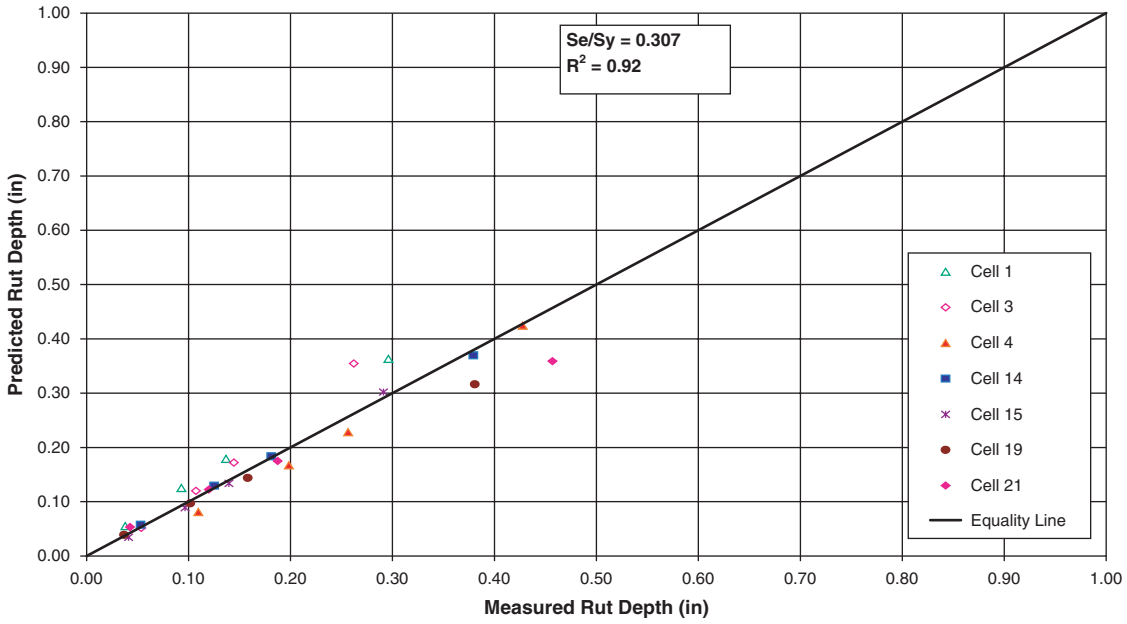

Figure 3-28. Measured versus predicted rut depth for MnRoad plant mixes (unconfined) using all cells.

Figure 3-28 shows the results of the linear optimization performed on the seven MnRoad mixes with four ESAL (traffic) levels. The figure shows an excellent correlation between the measured and predictive rut depth. Excellent statistical measure is shown with an R^2 of 0.92. The S_e for the model evaluated is fairly small and the S_e/S_y value of 0.30 indicates an excellent relative accuracy of the model.

From rut depth versus reduced flow number analysis, it was shown that Cell 1 was excluded from analysis for being an outlier. Excluding Cell 1, six MnRoad lane unconfined tests were used to get the model. By using the non-linear optimization model in Equation 3.5, the following model was found:

$$R_d = 1.2483 * (N)^{0.0425} * (Fn)^{0.1649 * Log(N) - 1.3745} \quad (3\text{-}13)$$

Figure 3-29 shows the results of this model, where excellent correlation between the measured and predictive rut depth was shown. An excellent statistical measure is shown with an R^2 of 0.93. The S_e for the model evaluated was fairly small and the 0.29 S_e/S_y value for the power model indicates an excellent relative accuracy of the model.

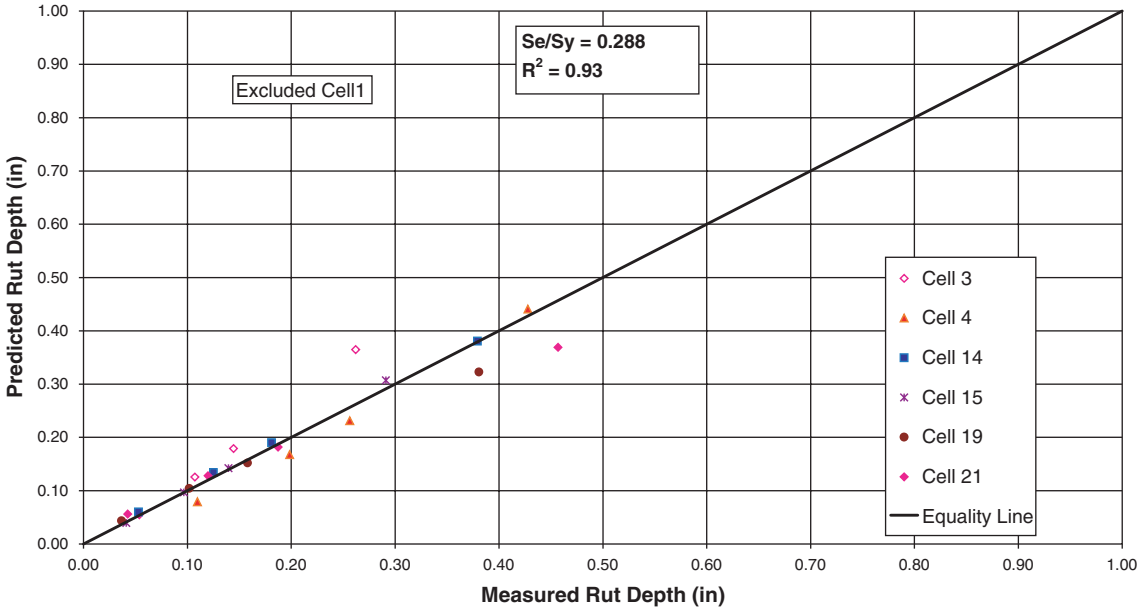

Figure 3-29. Measured versus predicted rut depth for MnRoad plant mixes (unconfined).

The two rutting models demonstrate that excluding the outlier (Cell 1) shows a higher R^2 value and lower S_e/S_y, which indicates increased model accuracy.

3.3.2.2 MnRoad—Plant Mixes Confined Flow Number

Six MnRoad lane unconfined tests were used in this analysis. By using the non-liner optimization model in Equation 3.5 the following model was found:

$$R_d = 1.20326 * (N)^{0.21255} * (Fn)^{0.28828 * Log(N) - 1.58221} \quad (3\text{-}14)$$

Figure 3-30 shows the results of the linear optimization performed on the six mixes with four ESAL (traffic) levels. The figure shows an excellent correlation between the measured and predictive rut depth. Excellent statistical measure is shown with an R^2 of 0.93. The S_e for the model evaluated is very small and the 0.28 S_e/S_y value for the model indicates an excellent relative accuracy of the model.

3.3.3 WesTrack

Plant mix samples were used from the WesTrack experiment. Reduced flow numbers from WesTrack plant mixes and field rut depth were used for developing the rutting model. Three traffic levels were used to develop this model. All test conditions were analyzed separately.

Rut depths at 10,000, 100,000, and 500,000 ESALs were used to get the model for measured and predictive rut depth. Reduced flow numbers were calculated by using the global temperature shifted master curve parameters and the model presented in Equation 3.1.

3.3.3.1 WesTrack—Plant Mixes Unconfined Flow Number

Eleven WesTrack cells incorporating three different traffic levels were used in this analysis. By using the non-liner optimization model in Equation 3.5 the following model parameters were found:

$$R_d = 0.00340 * (N)^{0.36068} * (Fn)^{0.00727 * Log(N) - 0.06018} \quad (3\text{-}15)$$

Figure 3-31 shows the results of the linear optimization performed on the 11 mixes with three ESAL (traffic) levels. The figure shows a good correlation between the measured and predictive rut depth. Good statistical measure is shown with an R^2 of 0.79 and S_e/S_y of 0.48. The 0.055 S_e for the model evaluated was very small compared to the mean rut depth.

From the rut depth versus reduced flow number analysis, it was shown that Cell 6 was excluded from analysis for being an outlier. Excluding Cell 6, 10 other WesTrack cells incorporating three different traffic levels were used to get the final rutting model. By using the non-liner optimization model in Equation 3.5, the following model parameters were found:

$$R_d = 0.00341 * (N)^{0.36446} * (Fn)^{0.00304 * Log(N) - 0.04683} \quad (3\text{-}16)$$

Figure 3-32 shows the results of the linear optimization performed on the 10 mixes with three ESAL (traffic) levels. The figure shows that a good correlation exists between the measured and predictive rut depth. Good statistical measure is shown with an R^2 of 0.89 and S_e/S_y of 0.35. The S_e for the model evaluated was very small compared to the mean rut depth.

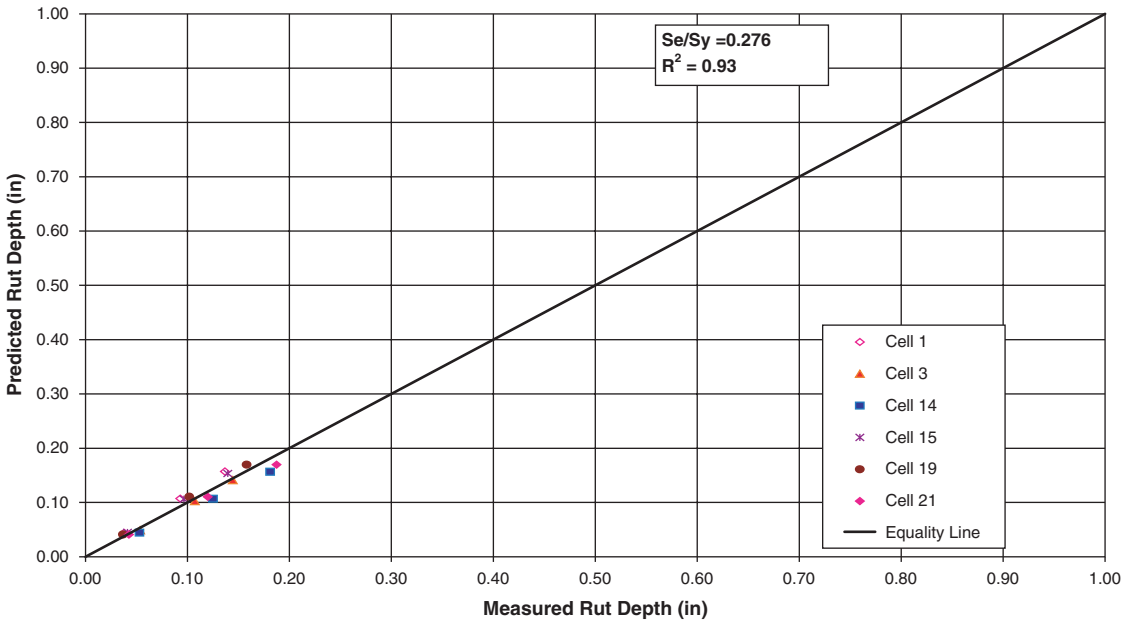

Figure 3-30. Measured versus predicted rut depth for MnRoad plant mixes (unconfined) using all cells.

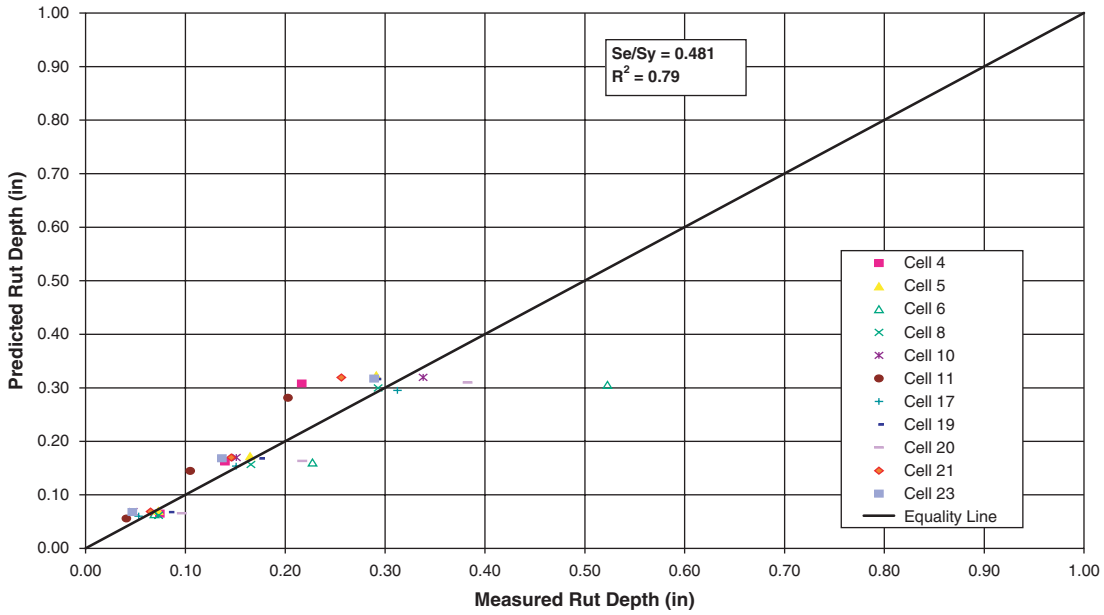

Figure 3-31. Measured versus predicted rut depth for WesTrack plant mixes (unconfined) using all cells.

3.3.3.2 *WesTrack—Plant Mixes Confined Flow Number*

Twelve WesTrack cells incorporating three different traffic levels were used in this analysis. By using the non-liner optimization model in Equation 3.5, the following model parameters were found:

$$R_d = 0.00041 * (N)^{0.59153} * (Fn)^{-0.05421 * Log(N) - 0.18822} \quad (3\text{-}17)$$

Figure 3-33 shows the results of the linear optimization performed on the nine mixes with three ESAL (traffic) levels. The figure shows an excellent correlation between the measured and predictive rut depth. Good statistical measure is shown with an R^2 of 0.78 and S_e/S_y of 0.49.

Three WesTrack cells were identified as outliers in the previous section. The model found without the three outlier data points was as follows:

$$R_d = 0.00042 * (N)^{0.60852} * (Fn)^{-0.05482 * Log(N) - 0.18035} \quad (3\text{-}18)$$

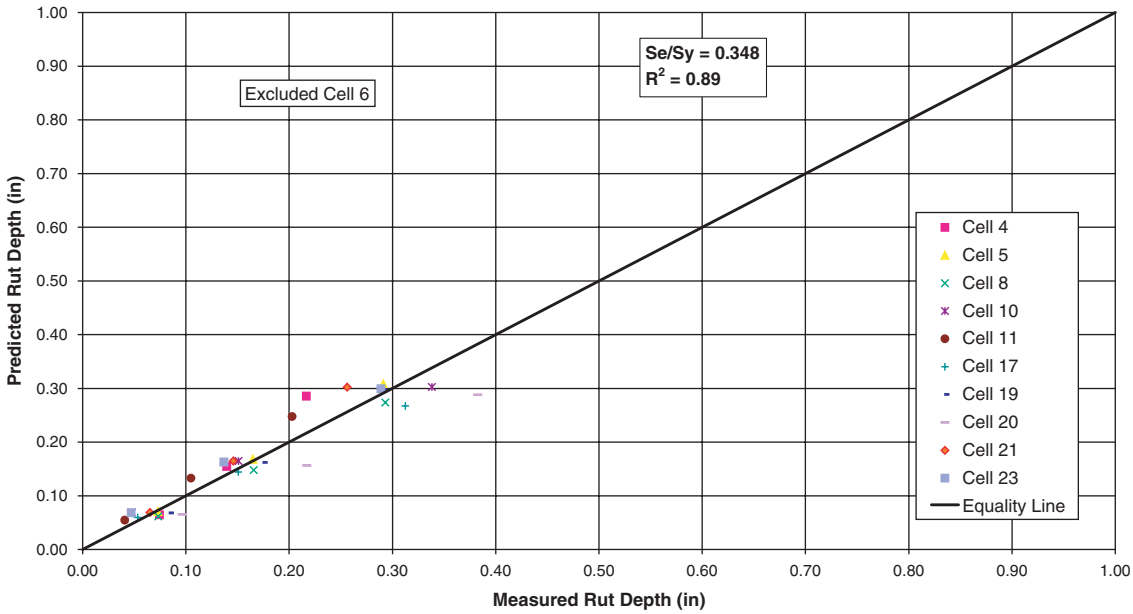

Figure 3-32. Measured versus predicted rut depth for WesTrack plant mixes (unconfined).

Figure 3-34 shows the results of the linear optimization performed on the nine mixes with three ESAL (traffic) levels. The figure shows an excellent correlation between the measured and predictive rut depth. Good statistical measure is shown with an R^2 of 0.95 and S_e/S_y of 0.24. The S_e for the model evaluated was very small compared to the mean rut depth.

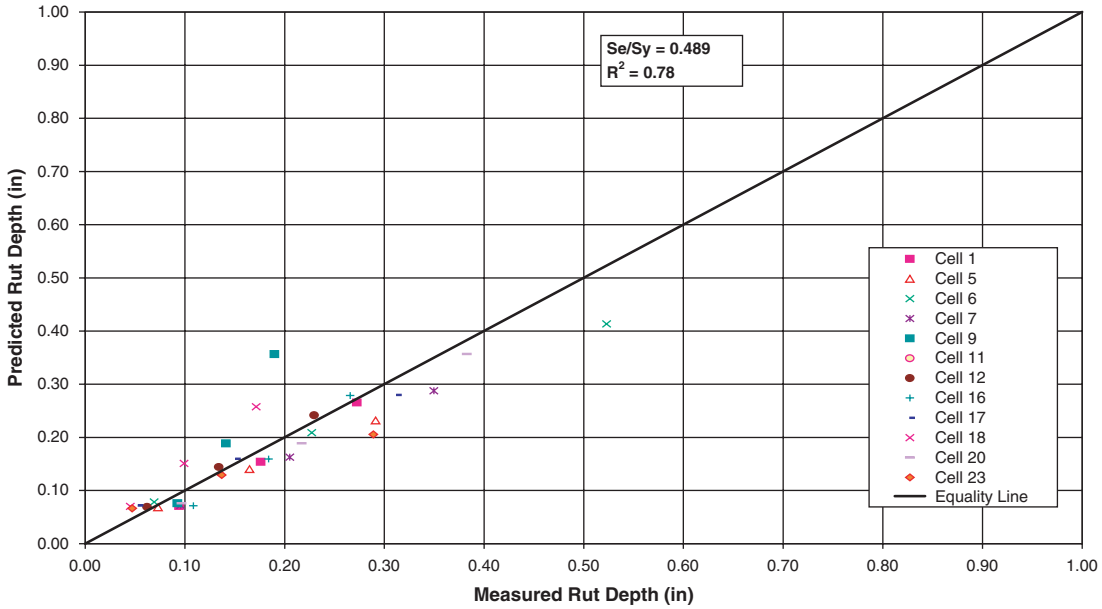

Figure 3-33. Measured versus predicted rut depth for WesTrack plant mixes (unconfined) using all cells.

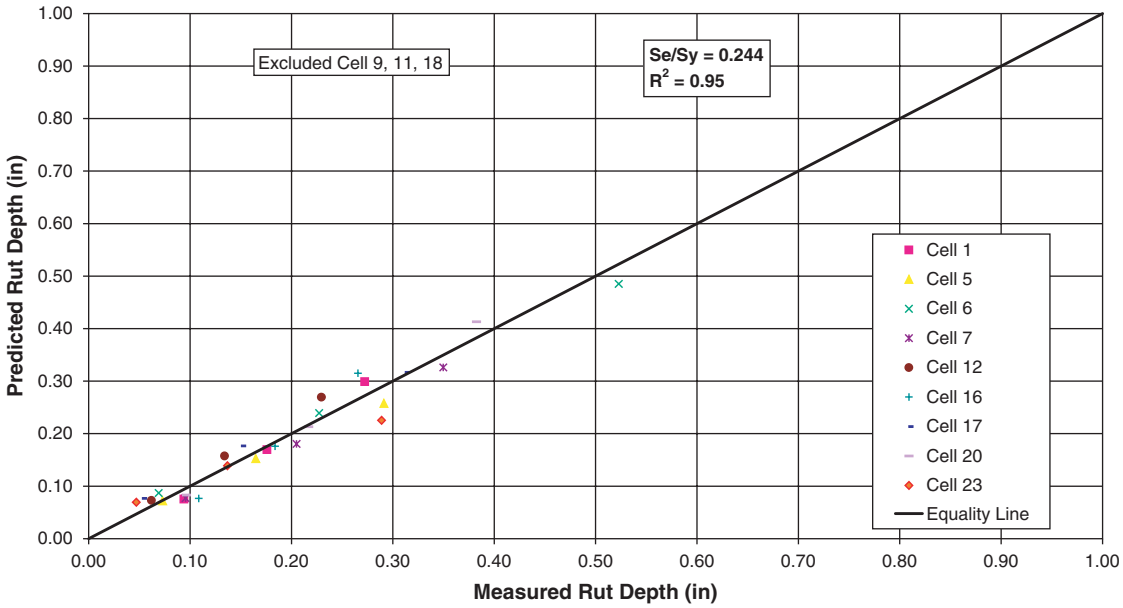

Figure 3-34. Measured versus predicted rut depth for WesTrack plant mixes (confined).

CHAPTER 4

Summary and Conclusions

4.1 Summary

A major objective of the research conducted in NCHRP Project 9-19 was to develop provisional SPT criteria for the prediction of permanent deformation in asphalt mixtures. This volume of the report dealt with criteria for the flow number and flow time simple performance tests.

The scope of this research covered the following:

- Performance of a literature search on HMA mixture characterization, including rutting prediction models;
- Performance of a comprehensive laboratory-testing program to measure the flow parameters for the repeated load flow number and static creep flow time tests; testing program included numerous asphalt mixtures under various temperature and stress levels;
- Establishment of the relationship between the two tertiary flow (failure) parameters as measured in the dynamic repeated load and static creep tests;
- Performance of a statistical analysis to evaluate relationships or trends between the flow parameters and the standard deviation of replicates;
- Investigation of the effect of mix and loading variables on the material strain parameters (i.e., total compliance at flow, plastic strain at flow, and the ratio of plastic to resilient strain at flow);
- Development of global time-temperature shift factors; and
- Development of a set of SPT failure criteria for HMA mixture rutting.

In this study, seven test sites were tested to assess the SPT ability to predict field performance over a wide range of mixes, traffic volumes, and climatic conditions. A total of 97 mixes were tested from NCHRP Project 9-19 experiments as well as mixes from ADOT. A total of 715 flow number and 374 flow time tests were conducted at a temperature range between 85° and 150°F with unconfined and confined testing conditions.

4.2 Conclusions

4.2.1 Statistical Analysis of Flow Number and Flow Time Results

Statistical analyses were conducted to measure the variability or dispersion between replicates of the flow number and flow time from the repeated load and static creep tests, respectively. Coefficient of variation and standard deviation were used as the statistical tools to measure variability. For every set of tests, the mean, standard deviation, and coefficient of variation were calculated.

The unconfined and confined testing data were analyzed separately and combined for both flow number and flow time. Standard deviation versus mean flow number or flow time was plotted. The plots showed that the variation of test results between replicates increased with increasing mean flow number and flow time. Power and linear models were used to fit the trends.

For flow number testing results, the correlations were fair. The following were observed:

- The standard deviation was higher for the confined testing than for the unconfined testing;
- The following relationship for standard deviation and flow number was obtained for combined confined and unconfined test data:

$$\sigma_d = 0.1441(F_n)^{1.0613} \; (R^2 = 0.73) \qquad (4\text{-}1)$$

- For measuring variability between replicates, the standard deviation was a better indicator than the coefficient of variation.

For flow time testing results, the correlations were also fair. The following were observed:

- The standard deviation of the confined testing was higher than the unconfined testing;

- For combined confined and unconfined test data, the following relationship for standard deviation and flow time was obtained:

$$\sigma_d = 0.4630(F_t)^{0.9361} \quad (R^2 = 0.61) \qquad (4\text{-}2)$$

- For measuring variability between replicates, the standard deviation was also shown to be a better indicator than the coefficient of variation.

4.2.2 Relationship of Flow Number and Flow Time

Comparison study was conducted to determine the type and degree of correlation that exist between the measured flow number and flow time.

Generally, unconfined tests showed fair correlation ($R^2 = 0.81$) using a large number of test data. Confined tests had a smaller data set and the correlation ($R^2 = 0.13$) was not as good as the unconfined testing. Using both unconfined and confined test data, the coefficient of determination was 0.71, which was the recommended final relationship for flow number and flow time.

Furthermore, it was observed that

- The relationship between $\log(F_n)$ and $\log(F_t)$ was linear in the log-log domain.
- At relatively low flow time (or flow number) values, the measured flow time was less than that of the flow number values. At higher values (>5500) the flow time and flow number values tend to converge. At relatively large values, the flow number values were generally less than that of the flow time results.
- The final relationship that was recommended between the two flow parameters was as follows:

$$log(F_n) = 1.904\,Log(F_t)^{0.5101} \quad (R^2 = 0.71) \qquad (4\text{-}3)$$

4.2.3 Factors Affecting Strain Failure Zones

The effect of mix and loading variables on the three material strain parameters at flow were investigated. Three unique parameters that were investigated were the total compliance at flow time ($D(t)_f$) for the static creep flow time test, the plastic strain at flow number (ε_{pf}) for the repeated load flow number test, and the ratio of plastic to resilient strain at flow number ($\varepsilon_{pf}/\varepsilon_r$) for the repeated load flow number test. The effect of six variables (confinement level, temperature, mix type, binder type, binder content, and air void level) on the three flow parameters were evaluated. Frequency distributions were done separately and combined for unconfined and confined tests. A summary of the statistical significance tests are presented in Table 4-1. The results of the analysis showed the following:

- None of the parameters was completely independent of the effects of testing variables,
- Confinement level and mix type had significant effects on all parameters for any testing condition and mix type, and
- The results indicated that there was no common failure envelope across the wide variety of mixture variables and the test conditions evaluated.

Table 4-1. Factors affecting strain failure zones—summary of statistical analysis.

Factors	ε_{pf} (F_n Test)				$\varepsilon_{pf}/\varepsilon_r$ (F_n Test)				$D(t)_f$ (F_t Test)			
	Unconfined		Confined		Unconfined		Confined		Unconfined		Confined	
	Plant Mix	Lab Blend	Plant Mix	Lab Blend	Plant Mix	Lab Blend	Plant Mix	Lab Blend	Plant Mix	Lab Blend	Plant Mix	Lab Blend
Confinement Level	Y	Y	Y	Y	Y	Y	Y	Y	Y	Y	Y	Y
Temperature	N	N	Y	X	N	Y	N	X	N	N	N	N
Mix Type	Y	Y	Y	Y	Y	Y	Y	Y	Y	Y	Y	Y
Binder Type	N	N	Y	Y	Y	Y	Y	Y	Y	Y	Y	Y
Binder Content	X	Y	X	Y	X	N	X	Y	X	Y	X	Y
Air Void	Y	Y	Y	Y	N	Y	Y	Y	Y	Y	N	Y

NOTE: Y = yes, effect is significant; N = no, effect in not significant; X = no evaluation was conducted or no data were available.

4.2.4 Development of Time-Temperature Global Shift Factors

Relationships between the flow number and E* time-temperature shift factors were the focus of this part of the study. The global shift factors would help to utilize time-temperature shift factors from the E* testing and directly apply them to the flow number or flow time test results to determine the response or values at any other desired temperature. This would significantly decrease the number of required testing and testing time for the flow number parameters. Several NCHRP Project 9-19 mixtures with various material properties and different test temperature conditions were utilized. Global temperature shift factors were developed using both confined and unconfined testing results. A summary of the findings is as follows:

- A shift factor relationship ratio was obtained to allow the determination of temperature-reduced flow number to one common reference temperature for all cells. This relationship, which is applicable to both confined and unconfined testing results, was as follows:

  Log a(T) Ratio = Log a(T) Fn / Log a(T) E*

- There was no constant ratio of flow number shift factors to E* shift factors. The shift factors ratio varied with temperature. The range of shift factor ratio varied from 60% to 100%.
- This methodology was developed to predict flow number at one temperature and stress level to any other combination of reference temperature and reference stress.

4.2.5 Global Temperature Shifted Master Curve Parameters

In this section, investigation was conducted to determine whether the two main factors affecting the flow number of a mix (temperature and stress level) can be reduced into one unique master curve. The reduced flow number using global shift ratios was plotted against the applied stress, and the fitting parameters (α, β, δ, and γ) of the sigmoidal function were calculated by non-linear optimization methods. The four master curve parameters were summarized for different testing sites. Each site's master curve parameters were then separated according to mix type and confinement level. Finally, statistical analysis was conducted to evaluate any consistency among the parameters. The outcome of the analysis was as follows:

- The parameter α was defined as minimum stress level that would cause the damage; $\delta + \alpha$ was defined as the maximum stress that would cause instantaneous damage; and β and γ were described as the shape of the sigmoidal function;
- α value was determined to be constant for every mixture and confinement level;
- The mix type and confinement level had a significant effect on δ;
- The mix type had a significant effect on β but little or no effect on γ; and
- The confinement level had little or no effect on β and a significant effect on γ.

4.2.6 Reduced Flow Number versus HMA Rut Depth at Different Traffic Levels

The relationship between the reduced flow number and field rut depth at different traffic level were investigated. Lab-measured flow numbers were reduced by global temperatures shifting. All the flow numbers were reduced to 100°F and 25 psi (172 kPa) for unconfined testing. For confined testing, a stress level of 150 psi (1034 kPa) was chosen except for the WesTrack experiment where confined testing at 200 psi (1379 kPa) was considered. Primarily, three NCHRP Project 9-19 test sites (ALF, WesTrack, and MnRoad) lab and field mixes were analyzed. The analysis showed the following:

- From the power relationship of reduced flow number and field HMA rut depth, there was a very good relationship between the slope and intercept values to traffic using the models as shown:

$b = m_1 * \text{Log}(N) - l_0$	$\text{Log}(a) = 1 - k * \text{Log}(N)$
m_1 = Slope	k = Slope
l_0 = Constant	l = Constant
N = ESAL (traffic)	N = ESAL (traffic)

- The relationship between slope and intercept to traffic was linear with a coefficient of determination of one.
- A model for predicting field rut depth (R_d) using lab-measured flow number (F_n) and traffic level (N) was developed for all mixtures and had the following form where i_1, m_2, m_1, and l_o are constants:

$$R_d = i_1 * (N)^{-m2} * (Fn)^{m1 * Log(N) - l0} \quad (4\text{-}4)$$

This model was used to get the predictive rut depth for a particular traffic (N) and reduced flow number (F_{nr}). All the models were statistically evaluated for their accuracy and engineering reasonableness. The statistics that were applied to measure the model accuracy were the coefficient of determination (R^2), standard error of estimate (S_e), and relative accuracy (S_e/S_y). The results of this study are as follows:

- All of the different test cell data were analyzed separately;
- Models for unconfined and confined testing were established separately, and Table 4-2 shows the final models for the different test sites; and
- All of the test cells, excluding the outlier cells, were used.

Table 4-2. Final rutting models for the individual test sites.

Test Site	Test Type	Rutting Model	R^2	S_e/S_y
ALF—Field Cores	U	$R_d = 1.0989 * (N)^{0.3848} * (Fn)^{-0.0115*Log(N) - 0.3201}$	0.97	0.20
ALF—Field Cores	C	$R_d = 1.2552 * (N)^{1.6972} * (Fn)^{-02429*Log(N) - 0.3201}$	0.89	0.40
ALF—Lab Blend	U	$R_d = 1.4646 * (N)^{0.2718} * (Fn)^{0.1885*Log(N) - 0.4629}$	0.56	0.78
MnRoad—Plant Mix	U	$R_d = 1.2483 * (N)^{0.0425} * (Fn)^{0.1649*Log(N) - 1.3745}$	0.93	0.29
MnRoad—Plant Mix	C	$R_d = 1.20326 * (N)^{0.21255} * (Fn)^{0.28828*Log(N) - 1.58221}$	0.93	0.28
WesTrack—Plant Mix	U	$R_d = 0.00341 * (N)^{0.36446} * (Fn)^{0.00304*Log(N) - 0.04683}$	0.89	0.35
WesTrack—Plant Mix	C	$R_d = 0.00042 * (N)^{0.60852} * (Fn)^{-0.05482*Log(N) - 0.18035}$	0.95	0.24

NOTE: U = unconfined testing; C = confined testing.

References

1. Witczak, M.W., K.E. Kaloush, T.K. Pellien, M. El-Basyouny, and H.L. Von Quintus. *NCHRP Report 465: Simple Performance Test for Superpave Mix Design.* Transportation Research Board, National Research Council, Washington, DC (2002).
2. Sousa, J.B., S.L. Weissman, L.J. Sackman, and C.L. Monismith. *A Nonlinear Elastic Viscous with Damage Model to Predict Permanent Deformation of Asphalt Concrete Mixtures*. Annual Meeting of the Transportation Research Board, National Research Council, Washington, DC (1993).
3. Yoder, E.J. and M.W. Witczak. *Principles of Pavement Design*. 2nd ed., John Wiley & Sons, Inc., New York, 1980.
4. Sousa, J.B., S.L. Weissman, J.A. Deacon, J. Coplantz, and C.L. Monismith. *Permanent Deformation Response of Asphalt Aggregate Mixes—Mix Design and Analysis*. Report No. SHRP-A-415. Transportation Research Board, National Research Council, Washington, DC (1994).
5. Sousa, J.B., A. Tayebali, J. Harvey, P. Hendricks, and C.L. Monismith. Sensitivity of Strategic Highway Research Program A-003A Testing Equipment to Mix Design Parameters for Permanent Deformation and Fatigue. In *Transportation Research Record 1384*. Transportation Research Board, National Research Council, Washington, DC, 1993, 69–79.
6. Sousa, J.B. and S.L. Weissman. Modeling Permanent Deformation of Asphalt Aggregate Mixes. *Proceedings*, The Association of Asphalt Paving Technologists, Vol. 63, 1994, 224–257.
7. Sousa, J.B. Asphalt-Aggregate Mix Design Using the Repetitive Simple Shear Test (Constant Height). *Proceedings*, The Association of Asphalt Paving Technologists, Vol. 63, 1994, 298–345.
8. SHRP Designation: M-003, *Determine the Shear Stiffness Behavior of Modified and Unmodified Hot Mix Asphalt with the Superpave Shear Test Device.* Report No. SHRP-A-379. Transportation Research Board, National Research Council, Washington, D.C., 1994.
9. Sousa, J.B. and M. Solaimanian. Abridged Procedure to Determine Permanent Deformation of Asphalt Concrete Pavements. Paper accepted for presentation at the Annual Meeting of the Transportation Research Board, National Research Council, Washington, D.C. (1994).
10. Solaimanian, M. and T. Kennedy. "Predicting Maximum Pavement Temperature Using Maximum Air Temperature and Hourly Solar Radiation." Paper accepted for presentation at the Annual Meeting of the Transportation Research Board, National Research Council, Washington, D.C. (1994).
11. Lytton, R.L. *Development and Validation of Performance Predication Models and Specifications for Asphalt Binder and Paving Mixes*. Report No. SHRP-A-357. Transportation Research Board, National Council, Washington D.C. (1993).
12. Kaloush, K.E. "Simple Performance Test for Permanent Deformation of Asphalt Mixtures." Ph.D. dissertation, Department of Civil and Environmental Engineering, Arizona State University, Tempe, AZ (2001).
13. Sullivan, B. "Development of Flow Number and Flow Time Candidate Simple Performance Test for Asphalt Mixtures." M.S. thesis, Department of Civil and Environmental Engineering, Arizona State University, Tempe, AZ (2002).
14. Leahy, R. and M. Witczak. The Influence of Test Conditions and Asphalt Concrete Mix Parameters on Permanent Deformation Coefficients Alpha and Mu, *Proceedings.* The Association of Asphalt Paving Technologists, Vol. 60, 1991, 333–363.
15. Ayres, M. and M. Witczak. AYMA Mechanistic Probablistic System to Evaluate Flexible Pavement Performance. In *Transportation Research Record 1629*, Transportation Research Board, National Research Council, Washington, D.C., 1998, 137–148.
16. Hafz. I.H.F. "Development of a Simplifed Asphalt Mix Stability Procedure for Use in Superpave Volumetric Mix Design," Ph.D Dissertation, Civil Engineering Department, University of Maryland, College Park, Maryland, 1997.

Abbreviations and acronyms used without definitions in TRB publications:

AAAE	American Association of Airport Executives
AASHO	American Association of State Highway Officials
AASHTO	American Association of State Highway and Transportation Officials
ACI–NA	Airports Council International–North America
ACRP	Airport Cooperative Research Program
ADA	Americans with Disabilities Act
APTA	American Public Transportation Association
ASCE	American Society of Civil Engineers
ASME	American Society of Mechanical Engineers
ASTM	American Society for Testing and Materials
ATA	Air Transport Association
ATA	American Trucking Associations
CTAA	Community Transportation Association of America
CTBSSP	Commercial Truck and Bus Safety Synthesis Program
DHS	Department of Homeland Security
DOE	Department of Energy
EPA	Environmental Protection Agency
FAA	Federal Aviation Administration
FHWA	Federal Highway Administration
FMCSA	Federal Motor Carrier Safety Administration
FRA	Federal Railroad Administration
FTA	Federal Transit Administration
IEEE	Institute of Electrical and Electronics Engineers
ISTEA	Intermodal Surface Transportation Efficiency Act of 1991
ITE	Institute of Transportation Engineers
NASA	National Aeronautics and Space Administration
NASAO	National Association of State Aviation Officials
NCFRP	National Cooperative Freight Research Program
NCHRP	National Cooperative Highway Research Program
NHTSA	National Highway Traffic Safety Administration
NTSB	National Transportation Safety Board
SAE	Society of Automotive Engineers
SAFETEA-LU	Safe, Accountable, Flexible, Efficient Transportation Equity Act: A Legacy for Users (2005)
TCRP	Transit Cooperative Research Program
TEA-21	Transportation Equity Act for the 21st Century (1998)
TRB	Transportation Research Board
TSA	Transportation Security Administration
U.S.DOT	United States Department of Transportation